PHARMACOLOGICAL AND STRUCTURE-ACTIVITY RELATIONSHIP EVALUATION OF MICROTUBULE-STABILIZING AGENTS

by

Charitha Madiraju

B.PHARM., Kakatiya University, 1996

M.S., University of Louisiana, 1999

Submitted to the Graduate Faculty of

the School of Pharmacy in partial fulfillment

of the requirements for the degree of Doctor of Philosophy

University of Pittsburgh

2005

UNIVERSITY OF PITTSBURGH

SCHOOL OF PHARMACY

This dissertation was presented

by

Charitha Madiraju

It was defended on

[September 22, 2005]

and approved by

[Janet Amico, M.D.]

[Patricia Eagon, Ph.D.]

[Soumitra Basu, Ph.D.]

[Michael Mokotoff, Ph.D.]

[Dennis P. Curran, Ph.D.]

[Billy W. Day, Ph.D.]
Dissertation Major Advisor

PHARMACOLOGICAL AND STRUCTURE-ACTIVITY RELATIONSHIP EVALUATION OF MICROTUBULE-STABILIZING AGENTS

Charitha Madiraju, M.S.

University of Pittsburgh, 2005

Microtubules are composed of α- and β-tubulin subunits and are highly dynamic elements of the cytoskeleton that help maintain fidelity during cell division. This aspect of microtubules makes them a very useful target for the treatment of tumors. The potent microtubule-stabilizing agent (+)-discodermolide is a sponge-derived polyketide natural product and is a polyhydroxylated and polymethylated, C24:4 fatty acid lactone carbamate. The microtubule-stabilizing action of discodermolide was predicted by computational chemistry. Biochemical, pharmacological, and antiproliferative activity studies with discodermolide showed it to have potent hypernucleating, microtubule-stabilizing and microtubule bundling properties. Synthetic analogues of discodermolide were made to establish a structure-activity relationship (SAR) for discodermolide. The library consisted of analogues with modifications made on the lactone and carbamate/diene portions, with altered stereochemistry on C-11 and C-17, conformational analogues based on the solution structure of discodermolide, and macrocyclic analogues of discodermolide. Biological evaluation of the analogues suggested the diene, the carbamate on C-19 and the stereochemistry on C-11 and C-17 to be important for the activity of the parent molecule, and that the lactone moiety is amenable to modifications. Of interest were the conformational and macrocyclic analogues that showed promising microtubule-targeting

activities. Furthermore, these studies paved way for the discovery of the related natural product dictyostatin as a potent microtubule stabilizer. Dictyostatin is a macrocycle with stereochemistry very much like discodermolide. Intensive biochemical and pharmacological studies showed dictyostatin to have comparable, or superior in some respects, properties to those of discodermolide and paclitaxel. Biological analyses of structural analogues of dictyostatin suggested that the macrolactone and the bottom half of dictyostatin have a critical role in the biological activity of the parent molecule. The top portion of the molecule was amenable for modifications without much loss of activity; however, this half of the molecule seemed crucial for the microtubule binding property of the parent molecule. These studies identified dictyostatin to be the most potent of the microtubule stabilizers studied. One interesting analogue, C16-normethyldictyostatin, was identified to have promising activity comparable to the parent molecule.

TABLE OF CONTENTS

LIST OF TABLES

LIST OF FIGURES

LIST OF SCHEMES

PREFACE

It brings an immense pleasure for me to write a note of acknowledgments for so many people whom I had come across and who have played a significant role during the years of my educational training. Top on the list would be my advisor, Dr. Billy Day for being my major dissertation advisor, for his support, and for his patience. Most of all, I thank Dr. Day for providing me with an opportunity and liberty for exploring science to its best, for sharing his scientific expertise in the field of drug discovery, for critical evaluation of my dissertation work, and for inculcating in me a never-ending interest in the project. My sincere acknowledgments for my committee members, Dr. Michael Mokotoff, Dr. Dennis Curran, Dr. Janet Amico, Dr. Patricia Eagon, and Dr. Soumitra Basu for willing to serve on my committee, for their excellent feedback during committee meetings, for sharing their expertise, and for their helpful suggestions. A special note of thanks and appreciation for our collaborator Prof. Dennis Curran and the synthetic chemists in his lab, Drs. Nicky Choy, Jose Minguez, Pui Qui Nguyen, Sun-Young Kim, Youseung Shin, Jean-Hughes Fournier, Yoshikazu Fukui, Arndt Brückner and Ms. Tiffany Turner for their effort in making molecules of great interest. I express my profound gratitude to Dr. Ernest Hamel at NCI (NIH) for providing me with great insight in microtubule literature and an opportunity to perform a portion of my dissertation work in his laboratories last summer. It was a great opportunity to get hands-on experience working with his 'salvaged' Gilfords. I am fortunate to have had financial assistantship from the School of Pharmacy for which I am grateful - all the faculty and staff here in the School of Pharmacy and at University of Pittsburgh deserve an acknowledgment. I acknowledge Drs. Donna Stolz, Simon Watkins,

Kenneth Giuliano, Andreas Vogt, Galina Kirillova, and Robert Bies for their help. Thanks to all the graduate students for their cheerful greetings and many thanks to all of Dr. Day's lab members (Drs. Balachandran and Schreiber, Brianne, and Guangyu who were involved with this project; others: Jenny, Jelena, Yun Fan, Miranda, and Ying) for the team work and the interesting discussions (science and non-science) during lab meetings.

Finally, I place on record the inspiration, love, and encouragement my parents provided me and I humbly thank my parents for their support in this venture. I thank my family members and friends for their congeniality and comradeship.

ABBREVIATIONS

ABC	-	ATP-binding cassette
ATP	-	Adenosine-5'-triphosphate
BimC	-	Blocked in mitosis C protein
$CaCl_2$	-	Calcium chloride
Cc	-	Critical concentration
cdk	-	Cyclin-dependent kinase
Bmax	-	Maximum bound
ddGTP	-	Dideoxyguanosine-triphosphate
DEAE	-	Diethylaminoethyl
Dis1	-	Defect in sister chromatid disjoining protein
DMEM	-	Dulbecco's Modified Eagle Medium
DMSO	-	Dimethylsulfoxide
DNA	-	Deoxyribo nucleic acid
EC_{50}	-	Concentration required to cause 50% effect
Eg5	-	Mitotic kinesin protein
EGTA	-	Ethylene glycol bis(2-aminoethyl ether)-N,N,N'N'-tetraacetic acid
EM	-	Electron microscopy
FBS	-	Fetal bovine serum
FITC	-	Fluorescein-5-isothiocyanate
GAB	-	Glycerol assembly buffer (contains GTP)
GAB-GDP	-	Glycerol assembly buffer (GTP replaced with GDP)
GDP	-	Guanosine-5'-diphosphate
GI_{50}	-	Concentration required to cause 50% growth inhibition
GTP	-	Guanosine-5'-triphosphate
HBSS	-	Hank's buffered salt solution
HCS	-	High content screening
HTS	-	High throughput screening
IC_{50}	-	Concentration required to cause 50% inhibition
K	-	Affinity
K_a	-	Association rate constant
K_b	-	Equilibrium binding constant
K_D	-	Binding dissociation constant
Ki	-	Inhibition constant
Kin1	-	Kinesin family 1 proteins
MAPs	-	Microtubule-associated proteins

MDECs	-	Minimum detectable effective concentrations
Mes	-	(4-Morpholino)ethanesulfonate
MOM	-	Methoxymethyl ether
$MgCl_2$	-	Magnesium chloride
MSG	-	Monosodium glutamate
MT	-	Microtubule
MTS	-	3-(4,5-Dimethylthiazol-2-yl)-5-(3-carboxymethoxyphenyl)-2 -(4-sulfophenyl)-2*H*-tetrazolium
$NaBH_4$	-	Sodium borohydride
nH	-	Hill slope
NCI/ADR	-	National Cancer Institute's adriamycin resistant
	-	breast cancer cell line
NMR	-	Nuclear magnetic resonance
NuMA	-	Nuclear protein that associates with the mitotic
	-	apparatus
P-gp	-	P-Glycoprotein
RCC1	-	Regulator of chromatin condensation
RPMI	-	Roswell Park Memorial Institute
RT	-	Room temperature
SAR	-	Structure-activity relationship
SD	-	Standard deviation
SEM	-	Standard error of mean
TEM	-	Transmission electron microscope
THP	-	Tetrahydropyranyl
XKCM1	-	*Xenopus* kinesin catastrophe modulator 1
XMAP215	-	*Xenopus* microtubule associated protein

1. INTRODUCTION

1.1. MICROTUBULES - A drug target for cancer therapy

Microtubules (MTs) are key elements of cytoskeleton that orchestrate many important events in the cell (Schiff *et al*. 1979). It was a century ago that tubulin/MTs were serendipitously discovered when the underlying complex process of cell division, called mitosis, was under investigation (Dustin 1984). A peripheral structure formed of minute parallel concentric fibrils [also referred to as tubules, the name 'microtubule' was coined by Mohri] was first observed in nucleated red blood cells. At the same time, colchicine, extracted from *Colchicum autumnale* administered as tincture for the treatment of gout, was observed for the first time to cause mitotic arrest (Borisy and Taylor 1967a). The same studies showed that [^{3}H]colchicine binds to (i) a cellular protein, (ii) a soluble protein in the 6S fraction, (iii) the mitotic apparatus in cell-free extracts, and (iv) a protein subunit from MTs (Borisy and Taylor 1967a, 1967b; Shelansky and Taylor 1967). Since then, rapid discoveries suggested good evidence for MTs' important regulatory role in many cellular processes. In cancer biology, MTs garnered much attention only after the discovery of the mechanism of the anticancer activity of paclitaxel (Taxol®), a natural product obtained from the pacific yew tree, *Taxus brevefolia* (Schiff *et al*. 1978).

Oncology therapeutics occupy a prominent place in drug design and discovery and contribute to over seventy-seven percent of global oncology revenues (Commercial insight). Amongst the oncology drugs available in the drug market, cytotoxics have occupied the cornerstone and are considered the drugs most prescribed for various kinds of cancers, ranging from benign to aggressive. Cytotoxics are now the first line of choice for the treatment of

refractory, hormone-resistant and metastatic cancers. One of the major classes of cytotoxics is the mitotic poisons, including MT stabilizers and destabilizers. The mechanism of action and clinical success of paclitaxel has drawn great interest for tubulin or MTs as a target for the cure of cancer, a disease state where patients bearing the rapidly and abnormally growing cells are in a desperate need for therapeutic intervention at any of the possible phases of cell cycle, not the least of which is the mitotic phase. Clinical studies have shown that cancer therapy with paclitaxel as the first line of choice for the treatment of metastatic cancers given either as a single agent or in combination with other cytotoxics like doxorubicin have met with good success (Rowinsky *et al*. 1990; Mamounas *et al*. 1995; Davidson 1995; Davidson 1996). However, the overall response observed in a clinical study is 32% for single agent therapy; combination therapy has shown an overall response rate observed of over 90% (Perez 1998; Perez 1999). Hence, continuous effort is ongoing in the search for potent MT-targeted chemotherapeutic agents to treat various types of cancers. One of the many clinical drug candidates that comprise the R&D pipeline of major pharmaceutical companies is invariably a microtubule-targeting agent (Mani *et al*. 2004). Success in using tubulin/MT as a target for the treatment of cancer has developed because of the sound knowledge gained over the years in understanding tubulin form, function and dynamics, along with advancements made in synthetic and high-throughput screening techniques for rapid compound development and identification. A discussion of MTs, their dynamic role in cell division (importantly during mitosis), factors influencing MT dynamicity and properties is given in the next section. This will be followed by a discussion on microtubule-targeting agents focused on microtubule stabilizers -- paclitaxel, discodermolide and dictyostatin.

1.2. Tubulin polymerization dynamics

MTs are polymeric forms of tubulin formed by self-assembly of α-β heterodimers (Dustin 1984). Longitudinal (head-to-tail) association of α-β tubulin dimers forms a protofilament of a MT (Nogales 2001). The primary structural element of the mitotic spindle involved in cell division is the MT (Wittmann *et al*. 2001). Two important properties regulate spindle assembly formation from the MT lattice, 1) MT dynamicity and 2) mechanochemical properties of MT-associated proteins (called motor proteins, dyneins and kinesins). The structure of the mitotic spindle is constituted of morphologically different subpopulations of MTs: kinetochore, interpolar and astral MTs -- the definition of all these is implicit in their nomenclature (Mastronarde *et al*. 1993). The spindle structure is highly dynamic with a turnover half-life of about 60-90 s (Saxton *et al*. 1984; Salmon *et al*. 1984). A representation of microtubules, the mitotic spindle and mitosis is shown in Figure 1. The rapid turnover of spindle MTs is characterized by catastrophe and rescue events; a catastrophe event is the rapid conversion of the polymerized state of MTs to the depolymerized state. The opposite holds true for the rescue events (Verde *et al*. 1992). The destabilization rate of MTs outweighs the stabilization process in a catastrophe event, and in a rescue event it is exactly the reverse.

The primary function of the mitotic spindle is to separate sister chromatids (chromosomes) so that each half of the replicated chromosome is positioned at the opposite ends of the spindle pole (Wittmann *et al*. 2001). This process involves a complex interplay of MTs, motor proteins, and the mechanochemical forces generated by proteins associated with kinetochores, chromosome arms and astral MTs. The mitotic phase in a cell starts at the condensation of chromatin to form chromosomes, during which kinetochores assemble at the centromeric regions of the chromosomes (Figure 1). Kinetochores form a high-affinity site on

the chromosomes to help search for and capture spindle MTs, attach spindle MTs to chromosomes, coordinate chromosome motility on the spindle, and regulate the transition from metaphase to anaphase (Zhai *et al*. 1995; Rieder and Salmon 1998). The mechanisms by which

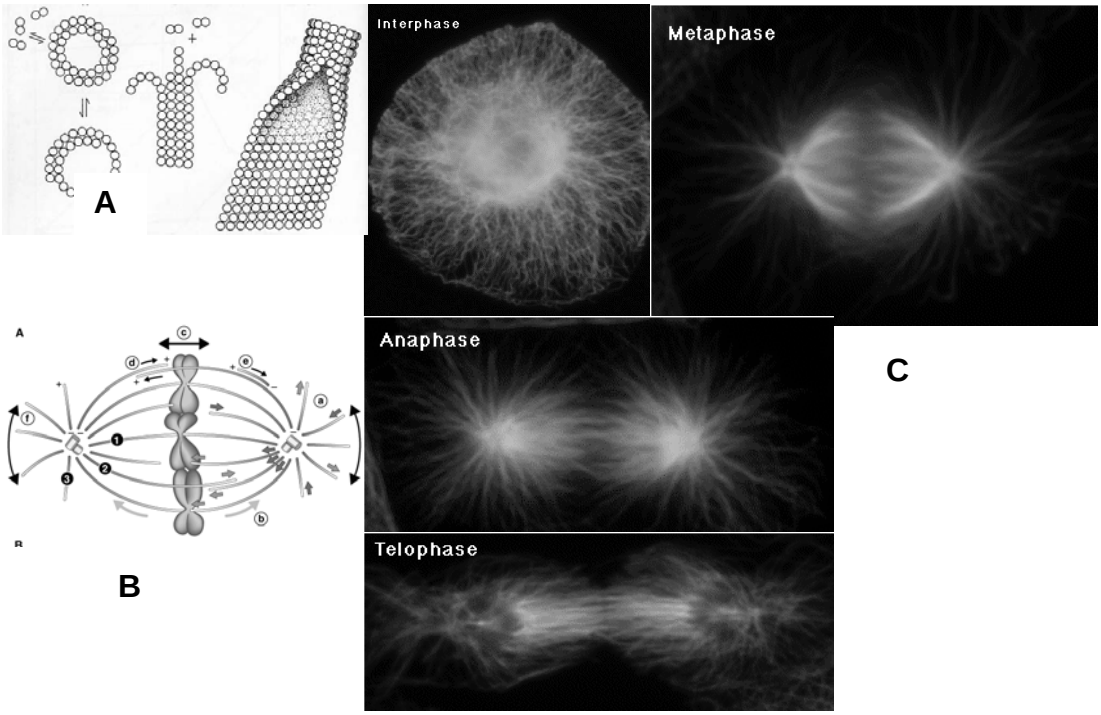

Figure 1. Representation of microtubules and mitosis

A. Tubulin subunits polymerize to form a sheet of protofilaments that assemble to form microtubule polymer (Adapted from: Dustin 1984). ***B***. Microtubule organization in the cytoplasm before cell division (Adapted from: Wittmann *et al*. 2001). Sister chromatids are tethered to the microtubules and aligned along the equatorial plate before cell division. ***C***. Different phases of mitosis. Microtubules play a crucial role in each of the four phases (interphase, metaphase, anaphase, and telophase) of mitosis.
(Adapted from: http://mitchison.med.harvard.edu/research/Microtubules.htm)

the 'search-capture-attach' and the other events controlled by kinetochores are still not well-understood. There are several factors in the cell that regulate the process of MT turnover that make up for the remarkable dynamicity of the spindle architecture. Important players during this process have been identified amongst which are guanosine-5'-triphosphate (GTP), motor proteins (dynein and kinesins), microtubule-associated proteins (MAPs), divalent cations (Ca^{++}, Mg^{++}), temperature, etc., that contribute to the process of mitosis in many ways (Kirschner and Williams 1974; Weingarten *et al*. 1975; Soifer 1986; Wittmann *et al*. 2001; Karsenti and Vernos 2001; Carazo-Salas *et al*. 2001). Quite a few of these factors, studied for their role as mitotic spindle regulators albeit not thoroughly understood, have been of immense interest and under extensive investigation. Most of the regulatory elements that control the spindle assembly process and the turnover rate are also known to be cell cycle-dependent (Karsenti and Vernos 2001). This feature of cell-cycle-dependent regulation explains the differing relative rates of MT turnover during different phases of cell cycle.

Dynamic events during polymerization of tubulin are, to a great extent, known to be regulated by the presence of the nucleotide GTP, MAPs and motor proteins (Soifer 1986; Grover *et al*. 1995; Weisenberg and Deery 1976; Kirschner and Williams 1974). Figure 2 represents the effect of GTP on the dynamic events of tubulin assembly. GTP is a crucial regulatory factor in MT assembly process. GTP is known to be localized in the exchangeable site on β-tubulin (i.e., GTP there can be hydrolyzed to GDP, and the GDP can be exchanged for GTP) and in a non-exchangeable site on α-tubulin (where the GTP is not hydrolyzed) (Mitchison 1993). Tubulin with GTP bound to β-tubulin (GTP-tubulin) is known to be competent for assembly and the GTP-cap maintains the stability of MTs (Desai and Mitchison 1997). Because the nucleotide at

the plus (growing) end of the MT is exchangeable, this end of a MT is capped by β-tubulin. MTs are thus known to exhibit polarity and are in a state of dynamic equilibrium, with assembly

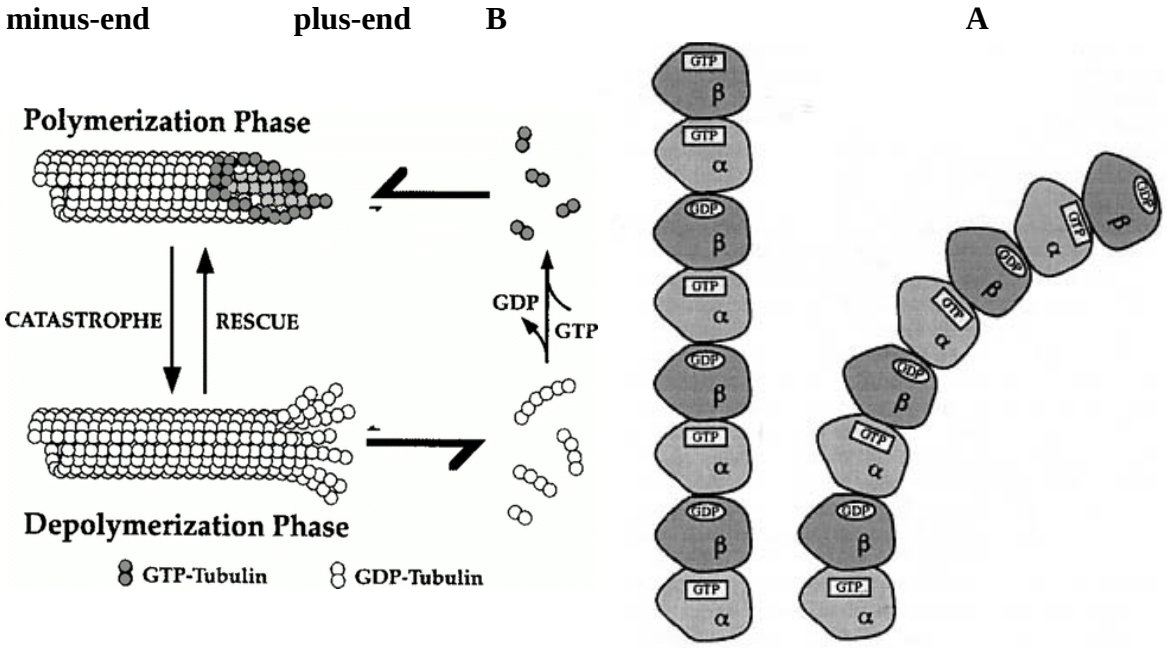

Figure 2. Schematic representation of the role of GTP in microtubule assembly process

A. GTP binds to β-subunit of tubulin, makes it competent for assembly (polymerization/rescue) and promotes polymerization at the plus-end of microtubules. GTP-cap maintains the stability of microtubules (Adapted from: Downing and Nogales 1998). ***B***. Representation of the state of dynamic equilibrium in microtubules, with assembly (polymerization/rescue) occurring at plus end and disassembly (depolymerization/ catastrophe) mainly occurring at the minus end. (Adapted from: Desai and Mitchison 1997)

(polymerization/rescue) occurring at the plus end and disassembly (depolymerization/catastrophe) mainly occurring at the minus end (Margolis and Wilson 1978).

These events contribute to the MT dynamic instability and treadmilling processes observed in MTs. The crystal structure of the paclitaxel-tubulin complex revealed the location of the nucleotides on each monomer (Downing and Nogales 1998; Downing 2000). The interactions along the protofilament interface (longitudinal contacts) involve binding of Glu254 on α-tubulin with the corresponding residue on β-tubulin. The primary interactions across the interprotofilament interface (lateral contacts) involve the M-loop from one dimer with helix H3 on the other dimer. GTP hydrolysis and phosphate release during the depolymerization process induces a conformational change that leads to the peeling or curving of protofilaments to form rings or sheets.

The dynamic behavior of MTs, the catastrophe, and the rescue events are largely under the influence of regulatory elements/proteins, motor proteins, and MAPs apart from GTP. Important factors/proteins identified to promote catastrophe events include Op18/stathmin and XKCM1-Kin I, the latter of which belongs to the kinesin superfamily (Wittmann *et al*. 2001; Belmunt and Mitchison 1996). The mechanism by which the two proteins induce MT disassembly could be one of the many possible. These include promoting GTPase activity, inducing catastrophe by sequestering tubulin dimers and disrupting interactions between protofilaments. Factors that help stabilize the MT polymerization process are termed MAPs (Wittmann *et al*. 2001). There are several MAPs identified to date, important ones include tau, MAP2, MAP4, Dis1-family MAPs and XMAP215. MAPs induce MT polymerization by protecting MT ends (decrease catastrophe rates) or by stabilizing the lateral contacts between the protofilaments (increase rescue rates). Literature reports suggest that Dis1-MAPs antagonize the kinesin family proteins (Kin1) preventing the depolymerization of MTs (Nabeshima *et al*. 1999). Kin1 is constitutive and the activity of Dis1 proteins is regulated by phosphorylation (Desai *et al*.

1999). There is good evidence that the levels of the factors that support spindle assembly, disassembly and rapid turnover of MTs during different phases of cell cycle are under the control of cell-cycle regulating factors. Studies done in frog oocyte systems reveal that spindle dynamics seemed to be under the influence of cyclins and cdc2, the levels of which vary at different phases of the cell cycle. Like Dis1 family proteins, XMAP215 during mitotic phase is phosphorylated by cyclin-dependent kinase 1 (cdk1), which in turn is regulated by cyclins (Vasquez *et al*. 1999). Stathmin, a known MT destabilizer, is hyperphosphorylated during mitosis by cdks (Andersen *et al*. 1997). While MAPs like XMAP215 are active during the mitotic phase, inhibitors of MTs (XKCM1) are active during interphase and metaphase (Tournebize *et al*. 2000).

MTs exhibit polarity with the plus-end of MTs in the polymerizing state and the minus-end in the depolymerizing state (Margolis and Wilson 1978; Margolis *et al*. 1978). The poleward movement of MTs is under the control of the MAPs and motor proteins that play a key role during mitosis. Several mechanisms have been identified for the organization and maintenance of bipolarity of the mitotic spindle. Motor proteins are essential for centrosome separation (regulated by cortical dyneins), for sorting of randomly growing MTs around chromatin into an array consisting of parallel and antiparallel MTs (BimC and Eg5 motors), for cross-linking MTs (minus-end directed dynein, dynactin, NuMA, etc.), and for movement of spindle poles away from chromosomes with the involvement of plus-end directed kinesins (Wittmann *et al*. 2001). The search-and-capture mechanism responsible for promoting the connection between kinetochores and spindle MTs is not the only important step in the spindle assembly process. The self-organization of the mitotic spindle by motor proteins and Ran-GTP-dependent nucleation of mitotic spindle around the chromosomes play important mechanistic

roles in the triggering of spindle assembly and dynamics (Carazo-Salas *et al*. 1999). The nucleation of dynamic MTs around chromosomes in the presence of centrioles, MT abundance, and MT length are all under the control of Ran-GTP. The generation of Ran-GTP around the chromosomes, promotion of nucleation and stabilization of centrosomal MTs is under the control of a factor named regulator of chromosome condensation (RCC1).

The self-organization, search-and-capture and centrosome-dependent nucleation of the mitotic spindle are all crucial for maintaining fidelity during cell division. All these steps involve perfect coordination of spindle assembly, MTs and motor proteins. Perturbation of any of the above components would lead to abnormal mitosis or mitotic arrest. This feature has been explored for cancer therapy in order to halt rapidly proliferating cells by discovering therapeutic interventions targeting one or more of the components of mitotic spindle. The studies reported here were done with this goal in mind for MT-targeting agents.

Tubulin or MT polymerization dynamics, regulated by so many factors, is under both kinetic and thermodynamic control. MT dynamics follows the classical Oosawa-condensation model wherein nucleation is a prerequisite for polymer formation (Oosawa and Kasai 1962). Nucleation of tubulin subunit assembly can either be a spontaneous process or can be induced by any polymer-promoting agent. This is followed by elongation of the nuclei to form MT polymer. The nucleation step in the process of tubulin/MT assembly confers a 'lag time' to the MT assembly process. Polymer formation is a time-, temperature- and reaction component-dependent process (Gaskin *et al*. 1974). Microtubule assembly and the factors regulating the assembly process can be understood most readily by employment of isolated protein-based experiments in the presence or absence of regulatory factors. This was one of the goals of the studies reported here. The rate processes during microtubule assembly follow the law of mass

action. The rate of formation of MTs (the forward reaction) is dependent on the association rate constant (K_{on}) for subunit assembly and the tubulin monomer concentration in the system. This reaction mechanism, similar to any other process, follows Newton's law: for every action there is an equal and an opposite reaction. Dissociation of the assembled tubulin counteracts the polymer assembly process and the rate of disassembly (the backward reaction) is dependent on the rate constant (K_{off}) of dissociation of MTs to tubulin. This process continues until equilibrium is reached, a stage at which the association and dissociation rates for tubulin polymerization process tend to be equal. The rate of polymerization equals that of depolymerization under this condition and the rate of change in the growth rate of the polymer is zero, also referred to as the steady-state condition. This reaction can be observed in a spectrophotometer (ideally at 37 ^{o}C) containing all the reaction components (tubulin and microtubule-inducer) as a turbidity profile represented as a change in O.D at 350 nm against increments of time (Gaskin *et al*. 1974). This profile is ideally a sigmoidal curve that shows saturation at equilibrium time points at which stage steady-state conditions are reached. Under this circumstance, the concentration of tubulin required to achieve steady-state is known as the critical concentration (Cc) of tubulin, which is a ratio of K_{off} over K_{on}. This parameter speaks about the MT polymer formation or inducing ability of test agent since Cc is inversely related to the affinity (K) of the monomer for microtubule polymer (Correia and Lobert 2001). Hence, the lower the Cc of tubulin required for MT polymer formation, the higher is the affinity of the monomers for polymers under a given set of reaction condition. In the case of a MT-promoting agent, this would translate to the ability of the test agent to promote tubulin assembly and hence to the potency of the agent as a MT stabilizer. The Cc can be quantified and related to the energetics of the assembly mechanism under known reaction conditions using a simple equation

for Gibb's free energy: $\delta G = -RT\ln K$. The lower the Cc for assembly, the higher is the affinity and the lower is the free energy for polymer formation or stabilization (Kasai 1969). The Cc is one of the parameters that provides information on the both the kinetic and thermodynamics processes underlying the tubulin assembly mechanism.

The tubulin polymerization process is known to be influenced by temperature - the free energetics for MT assembly process are lower with rises in temperatures (Inoue and Sato 1967). An Arrhenius plot of 1/T versus lnK illustrates the temperature-dependency of a ligand-induced assembly process. The slopes and intercepts yield enthalpy and entropy parameters that can be used to explain the thermodynamics of the MT assembly mechanism. At lower temperatures, the nucleating ability of tubulin subunits to form MT polymer is low in the presence of GTP. Hence, at 0-20 ^{o}C GTP does not induce assembly. Increasing the temperature to 37 ^{o}C drives the polymer forming reaction forward, thus suggesting that MT assembly process is energy-dependent. However, in the presence of an inducer like paclitaxel, or a more potent compound like discodermolide, the nucleation process is more spontaneous and the assembly process occurs at much lower temperatures (10-20 ^{o}C for paclitaxel, 0 ^{o}C for discodermolide). The ability of a MT-inducing agent to nucleate assembly at lower temperatures is referred to as 'hypernucleation' and this parameter reflects on the binding energetics, and hence potency, of a test agent to induce MT-polymer formation. Literature reports suggest that paclitaxel-induced microtubule polymer formation is an enthalpy-driven, exothermic process (Edler *et al*. 2005).

Binding kinetics and energetics provide good information on building protein-ligand models. Parameters like Cc, binding constants (K_D and K values) and inhibition constants (K_i values) are enough to assess a ligand-induced MT assembly mechanism both *in vitro* and *in vivo*. Studies done here using isolated tubulin were aimed at understanding the microtubule assembly

process under different sets of reaction conditions, and emphasized the qualitative and quantitative aspects of the MT polymerization dynamics. Others have investigated the energetics of tubulin polymerization dynamics in the presence of MT stabilizers and/or destabilizers. The studies done here made an attempt towards rationalizing the experimental observations for structure-activity and pharmacological evaluations on MT perturbing libraries on the basis of binding energetics. Biochemical experiments done supported the *in silico* observations and the data generated could be of valid use in understanding structure-activity relationships for future drug design studies.

1.3. Microtubule-targeting agents

Mitotic poisons that target MTs are known to either stabilize MTs by inducing polymerization of tubulin or destabilize MTs by triggering depolymerization events (Hamel 1996). Based on the mechanism by which they block assembly or disassembly, MT-targeting agents have been broadly classified as 1) MT-stabilizing (polymerizing) agents, e.g., paclitaxel, or 2) MT-destabilizing (depolymerizing) agents, e.g., vinca alkaloids and colchicine. Furthermore, MT binding domains have been categorized based on the site of binding to tubulin or tubulin polymer: the taxoid site (T), the vinca domain (V), and the colchicinoid site (C). The studies done here were focused on MT-stabilizing agents and hence the discussion in the following pages will be limited to MT stabilizers.

1.3.1. Paclitaxel

Structure, discovery of the mechanism of action and location of paclitaxel binding site on tubulin polymer

In the early 1960's the National Cancer Institute organized a collection of plants from the U.S. for evaluation as potential sources of anticancer drugs (Horwitz 2004; Cragg and Newman

2004). The Pacific yew (*Taxus brevifolia*) was collected and the extract from this tree was confirmed to be active against 9KB cancer cells in culture and in animal carcinoma test systems. By 1971, a crystalline derivative of a compound, originally called taxol but later renamed to paclitaxel was examined by X-ray crystallography and the structure of this interesting agent was determined (Figure 3) (Wani *et al*. 1971). By 1978, the efficacy of paclitaxel against tumors was first reported. Upon exposure to this compound, there was an increase in the mitotic index of P388 cells and an inhibition of human HeLa and mouse fibroblast cells (0.25 μM) in the G2 and M phases of the cell cycle (Schiff *et al*. 1979). Tubulin polymerization experiments identified paclitaxel to be a promoter of MT assembly. This compound caused a concentration-dependent increase in turbidity, decreased the lag time for assembly independent of tubulin concentration, and decreased the Cc of tubulin required for assembly. Paclitaxel-induced MTs were found to be resistant to depolymerization in the presence of 4 mM $CaCl_2$. The MTs it causes are shorter in length and more in number in than those induced by GTP. Eva Nogales and Kenneth Downing first resolved the 3D structure of tubulin in complex with paclitaxel by high resolution cryoelectron microscopy (electron crystallography) analysis of tubulin-paclitaxel assembled as a monolayer on zinc sheets (Nogales *et al*. 1995; Nogales *et al*. 1998). These studies revealed that paclitaxel binds to the amino-terminal region of β-tubulin near the interprotofilament contacts and that there is one paclitaxel site per tubulin heterodimer. This data was supported by biochemical experiments where photoaffinity labeled paclitaxel derivatives bound to residues in this region of the protein - Gly368, Thr274, Val23, His227 and Asp224 (Rao *et al*. 1995).

Considering that paclitaxel is a natural product available in very limited amounts and the fact that it is one of the very few drugs to show high success in the clinic for the treatment of

various tumors of malignant phenotype, many efforts have been put forth for devising semisynthetic strategies and synthetic variants of paclitaxel (Miller and Ojima 2001). However,

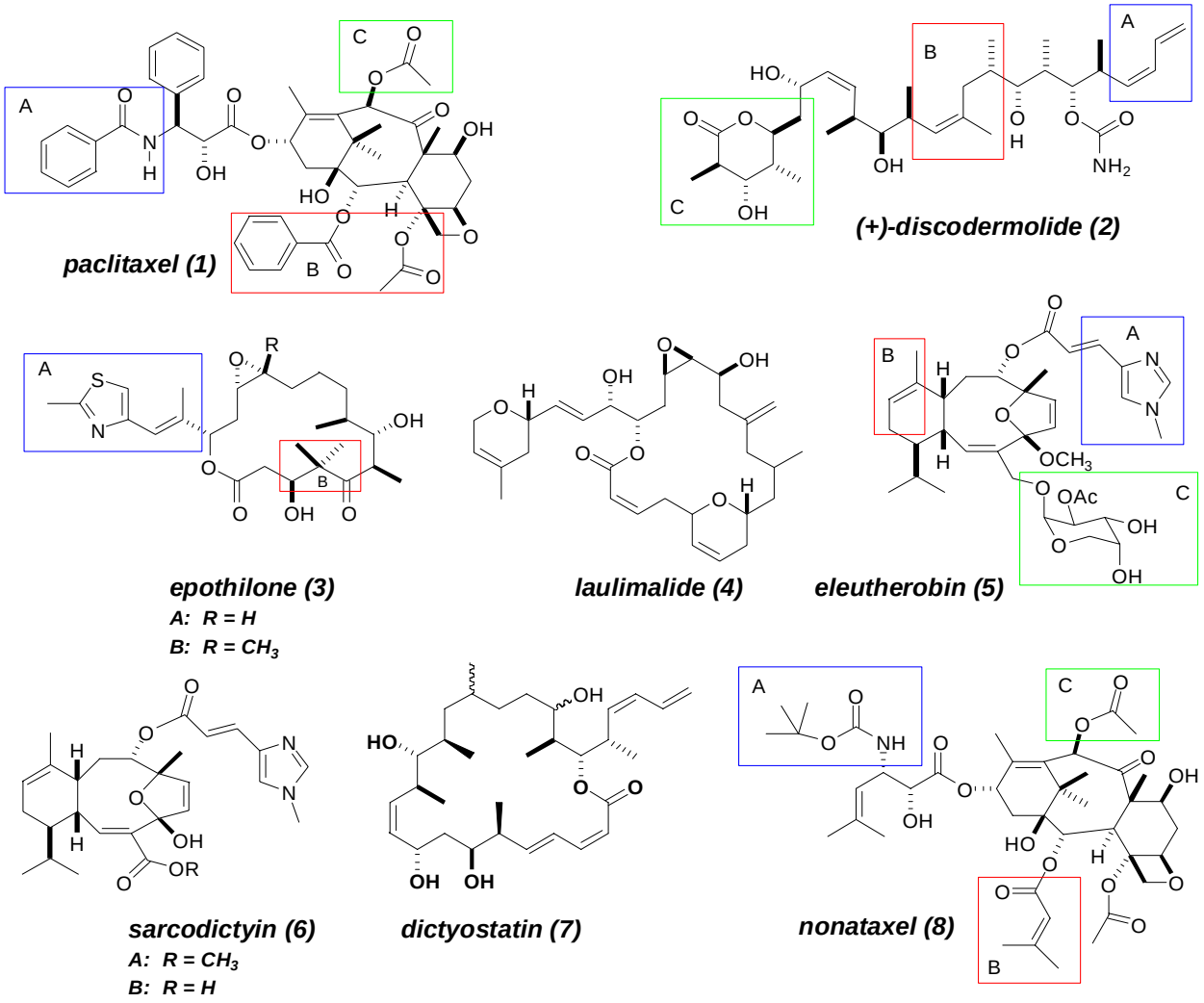

Figure 3. Structures of microtubule-stabilizing agents

Ojima's pharmacophore model is depicted. Domains A, B, and C in paclitaxel, the epothilones, discodermolide, and the eleutherobin have identical pharmacophore groups.

(Adapted from: Ojima *et al*. 1999)

because of undesirable effects, poor solubility and drug resistance associated with paclitaxel and its analogues, there is continuing hope for the discovery of paclitaxel-like MT-targeting agents that can have equivalent or superior anticancer properties without having any of the undesirable effects. One of the well known structural analogues of paclitaxel, docetaxel (Taxotere®), received FDA approval and is showing great promise in the clinic (Guenard *et al*. 1993). Structurally, docetaxel differs from paclitaxel in that it has a C-3'-^{t}butyloxy carbonyl group (instead of a C-3'-benzamido group) and a free hydroxyl group at C-7 (instead of an acetate group). Quite a few novel and potent chemical entities from natural products have shown interesting biological activities and have outpaced the taxane group of compounds. The post-taxane era of natural product-derived MT-stabilizing agents includes discodermolide (Gunasekera *et al*. 1990; ter Haar *et al*. 1996a; ter Haar *et al*. 1996b), the epothilones (Gerth *et al*. 1996; Bollag *et al*. 1995; Kowlaski *et al*. 1997; Altmann, K-H *et al*. 2000a; Altmann, K-H *et al*. 2000b), laulimalide (Quinoa *et al*. 1988; Corley *et al*. 1988; Mooberry *et al*. 1999), the eleutherobins (Lindel *et al*. 1997; Long *et al*. 1998), the sarcodictyins (D'Ambrosio *et al*. 1987; Ciomei *et al*. 1997), peloruside A (West *et al*. 2000; Hood *et al*. 2002) and, most recently, dictyostatin (Shin *et al*. 2002, Isbrucker *et al*. 2003). The structures of some these agents are represented in Figure 3. Following the discovery of these many structurally different molecules, all having MT-stabilizing actions, efforts were made towards establishing a common pharmacophore model for MT stabilizers.

Ojima *et al*. (1999) derived a common pharmacophore model using NMR, X-ray crystallography and molecular modeling studies. Using nonataxel as the model, the regions of possible overlap were identified for a set of MT stabilizers known to bind to the taxoid site on tubulin polymer. Figure 3 represents the regions of common overlap for some of the

microtubule-stabilizing agents. The binding interactions suggested for paclitaxel show that the side chains as well as the baccatin core of the molecule are involved in the interactions with the β-subunit of the tubulin. Very recently, however, electron crystallography, NMR and molecular modeling studies done with epothilone A (epoA) bound to α,β-tubulin suggest a far different pharmacophore model (Nettles *et al*. 2004). The major differences between the paclitaxel and epoA binding models, shown in Figure 4, will be briefly discussed in the following section:

Paclitaxel binds to the β-tubulin subunit of tubulin polymer primarily through hydrophobic interactions with complementary residues on the M-loop, helices H7 and H10, and β-strand B9. The important pharmacophoric groups are the C-3'-benzamido phenyl, the C-3'-phenyl and the C-2-benzoyl phenyl that are involved in hydrophobic interactions with segments of helices H6 and H7 (Snyder *et al*. 2001). The complementary residues interacting with the C-2-benzoyl phenyl include Leu-217, Leu-219, a CH_2 of Asp-226 and His-229 on and adjacent to helix H7. The consequence of His-229 positioned in between the C-2 and C-13 paclitaxel side chains affords a "T"-form for paclitaxel in the binding model. The C-3'-phenyl group is in close contact with the β-sheet strands B8 and B10. The C-3'-benzamido phenyl binds to the N-terminal amino acids on helix H1, critical residues being the isopropyl group of Val-23, methylene groups of Lys-19, Glu-22 and Asp26. The C-4-acetate is tethered above the hydrophobic pocket encompassing helix H7, the M-loop and the B9-B10 loop. The C-8-methyl is oriented towards Thr-276 and Gln-281 of the M-loop, the O-21 interacts with Thr-276 and the C-12 methyl lies in close contact with Leu-371 on the B9-B10 loop. Epothilone A conformational analyses suggested a different pharmacophore model as compared to the one for paclitaxel, even though these two molecules share a common binding site (Nettles *et al*. 2004). This binding model supports the existing antiproliferative activity data for mutated ovarian carcinoma cell lines in

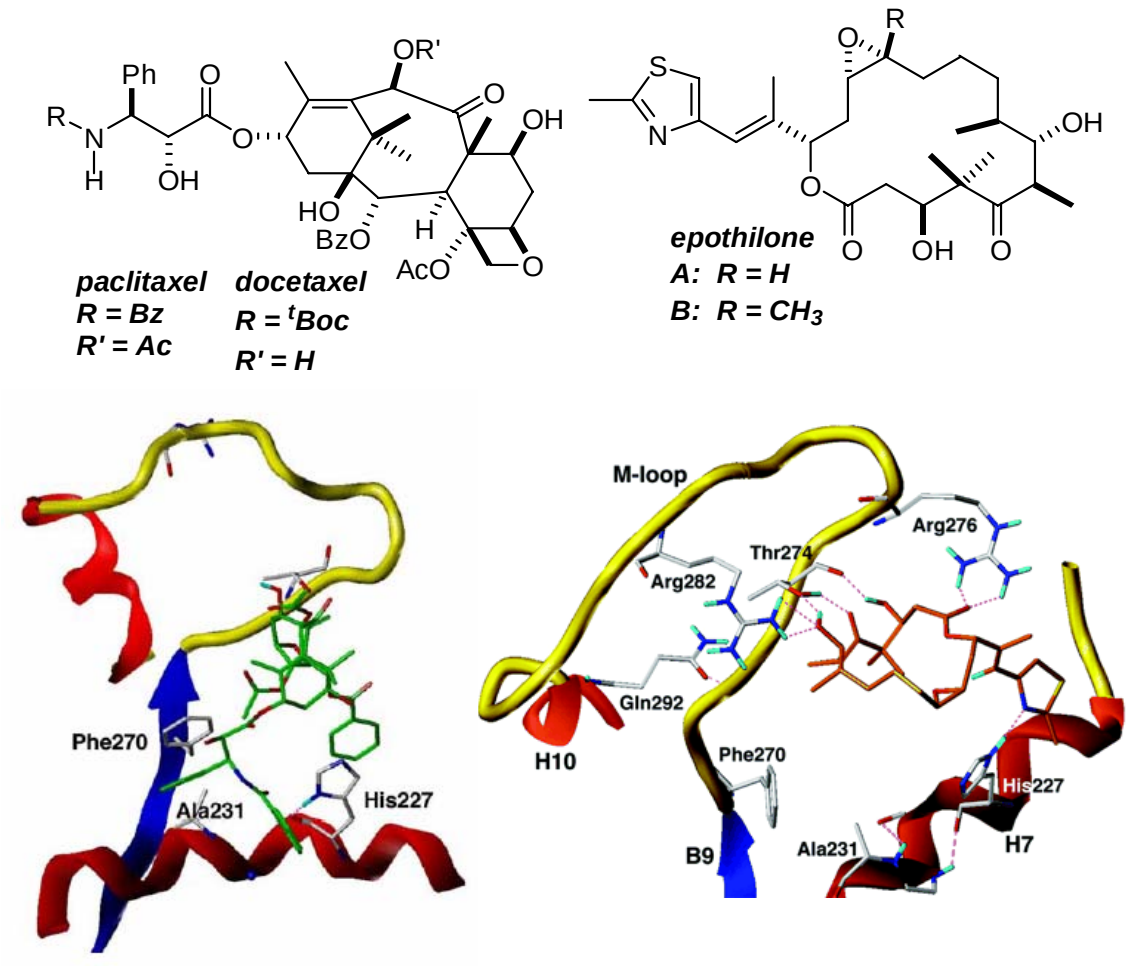

Figure 4. Representation of binding models for paclitaxel and epothilone A

The upper half of the figure has structures of paclitaxel, docetaxel, epothilone A, and epothilone B. The lower half of the figures represents the two different binding models for microtubule-stabilizing agents bound at the taxoid site of tubulin polymer. The model on the left represents paclitaxel binding model and the one on the right epothilone A binding model.

(Adapted from: Nettles *et al*. 2004)

the presence of paclitaxel and epoA. The 1A9PTX10 cell line, which has Phe270 mutated to Val270, is resistant to paclitaxel but is quite sensitive to epoA. The predicted model is supported by biochemical data and suggests that the macrocycle of epoA is drawn more toward the M-loop and is away from Phe270 that lies in the hydrophobic cavity comprised of strand B9. Hence, the mutation of Phe270→Val270 did not influence the biological activity of epoA. The polar functional groups spanning C1-C7 of epoA are involved in hydrogen bonding interactions with M-loop residues mainly, Thr274, Arg278 and Arg282. Cells expressing the β-tubulin mutation of Ala364 on B10 loop are resistant to paclitaxel (1A9PTX22 cells); however, this cell line retained sensitivity towards epoA. This re-emphasizes the fact that the epoA macrocycle and the hydrophilic functional groups are away from B10 and are not involved in any interaction with residues of loop B10. The thiazole ring of epoA, analogous to the C-2-benzoyl group of paclitaxel, tethers to His227. These two new pharmacophore models stand as valuable references for drug design of taxoid site binding agents. Noteworthy from these studies is the fact that these agents have a common taxoid binding site on β-subunit of tubulin polymer, but share minimum overlapping binding interactions within this region. Modeling studies might give clues to the synergistic or additive effects of paclitaxel-mimetics on MT polymerization dynamics.

1.3.2. Discodermolide

Structure, discovery of the mechanism of action and conformational & pharmacophore studies

The MT-stabilizing agent (+)-discodermolide is a sponge-derived polyketide natural product obtained from the Caribbean sponge *Discodermia dissoluta*, originally shown to possess immunosuppressive action and antiproliferative activity in various cell lines (Gunasekera *et al*.

1990). The MT-stabilizing action of discodermolide (structure shown in Figure 3) was discovered when in silico studies for quantitative structure-activity relationship evaluations on tubulin polymerization perturbing agents were done with a goal to search for new potent antimitotic agents (ter Haar *et al*. 1996a). Computational studies utilizing the algorithms CASE and MultiCASE revealed that the substructural moieties statistically most responsible for activity (biophores) identified for discodermolide were isosteric with those observed for steganacin, a known colchicine-site binding agent and an inhibitor of MT polymer formation. These biophores were shared with paclitaxel. Discodermolide was thus predicted to have tubulin binding activity and it was of interest then to observe for the effect of discodermolide on tubulin dynamics. Studies *in vitro* using isolated bovine brain tubulin preparation show discodermolide, like paclitaxel, to have a potent MT-stabilizing action (ter Haar *et al*. 1996b). It was also observed that discodermolide is superior to paclitaxel in that it hypernucleates tubulin assembly to form MTs and stabilizes the polymer against cold-induced disassembly much more potently than paclitaxel, competes with paclitaxel for binding to tubulin polymer and inhibits the growth of paclitaxel-resistant cancer cell lines (Kowalsky *et al*. 1997). Furthermore, *in vivo* growth inhibition, cell and nuclear morphological, electrophoretic and flow cytometric analyses on human breast carcinoma cells show it to have potent growth inhibitory (low nM range), cell cycle perturbing (G2/M block) and apoptosis-inducing activities similar to or even greater than that observed for paclitaxel (Balachandran *et al*. 1998). Moreover, considering that the clinical use of paclitaxel has been limited because of undesirable effects, poor solubility, and drug resistance, one would anticipate discodermolide to be a promising and novel chemotherapeutic agent against different kinds of cancers. This compound was one of the candidates taken into phase II clinical trials in the Novartis R&D pipeline. Pre-clinical and Phase I clinical trials on

healthy volunteers showed it to be very effective with less toxicity than paclitaxel symptoms. This molecule was going through Phase II clinical until recently but, unfortunately, recent reports from Novartis indicate termination of clinical trials with discodermolide owing to toxicity issues met with this compound upon dose escalation done on a group of patients recruited for a Phase II clinical trial (Novartis 2005).

Discodermolide is a polyhydroxylated, polymethylated, C24:4 fatty acid lactone carbamate. Its structure consists of a linear polypropionate backbone with 13 stereogenic centers, three (*Z*)-olefenic bonds at C8-C9, C13-C14, and C21-C22, a tetrasubstituted δ-lactone (C1-C5), a carbamate (C19) and a terminal *cis*-diene (C21-C24). X-Ray crystallographic studies suggested that the molecule adopts a corkscrew shape (Gunasekera *et al*. 1990; Ballone *et al*. 1999). NMR analysis of this compound in acetonitrile showed that the molecule assumes a helical form and this observation is in congruence with the designated solid state conformation (Smith *et al*. 2001). The conformation of discodermolide appears to be a curved, tilde ('~') shape in which an elongated hydrophobic core is surrounded by polar groups projecting outward. The center part of the molecule adopts a U-turn shape to minimize *syn*-pentane interactions by the methyl groups in the main chain and to avoid A-1,2 strain by the vinyl groups projecting from the methyl-bearing stereocenters (Jimenez-Barbero *et al*. 2002). Different conformations were found by NMR analysis of discodermolide dissolved in DMSO-d_6, with the X-ray structure contributing only 1% of the total number of conformers (Monteagudo *et al*. 2001). The major conformers included corkscrew, sickle and awl types. Modeling studies attempted to identify a common pharmacophore at the taxol/β-tubulin site for paclitaxel and discodermolide have proposed a low energy discodermolide conformation with a protein-ligand hydrogen-bonding pattern similar to that observed for paclitaxel (Ojima *et al*. 1999). Molecular dynamic

calculations and conformational analysis suggest the C-11 and C-19 fragment of discodermolide is in superposition with the hydrophobic surface (C2 side chain) of nonataxel. It was also observed that C-20 to C-24 diene of discodermolide could be overlaid on the C3'-*N*-^{t}Boc group of nonataxel. The dataset here represented a collection of several thousand conformations/energy manifolds that are possible for discodermolide, implying/indicating conformational mobility and a high degree of flexibility possessed in this molecule; however, avoidance of A-2,3 and A-1,2 interaction strain was not taken into account. Regardless, the biological activity made this molecule attractive for synthesis and SAR studies. Understanding the SAR of discodermolide on a structural basis will provide important clues for building protein-ligand models and for discerning the optimum binding conformation for discodermolide.

1.3.3. Dictyostatin

Structure and mechanism of action

Dictyostatin is a marine natural product derived from *Lithisda* species belonging to *Corallistidae* family. Pettit *et al*. were the first to isolate and attempt structural assignment for this molecule (Pettit *et al*. 1994). Structurally, dictyostatin resembles discodermolide and this molecule was hypothesized to be similar in biological activity to that of discodermolide (Shin *et al*. 2002). A discussion on the accurate assignment of structure and the potential of dictyostatin as a microtubule-stabilizing agent is given in Chapter 4 (and for now I prefer holding it to maintain a good level of suspense).

Investigations done towards the dissertation project were aimed at understanding the biochemistry, pharmacology, and structure-activity relationship aspects of novel synthetic microtubule-stabilizing agents. The objectives of the dissertation studies were the following:

1. Pharmacological and structure-activity relationship studies of synthetic discodermolide analogues

2. Biochemical, pharmacological, and structure-activity relationship evaluation of dictyostatin, a structural congener of discodermolide.

3. Kinetic and thermodynamic evaluation of discodermolide, dictyostatin, and their synthetic analogues binding to microtubule polymer.

2. MATERIALS AND EXPERIMENTAL PROCEDURES

2.1. Materials

Discodermolide analogues, dictyostatin and dictyostatin analogues were synthesized as described (Shin *et al*. 2002; Shin *et al*. 2004; Shin *et al*. 2005; Shin *et al*. (unpublished); Minguez *et al*. 2003; Choy *et al*. 2003). Paclitaxel and [^{3}H]paclitaxel (specific activity 16.2 Ci/mmol) were provided by the Drug Synthesis and Chemistry Branch, National Cancer Institute. (+)-Discodermolide and [5-^{3}H]discodermolide (14.4 Ci/mmol) were generous gifts from Novartis Pharmaceuticals Corp., and epothilone B and [^{14}C]epothilone B (111 mCi/mmol) from Novartis Pharma AG. Docetaxel was obtained from the pharmacy at the University of Pittsburgh Cancer Institute. GTP was obtained from Sigma and purified by triethylammonium bicarbonate gradient chromatography on DEAE-Sephacel. DideoxyGTP (ddGTP) was obtained from US Biochemicals. Purified tubulin and heat-treated MAPs were prepared as described previously (Hamel and Lin 1984). Bovine brain tubulin free from unbound nucleotide was prepared as reported earlier (Grover and Hamel 1994). Ca^{2+}- and Mg^{2+}-free RPMI-1640 culture medium were from GIBCO/BRL-Life Technologies. Fetal bovine serum (FBS) was from Hyclone. Human carcinoma cell lines (1A9, 2008, PC3, MDA-MB-231 and T47D) were all available by previous acquisitions in the Day laboratory. Parental human ovarian carcinoma 1A9 and the β-tubulin mutant subclone 1A9PTX10 and 1A9PTX22 cell lines were generous gifts from Drs. Tito Fojo and Paraskevi Giannakakou at the National Cancer Institute. Since cytotoxics are used in the clinic primarily to treat hormone-resistant and hormone-refractory cancers of malignant phenotype, cell culture experiments were done utilizing cell lines that are mostly hormone-

resistant. A brief description of each cell line is as follows: 1A9 is a subclone derived from A2780 ovarian carcinoma cell line. 1A9PTX10 is the mutant form of 1A9 ovarian carcinoma cell line that has Phe270 mutated on β-tubulin to Val270. 1A9PTX22 is also derived from 1A9 parental ovarian carcinoma cell line that has Ala364 mutated to Thr. 2008 is a human ovarian carcinoma cell line, PC3 is an androgen-independent prostate cancer cell line, MDA-MB-231 is an estrogen receptor alpha-independent breast cell line, and T47D is a breast carcinoma cell line. Mouse anti-α-tubulin was from LabVision. Rabbit anti-phosphohistone H3 was from Upstate Cell Signaling, and fluorophore donkey anti-rabbit and -mouse antibodies were from Jackson Immunoresearch. Flutax-2 was from Invitrogen. All other chemicals were obtained from either Sigma or Fisher Scientific and used as received.

2.2. Experimental procedures

A. Paclitaxel site inhibition assay: The abilities of test agents to displace radiolabeled paclitaxel from tubulin polymer were determined with a procedure described previously (Hamel *et al*., 1999). [^{3}H]Paclitaxel solutions were prepared in 0.75 M monosodium glutamate (MSG). Test agents (4 μM final concentration), prepared in 25% (v/v) DMSO-0.75 M MSG, were mixed with radiolabeled agents and warmed to 37 ^{o}C. A reaction mixture (50 μL) containing 0.75 M MSG, 4.0 μM tubulin and 40 μM ddGTP was prepared and incubated at 37 ^{o}C for 30 min to preform MTs. Drug mixtures with the radiolabeled tracer were added to preformed polymer and incubated for 30 min at 37 ^{o}C. Bound tracer was separated from free tracer by centrifugation of the reaction mixtures at 14,000 rpm using a Beckman Coulter AllegraTM 64R centrifuge for 20 min at room temperature. Radioactive counts from the supernatant (50 μL) were determined by scintillation spectrometry (LS6500-Beckman Coulter multi-purpose scintillation counter). Bound

tracer was calculated by subtracting the amount of tracer found in the supernatant from the amount of total tracer added to each reaction mixture. Percent inhibition values were determined with respect to controls.

B. Saturation binding kinetics of [^{3}H]paclitaxel on tubulin polymer: The saturation binding kinetics of paclitaxel were established before evaluating the kinetics in the presence of test agents. Pre-warmed [^{3}H]paclitaxel solutions in the concentration range studied (0.025-2 μM) were added to and incubated at 37 ^{o}C for 30 min with 4.0 μM tubulin polymer preformed in 0.75 M MSG containing 40 μM dideoxyGTP. Unbound [^{3}H]paclitaxel was determined by scintillation spectrometry after centrifugation as described above, and bound [^{3}H]paclitaxel values were calculated. Nonspecific binding of [^{3}H]paclitaxel in the presence of docetaxel (12 μM) was determined. Specific binding of [^{3}H]paclitaxel in nmol/mg was determined from the difference between total and nonspecific binding values. Saturation binding kinetic parameters, K_D and B_{max}, were then determined using PRISM software version 4.0 (GraphPad Software, Inc., San Diego, CA, USA) based on the best-fit model fitting strategy.

C. Inhibition kinetics of discodermolide and dictyostatin: The inhibition kinetics of dictyostatin at the taxoid site on tubulin polymer were determined as follows. An equal volume of the test agent, in the concentration range studied, was mixed with a [^{3}H]paclitaxel solution (varied concentrations) and the resulting solution was warmed to 37 ^{o}C. Test agent mixtures were added to preformed polymer containing a mixture of 0.75 M MSG, 4.0 μM tubulin and 40 μM dideoxyGTP, and incubated for 30 min at 37 ^{o}C. Radioactivity in the supernatant, obtained by centrifugation at 14000 rpm for 20 min, was determined by scintillation spectrometry. Nonspecific binding and specific binding of [^{3}H]paclitaxel in the presence of inhibitors were determined as described above. The percent inhibition values were calculated. Kinetic analyses

of the data were performed using PRISM software version 4.0 (GraphPad Software, Inc., San Diego, CA, USA) for the determination of the inhibition pattern(s) and inhibition constants (Ki values) for discodermolide and dictyostatin.

D. Purity check of [^{3}H]paclitaxel by HPLC-radiometry: Radiochemical purity of [^{3}H]paclitaxel was determined by high pressure liquid chromatography (HPLC) connected to a radiochemical detector. HPLC conditions were as follows. A phenyl column (Alltech® Alltima, 5 μ, 4.6 mm x 250 mm) was used for separation under gradient conditions. Mobile phases consisted of solvents A and B run under gradient conditions. Solvent A composed of $CH_3OH/CH_3CN/H_2O$ in the ratio 4:3:13 and solvent B composed of $CH_3OH/CH_3CN/H_2O$ in the ratio 4:11:5. Gradient conditions included 30 min 100% A, 31-40 min 100% B, 41-45 min 100% A. The flow rate was 1 mLl/min. The injection volume was 50 μL, the run time was 45 min, and the retention time was 20 min. The UV wavelength used for single mode detection was 227 nm and a Radiomatic tandem radiochemical detector was used.

E. Cell culture experiments: Test agent-induced growth inhibition of human carcinoma cell lines (1A9, 1A9PTX10, 1A9PTX22, MDA-MB231, T47D, PC3 and 2008) were evaluated following the antiproliferative assay protocol as described earlier (Lazo *et al*. 2001). Cells were maintained in RPMI medium with 10% FBS. The maintenance medium of 1A9PTX10 and 1A9PTX22 cells also contained 17 nM paclitaxel and 10 μM verapamil. Maintenance medium for T47D carcinoma cell lines was DMEM. Prior (48-72 h) to experimentation, resistant cells were transferred to verapamil- and paclitaxel-free RPMI containing 10% FBS. Cells were seeded into 96-well plates, allowed to attach and grow for 48 h, then treated with either vehicle (DMSO; N=8) or a range of concentrations of test agent (each concentration in quadruplicate) for 72 h. Cell number was determined spectrophotometrically at 490 nm minus absorbance at 630

nm after exposure to 3-(4,5-dimethylthiazol-2-yl)-5-(3-carboxymethoxyphenyl)-2-(4-sulfophenyl)-2*H*-tetrazolium and *N*-methylphenazine methylsulfate (MTS) at both the time zero of the experiment as well as at the 72 h time point. The fifty percent growth inhibitory concentrations (GI_{50}) of test agents were calculated from the spectrophotometrically determined expansion of the control cells over the 72 h period.

F. Tubulin polymerization assay: Tubulin assembly was monitored turbidimetrically at 350 nm in temperature-controlled, multichannel Gilford 250 spectrophotometers as described previously (ter Haar *et al*. 1996b). Reaction mixtures without test compounds consisted of tubulin (1 mg/ml), heat-treated microtubule-associated proteins (MAPs; 0.75 mg/ml, if present), GTP (100 μM, if present), and 0.1 M (4-morpholino)ethanesulfonate (Mes), pH 6.9. Baselines were established after addition of all reaction components (except the test agents) to the cuvettes held at 0 ^{o}C. Test agents, predissolved in DMSO, were then added to give the indicated final concentrations (and a constant DMSO concentration of 4% v/v). Each reaction mixture (0.25 mL final volume) was then subjected to the temperature changes indicated in the text and figures. The positive controls were either paclitaxel (typically 10 μM) or GTP. The negative control was 4% v/v DMSO. Tubulin polymerization assays done in the Beckman-Coulter DU7400 spectrophotometers had the same protocol as described above except that the MSG, pH 6.6, was used in place of Mes, and the reaction mixtures contained no heat-treated MAPs nor GTP.

G. Electron microscopy: Samples for electron microscopic analyses were aliquots taken directly from cuvettes during the turbidimetry determinations. Each aliquot was placed on a 200-mesh, carbon-coated formvar-treated copper grid and stained with 1% (w/v) uranyl acetate (ter Haar *et al*. 1996b). Excess staining solution was removed by wicking with torn Whatman filter paper and the grid was allowed to dry while protected from dust at room temperature. Grids were

examined in a JEM 1210 TEM 120 kV electron microscope. The images obtained were examined visually for polymer morphology. MT lengths in the digital images were measured using Metamorph® version 6.1r2, Universal Imaging Corp.) image analysis software.

H. Critical concentration experiments: The critical tubulin concentrations for 10 μM test agent to induce polymerization at 37 ^{o}C were determined with a centrifugation-based procedure described previously (Dabydeen *et al*. 2004). Briefly, reaction mixtures (0.1 ml) containing varying concentrations of tubulin in 0.1 M Mes, pH 6.9, 4% DMSO and test agents as appropriate were prepared and incubated for 30 min at 37 °C. The reaction mixtures were centrifuged for 15 min at 14,000 rpm at room temperature (20-22 °C). A metered aliquot was removed from the supernatant and its protein concentration determined by the Lowry method. Data were analyzed using PRISM software version 4.0 (GraphPad Software, Inc., San Diego, CA, USA).

I. Lowry assay: The procedure was based on the Lowry protocol reported in the literature (Lowry *et al*. 1951). A 1 L, 2x Lowry solution A was prepared by adding 40 g of Na_2CO_3, 8 g of NaOH and 0.4 g Na/K tartrate. Lowry solution B consisted of 0.5% w/v (i.e., 5 g/L) $CuSO_4.5H_2O$. Within 1 h of beginning the assay, Lowry solution C was prepared by mixing the 2x solution A with H_2O and solution B in a 25:25:1 v/v/v ratio. One ml of solution C was added to each sample (all samples, blanks and standards had the same volume, whether 25, 50 or 100 μl). All samples were vortexed. Fifty μl of the Folin-phenol reagent was added to each sample and the samples vortexed again. The samples were incubated for at least 1 h until the reaction reached equilibrium (i.e., a stable blue color). The absorbances of samples at 650 nm were determined with a Beckman coulter DU640 spectrophotometer.

J. Pelleting assay (for determination of EC_{50}): The EC_{50} value is defined as the concentration of test agent required to polymerize 50% of the tubulin compared to amount of tubulin polymer found in the pellet of the DMSO control incubation, and was determined with a procedure reported earlier (Gapud *et al*. 2004). The reaction condition included 0.2 M MSG, 10 μM tubulin, 5% v/v DMSO and varying concentrations of test agents. The reaction mixtures were incubated at room temperature for 15 min, centrifuged for 10 min at 14,000 rpm, and protein concentration determined by the Lowry method. On average, 5.5 ± 4.0 % of the tubulin pelleted in the DMSO control.

K. Multiparameter fluorescence microscopy: High information content cell-based fluorescence screening was carried out under previously detailed conditions (Minguez *et al*. 2002). Human cervical epithelial HeLa (for Henrietta Lacks, from whom they were derived in 1951) carcinoma cells were used for this experiment. HeLa cells growing at log phase were trypsinized and plated in 40 μL at a density of 7,000-8,000 cells per well in calf skin collagen I-coated 384well plates (Falcon #3962; Fisher Scientific). Cells were exposed to test agents or 0.5% DMSO within 2-8 h of plating. Concentrated DMSO stock solutions of all test agents were diluted into solutions of HBSS medium plus 10% FBS and added to the microplate wells (10 μL per well), using an automated liquid handling system (Biomek® 2000; Beckman-Coulter, Inc.) to provide a serial 2-fold dilution of each test agent. The cells were incubated in the presence of test agents for 24 h. At the end of the incubation, the medium was removed and replaced with HBSS containing 4% formaldehyde and 10 μg/mL Hoechst 33342 (25 μL/well) to fix the cells and fluorescently label their chromatin, respectively. After incubation at room temperature for 20-30 min, the solution was removed from each well and replaced with HBSS (100 μL/well). Further reagent additions were made to the microplates using the Biomek 2000. After removing the HBSS from each well,

cells were permeabilized for 5 min at room temperature with 0.5% w/w Triton X-100 in HBSS (10 μL/well). This step extracts a fraction of the soluble cellular components, including soluble tubulin. The wells were washed with HBSS (100 μL/well), followed by addition of a primary antibody solution containing mouse anti-α-tubulin (at a 1:3000 dilution) and rabbit anti-phosphohistone H3 (at a 1:500 dilution) in HBSS (10 μL/well). After 1 h at room temperature, the wells were washed with HBSS as above, followed by the addition of a secondary antibody solution containing fluorescein-5-isothiocyanate (FITC)-labeled donkey anti-mouse (at a 1:300 dilution) and Cy3-labeled donkey anti-rabbit (at a 1:300 dilution) antibodies diluted in HBSS (10 μL/well). After 1 h at room temperature, the wells were washed as above, and HBSS was added (100 μL/well). The plates were placed in an ArrayScanII® HCS Reader with the Target Activation BioApplication Software coupled to Cellomics® Store and the vHCS™ Discovery Toolbox (Cellomics, Inc.) to analyze images. Briefly, the instrument was used to scan multiple optical fields, each with multiparameter fluorescence, within a subset of the wells of the 384-well microplate. The BioApplication software produced multiple numerical feature values, such as subcellular object intensities, shapes, and location for each cell within an optical field. Data were acquired from a minimum of 1,000 cells per well, except in cases where added test agents reduced the attachment of cells to the substrate. A nuclear mask was generated from Hoechst 33342-stained nuclei, and object identification thresholds and shape parameters were set such that the algorithm identified over 90% of the nuclei in each field. Objects that touched each other or the edge of the image were excluded from the analysis. Tubulin mass was defined as the average green (FITC) pixel intensity in an area defined by the Hoechst-defined nuclear mask. This cytoplasmic area around the nucleus contains cytoskeletal components and has been shown to be a region from which sensitive measurements of cytoplasmic characteristics can be made

(Giuliano and Taylor 1994). The percentage of phospho-histone H3 positive cells was defined as the number of cells whose average red (Cy3) staining intensity exceeded the average Cy3 intensity plus two standard deviations of vehicle-treated cells, divided by the total number of cells. Data were analyzed using PRISM software version 4.0 (GraphPad Software, Inc., San Diego, CA USA).

L. Flutax-2 binding experiments: Glutaraldehyde-fixed microtubules and a fluorescent analogue of paclitaxel (Flutax-2) were used to determine the binding kinetics and thermodynamics of test agent-tubulin interactions using methods recently described (Andreu and Barasoain 2001; Diaz *et al*. 2003). A fluorescent-labeled paclitaxel derivative called Oregon Green® 488 paclitaxel conjugate (commonly referred to as Flutax-2) was obtained from Invitrogen. The fluorescent label on this probe was obtained by derivatizing the 7β-hydroxy group of paclitaxel with difluorocarboxyfluorescein group (Figure 34 in the Appendix).

Flutax-2 binding experiments were done to obtain binding kinetic as well as thermodynamic parameters and are based on fluorescence anisotropy technique. The set of experiments involved were preparation of gluraldehyde-fixed microtubules, determination of concentration and number of binding sites, and determination of inhibition constants by fluorescence competitor assay. Each one of these experiments will be discussed below. Flutax-2 experiments with no inhibitor provide information on the concentration and number of binding sites, stoichiometry of binding sites, equilibrium binding constants and thermodynamic parameters.

Preparation of cross-linked microtubules: Microtubules were cross-linked with glutaraldehyde following the experimental procedure described previously (Andreu and Barasoain 2001). Bovine brain tubulin was dialyzed against a buffer consisting of 10 mM sodium phosphate, 1 mM EGTA, 0.1 mM GTP, and 3.5 M glycerol pH 6.8 for about 2 h after

which $MgCl_2$ (6 mM) and GTP (1 mM) were added to the solution. This is glycerol-induced assembly buffer (GAB, pH 6.5). The solution consisting of tubulin (50 μM) was assembled into microtubules at 37 ^oC for 30 min. The assembled microtubules were cross-linked with 20 mM glutaraldehyde at 37 ^oC for 10 min and the reaction quenched with 60 mM $NaBH_4$. The morphology of the cross-linked microtubules was verified by EM. The cross-linked microtubules were dialyzed against the desired buffer (which was GAB-0.1 mM GDP buffer) for 2 h in the cold and stored at 4 ^oC with 0.05% sodium azide. The total tubulin concentration was determined by Lowry method.

Determination of the concentration of taxoid binding sites: The concentration of taxoid binding sites was determined following the procedure described earlier (Andreu and Barasoain 2001). Flutax-2 concentration was determined after diluting the sample in 50 mM dipotassium phosphate buffer pH 9.0 at an extinction coefficient of 80, 000 M^{-1} cm^{-1} at 494 nm. The assay was done in a 96-well plate. Increasing concentrations of cross-linked microtubules (0.004-12.5 μM) were added to 25 nM Flutax-2 in the GAB-GDP buffer, pH 6.5 in the presence and absence of 10 μM docetaxel. The plate was scanned using a fluorescence plate reader with polarizer filters installed in it. Each well was scanned in λ_{exc} 495 and λ_{ems} 520 range using fluorescein filter and a dichroic mirror as the beam splitter that operates at 520 nm (Figure 34 in the Appendix). Fluorescence anisotropy was determined from the raw parallel and perpendicular fluorescence intensity data. The concentration of bound Flutax-2 (F_b) was determined using the following equation:

$$[F]_b = [F]_o[(r-r_{min})/(r_{max}-r_{min})]$$

where, 'r' is the observed anisotropy value, r_{min} is the minimum anisotropy observed for Flutax-2 only sample containing no protein, and r_{max} is the maximum anisotropy obtained for Flutax-2 in

the presence of highest concentration of cross-linked microtubules. The experimental r_{min} and r_{max} values were in the range of 0.05-0.08 and 0.25-0.28. The concentration of free binding sites was determined from the difference between total concentration of microtubules and bound concentration of Flutax-2, the equation for which is:

$$[S] = [S]_o - [F]_b$$

where, [S] is the concentration of free binding sites determined from total concentration of microtubule binding sites $[S]_o$ and bound concentration of Flutax-2 $[F]_b$.

The equilibrium binding constant (K_b) from the free concentration of microtubule binding sites versus anisotropy data was determined from the following equation. Iterations were done using WINNONLIN version 3.0 from which the best-fit values for r_{min} and r_{max} were determined.

$$r = r_{min} + (r_{max}-r_{min})K_b[S]/(1 + K [S])$$

Determination of the number of taxoid binding sites for Flutax-2: The number of taxoid binding sites was determined by adding increasing concentrations of Flutax-2 to 50 nM or 100 nM of cross-linked microtubules in the presence and absence of 10 μM docetaxel. The samples were rotary shaken for 5 min and incubated at 37 ^oC for 20 min at different temperature conditions (room temperature and 37 ^oC). GAB-GDP, pH 6.5 buffer was used. The bound and free Flutax-2 concentrations were determined, as described above, from which the number of binding sites (n) were determined using appropriate equations.

$$[F]_b/[S]_o = [F]_o (r - r_{min})/[S]_o (r_{max} - r_{min})$$

$$[F] = [F]_o - [F]_b$$

$$[F]_b/[T]_o = nK_bF/(1 + K_b[F])$$

Iterations were done using WINNONLIN version 3.0 from which the best-fit values for n and K_b were determined.

Competitive fluorescence assay for microtubule-stabilizing agents: A solution of 50 nM Flutax-2 and 50 nM cross-linked microtubules were prepared in GAB-GDP buffer, pH 6.5. The assay was performed in a 384-well plate and the total volume was 40 μL. The competitors were added in increasing concentrations into each well (concentration range: 1 nM-1 μM), final DMSO concentration was 2% v/v. The samples were rotary shaken for 5 min and incubated for 20 min at the desired temperatures (room temperature and 37 ^{o}C). Measurements were taken in a microplate reader twice within 30-90 min after equilibration. The λ_{exc} is 480 nm and λ_{emi} is 520 nm. A sample consisting of 50 nM paclitaxel binding sites was the blank and another sample of 50 nM Flutax-2 solution in GAB-0.1 mM GTP was the anisotropy standard. Measurements of anisotropy of Flutax-2 in the presence of docetaxel (excess, 1 μM or 10 μM) and also in the absence of competitors were required for data analysis. Inhibition constants were to be calculated for competition experiments. This set of experiments is in progress.

Data analyses: Data were analyzed using either WINNONLIN version 3.0 or PRISM software version 4.0 (GraphPad Software, Inc., San Diego, CA USA). Equilibrium binding constants and thermodynamic parameters were calculated from fluorescence anisotropy data.

3. DISCODERMOLIDES - BIOLOGICAL AND SAR EVALUATIONS

3.1. Introduction and literature cited

The yield of discodermolide from its natural source is very low (0.002%); hence intensive efforts were put in place to devise efficient strategies to synthesize this complex molecule in high yields. Several total and partial syntheses of discodermolide have been developed based on convergent retrosynthetic approaches, but all these require not less than thirty steps from commercially available starting materials to the final product (Curran *et al*. 2002; Day *et al*. 2002; Francavilla *et al*. 2003; Harried *et al*. 2003; Hung *et al*. 1996a; Marshall *et al*. 1998; Mickel *et al*. 2004a, Mickel *et al*. 2004b, Mickel *et al*. 2004c; Mickel *et al*. 2004d; Mickel *et al*. 2004e; Paterson *et al*. 2000; Paterson *et al*. 2001; Smith *et al*. 1999). Consequently, few analogues have been reported and SAR data on discodermolide is not complete. Hence, one goal over the past decade has been to make simpler analogues of discodermolide in fewer synthetic steps than necessary for the natural product. Moreover, clinical trials of discodermolide were put on hold, presumably because of previously unseen toxicity (Novartis 2005). Hence, efforts made towards the synthesis of potent analogues of discodermolide could give rise to new lead molecules for drug development.

The initial structural variants of discodermolide were prepared by Schreiber's group and tested for biological activity (Hung *et al*. 1996a and Hung *et al*. 1996b). These are stereoisomers prepared from the epimeric side products obtained in the synthesis of discodermolide. The biological activities of these isomers show that the 16-normethyldiscodermolide is as active as discodermolide in cytotoxicity assays. The configuration at C16 and C17 positions is very

important for the activity of the parent molecule. The analogue with *R*-configuration at C16 had an IC_{50} of about 300 nM and the one with *S*-configuration at C17 was totally inactive.

Truncated versions of discodermolide, fragments including the C1-C15 or C8-C24 regions of the parent molecule, were also made and tested. These two compounds lacked biological activity, implying that the full length of discodermolide is necessary. The authors also studied the importance for activity of the four hydroxyl functionalities of discodermolide by examining acylated analogues. 17-Acetyldiscodermolide had a reasonably good antiproliferative IC_{50} value (70 nM), though it is less potent than discodermolide (6 nM). The descarbamoyl analogue, C19-acetyldiscodermolide, was inactive. Modification of the terminal diene through replacement with a pivaloyl group led to an analogue with activity less than that observed for discodermolide. The α- and β-thiophenyl anomers at C1 of the lactol form of the lactone ring of discodermolide retained activity equivalent to that of the parent molecule. Finally, removal of the C16 methyl group and extending the C16 carbon yielded an analogue with no activity, indicating that modifications at the C16 position of the C16-normethyldiscodermolide would not lead to analogues possessing good biological activity.

Longley and co-workers reported that effects of semisynthetic acetyl analogues of discodermolide on microtubule function (Gunasekera *et al*. 2001; Isbrucker *et al*. 2001) by selective acetylation of the hydroxyl groups at C3, C7, C11, and/or C17 of discodermolide. The resultant mono-, di-, tri-, and tetra-acetates of discodermolide were studied for biological potency in *in vitro* cytotoxicity assays. The IC_{50} values of these analogues towards A459 cells were quite interesting; while C3- and/or C7-acetylated versions showed biological activities greater than/or equivalent to discodermolide, acetylation of the C11 (discodermolide 3, 11-diacetate and discodermolide-3,7,11-triacetate) and C17 (3,7,11,17-tetraacetate, discodermolide-

3,7,17-triacetate, discodermolide-3,17-diacetate) hydroxyl groups caused a decrease in the biological potency. The effect was more drastic with C17 substitution than that observed with C11 substitution. These studies are in agreement with that reported by Schreiber's group where reduced activity of the C17-substituted compounds was observed. Moreover, the C3- and/or C7-acetylated versions, like the parent molecule, blocked the cell cycle at the G2/M phase and the proliferation of A459 cell line (at 100 nM). The remaining analogues had no effect on cell cycle distribution at this concentration. Further studies of these analogues on microtubule morphology revealed that at 100 nM the C3- and/C7-acetylated compounds induce microtubule bundling comparable to discodermolide. Discodermolide-7-acetate and discodermolide-3,7-diacetate caused more pronounced microtubule bundling than did discodermolide itself when all were studied at 10 or 100 nM. The other analogues were less active. Temperature-controlled tubulin polymerization experiments also show similar trends in that the C3- and/or C7- acetylated analogues of discodermolide, at 10 μM with 1 mg/mL purified bovine brain tubulin, induced assembly of tubulin at low temperatures (at and above 6^{o}C, for discodermolide it is $>4^{o}$C) and that the assembled tubulin was quite resistant to cold-induced disassembly (discodemolide-stabilized polymer is not affected by changes in temperature). The remaining analogues were all inactive. These SAR studies on the acetylated derivatives of discodermolide provide conclusive evidence that the C11 and C17 hydroxyl groups are important for the cytotoxic action of the parent molecule and that the hydroxyl groups at C3 and C7 are amenable to modifications.

Smith's group reported that syntheses of C14-normethyl (i.e., the C8-C9 *cis*-disubstituted olefin) and C7-deoxygenated analogues were feasible during the course of total synthesis of the parent molecule (Smith *et al*. 1999; Martello *et al*. 2001. Of all the analogues, the C3-dehydro and C3-dehydro/C7-deoxy analogues are approximately 2-fold more and 3-fold less cytotoxic

than discodermolide. This suggests extreme sensitivity to structural changes at C1-C14 portion of the parent molecule. The α,β-unsaturated lactone containing ring analogue analogue was found to be more or less as active as discodermolide. This indicates that the lactone ring is a flexible moiety in terms of modifications it can withstand and still provide analogues with potent biological activity. The C14-normethyl and C7-deoxy analogues were less active than discodermolide and its α,β-unsaturated lactone containing ring analogue. The nucleating ability of all the analogues differed significantly from that of the parent molecule. The cytotoxic action of these compounds was studied in A549 and SKOV3 cells. Discodermolide and its α,β-unsaturated lactone analogue had similar growth inhibitory IC_{50} values in A549 cells, and discodermolide was shown to be less cytotoxic. This indicates that the methyl group at C14 and the hydroxyl group at C7 are important for the activity of the parent molecule. These analogues were approximately 2- and 3-fold less cytotoxic than discodermolide. Flow cytometry and immunofluorescence analyses using A549 cells also showed these analogues caused G2/M block and microtubule bundling, though each compound showed these effects at different concentrations. The geometry at C14-C15 is important for activity. This group reported that C14-*cis*-C14-normethyl discodermolide is only 2-fold less cytotoxic than discodermolide, while its C14 *trans*-C14-normethyl geometric isomer is far less biologically active. The SAR studies by this group also suggest that at least one of the hydroxyl groups at C3 or C7 is required for discodermolide-like activity.

3.2. Simplified discodermolide analogues - design and synthesis

Based on the structure-activity studies reported in the literature for discodermolide, it was hypothesized that the left and the right portions of the molecule (lactone, carbamate and the

diene) are amenable for structural manipulation to make synthetically easier and simpler discodermolide analogues that would retain biological activity. Hence, the goal of this study was to establish structure-activity relationship (SAR) for discodermolide by evaluating simpler analogues of discodermolide for microtubule-targeting activities.

Hypothesis I: Simplified analogues of discodermolide would retain the biological activity of and have microtubule-targeting (binding, stabilizing, and antiproliferative) activities similar to the parent molecule.

Rationale: Literature reports suggest that discodermolide binds to paclitaxel site on tubulin polymer (ter Haar *et al*. 1996b; Kowalski *et al*. 1997). Discodermolide was known to bind with high affinity at the taxoid site and is known to competitively inhibit Paclitaxel from binding to microtubules. Studies performed to understand mechanisms of synergism also suggest minimum overlapping binding sites for discodermolide and paclitaxel (Martello *et al*. 2000). Discodermolide analogues were evaluated for their ability to inhibit paclitaxel from binding to tubulin polymer in comparison to the parent molecule discodermolide. Understanding the SAR of discodermolide on a structural basis provides important clues for establishing protein-ligand models and for discerning the optimum binding conformation for the molecule. Hence, paclitaxel binding experiments were set up to look at the binding properties of the analogues. The potent antiproliferative activity of discodermolide is primarily attributed to its ability to hypernucleate tubulin assembly and to stabilize assembled microtubule thereby causing cell cycle arrest (ter Haar *et al*. 1996b). Therefore, along with the binding experiments, analogues were examined for microtubule stabilization and antiproliferative activities.

The first library of discodermolide analogues was synthesized by Drs. Jose Minguez and Sun-Young Kim in the laboratories of Prof. Dennis Curran at the University of Pittsburgh

Department of Chemistry. The modifications introduced in the design of the analogues are represented in Figure 5 (Minguez *et al*. 2003).

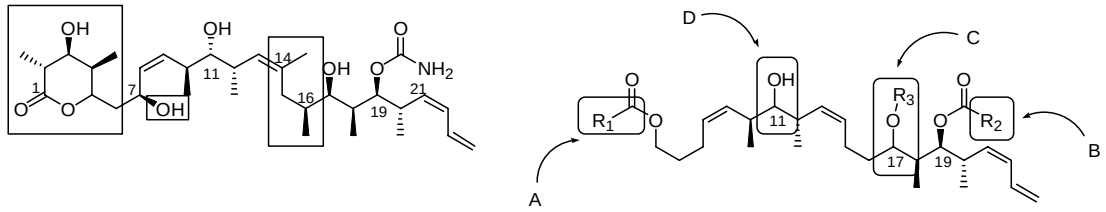

Figure 5. Configuration of discodermolide and domains of variation for SAR studies

Domain A. Replacement of the lactone with simple esters. Domain B. Replacements of the carbamate on C19 with an acetoxy group. Domain C. Inversion of the configuration at C17 and derivatizing the hydroxyl group at this carbon keeping the hydroxyl group at C19 free.

Domain D. Inversion of the configuration at C11. Note: The analogues also differed from the natural product, apart from removal of the lactone, in that the methyl groups at C14 and C16 as well as C7 hydroxyl group were omitted.

The strategy of convergent retrosynthetic plan of fragment coupling by Wittig-olefinations was utilized to build the library of diverse set of analogues for extensive SAR analysis. Details of the experimental procedures and schemes for the synthesis of the first library of discodermolide analogues can be found in Minguez *et al*. 2003. A simpler scheme adopted for the synthesis of the first set of discodermolide analogues is shown in Scheme 1. Retrosynthetically, the polypropionate backbone was divided into three fragments disconnecting at the C8-C9 and C13-C14 double bonds: a THP-protected phosphonium salt as the 'left display', a diene phosphonium salt as the 'right display', and an aldehyde as the central scaffold. The latter two fragments

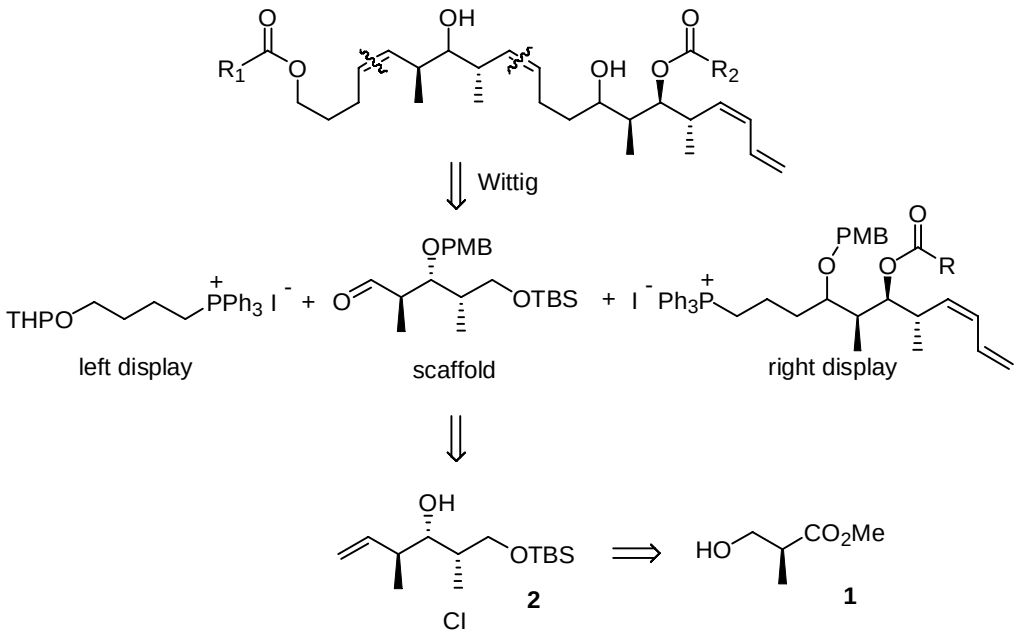

Scheme 1. Retrosynthetic strategy adopted for the synthesis of the first library analogues

have a common stereochemical triad that can be retrosynthetically reduced to a common intermediate, the homoallylic alcohol **2**, the starting material for which was the commercially available hydroxy ester, methyl (*S*)-(+)-3-hydroxy-2-methylpropionate **1**. The first library consisted of the following discodermolide analogues:

1) 11*S*, 17*R*, 19*S*-carbamoyloxy analogues

2) 11*S*,17*R*,19*S*-acetoxy analogues

3) 11*S*,17*R*-carbamoyloxy and 11*S*,17*R*-acetoxy analogues

4) 11*R*,17*R*-carbamoyloxy and 11*R*,17*R*-acetoxy analogues

5) 11*S*,17*S*,19*S*-carbamoyloxy analogues

3.2.1. Biological evaluation of discodermolide analogues

The first library of discodermolide analogues were evaluated for their ability to inhibit tritiated paclitaxel ([^{3}H]paclitaxel) from binding to tubulin polymer.

Experimental procedures:

Paclitaxel site inhibition assay: The abilities of test agents to displace radiolabeled paclitaxel from binding to tubulin polymer were determined following the procedure described in the Chapter 2. Monosodium glutamate at pH 6.6 was used in this experiment since tubulin and microtubule polymer were known to be stable in this vehicle. The critical concentration to polymerize tubulin to form microtubules was previously reported to be lower in the presence of ddGTP, a dideoxy analogue of GTP, than GTP itself. Hence, ddGTP was used to assemble tubulin to microtubule polymer at 37 ^{o}C. Radioactive counts from the supernatant (50 μL) were determined by scintillation spectrometry. Bound tracer was calculated from the amount of total tracer added to each reaction mixture minus the amount of tracer found in the supernatant. Percent inhibition values were determined with respect to controls.

Microtubule stabilization assay: Tubulin polymerization assays were done in Beckman-Coulter DU7400 spectrophotometers as described in the Chapter 2. The percent microtubule stabilization was calculated for each analogue with respect to the turbidity readings obtained for positive (in the presence of 10 μM paclitaxel) and negative controls (in the presence of DMSO).

Antiproliferative assay: Three different human carcinoma cell lines were used to determine the antiproliferative potency of these compounds. MDA-MB-231 is an estrogen receptor alpha negative breast cancer cell line, PC3 is an androgen-independent prostate cancer cell line, and 2008 is an ovarian cancer cell line. The protocol as described in Chapter 2 used the mitochondria-catalyzed formation of a water-soluble MTS formazan that was

spectrophotometrically detected at 490, minus non-specific absorbance at 650 nm, to estimate cell number.

3.2.2. 11*S*, 17*R*, 19*S*-carbamoyloxy discodermolide analogues

This set of analogues was modified on the left portion of the molecule. The lactone moiety was replaced with simple to bulkier esters. The biological activity data for these analogues is summarized in Table 1. Analogue JMM452, having a bulkier tertiary butanoyl ester replacing the lactone ring, was the most active of all these analogues in all the biological assays. Antiproliferative assays showed that all the analogues (except for one) had GI_{50} values in the low micromolar range (1-8 μM). JMM452 showed antiproliferative activity in low micromolar range (1-15 μM) in all the three cell lines. Analogues having either a phenyl (JMM450), a methyl (JMM451), a hydroxyl methyl (JMM496) or a heteroaryl (JMM490 and JMM499) functionality substituted for the lactone ring of discodermolide were less active than JMM452. JMM496 was the least active of all the analogues in cell-based assay. The GI_{50}s were in the range of 25-50 μM in the three cell lines studied. The esterified analogues, although less effective than discodermolide, inhibited [^{3}H]paclitaxel from binding to tubulin polymer when present in 2-fold molar excess over that of paclitaxel. JMM452 at 4 μM inhibited [^{3}H]paclitaxel binding to microtubule polymer to an extent of about 32%. However, the analogues showed lower GI_{50} and % [^{3}H]paclitaxel inhibition values when compared with either discodermolide or paclitaxel All these analogues showed some ability, although weak, to cause polymer assembly of isolated bovine brain tubulin (Minguez *et al*. 2003). These two studies suggest that these analogues bound at a site coincident with or overlapping that of paclitaxel.

Table 1. Biological activity data for 11*S*, 17*R*, 19*S*-carbamoyloxy analogues

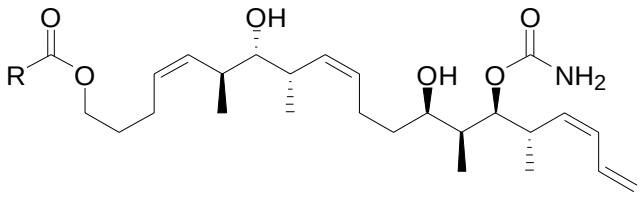

Analogue	**%MT Assembly**	**Antiproliferative activity GI_{50}(μM); N=4**			**%Paclitaxel Inhibition N=6**
		MDA-MB-231	**PC-3**	**2008**	
JMM450 R=Ph	13	7.2±0.4	11±1	7.7±0.5	19±3
JMM451 R=Me	5	12±1	6.6±0.3	5.8±0.7	19±4
JMM452 R=^{t}Bu	14	2.6±0.9	3.0±0.8	1.5±1.0	32±6
JMM490 R=2-Methylthiophene	10	8.0±0.3	15±2	7.1±0.6	23±9
JMM496 R=CH_2OH	<5	41±2	>50	24±2	23±1
JMM499 R=2-Methylfuran	21	7.5±0.1	14±1	6.4±0.6	18±1
Discodermolide	>100	0.016±0.003	0.067±0.004	0.072±0.005	64±2
Paclitaxel	100	0.0024±0.0016	0.015±0.002	0.0092±0.0016	37±1

3.2.3. 11*S*, 17*R*, 19*S*-acetoxy discodermolide analogues

This set of analogues had an acetoxy group at C19 in place of the carbamate moiety of discodermolide, and as in the previous set of analogues, the lactone moiety was substituted with simple esters. The ability of the acetoxy analogues to inhibit [^{3}H]paclitaxel from binding to

tubulin polymer, to induce microtubule stabilization and to inhibit carcinoma cell lines from proliferating are represented in Table 2. At 4 μM, these analogues showed some inhibition of radioligand binding to polymer to an extent almost similar to the previous set of analogues. However, the assembly-inducing properties and antiproliferative activities of the acetoxy analogues were decreased to a considerable extent, indicating that the carbamate moiety at C19 is important for the activity of the parent molecule. The GI_{50} values were in mid-μM range for all the analogues except the tertiary butanoyl derivative that had GI_{50} values in low-mid μM range. The analogues had lower biological activity compared to either discodermolide or paclitaxel.

Table 2. Biological activity data for 11*S*, 17*R*, 19*S*-acetoxy analogues

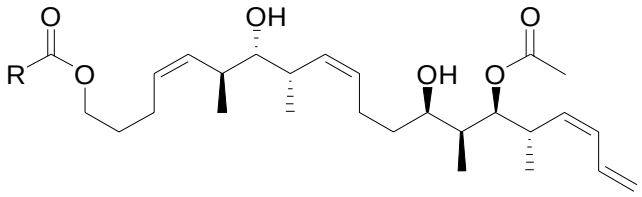

Analogue	**%MT Assembly**	**Antiproliferative activity - GI_{50}(μM); N=4**			**%Paclitaxel Inhibition N=6**
		MDA-MB-231	**PC-3**	**2008**	
JMM460 R=Me	18	22±2	25±4	15±1	19±2
JMM461 R=Ph	9	20±2	21±2	20±2	17±1
JMM462 R=^{t}Bu	8	6.8±1.9	14±1.0	14±2	24±2
Discodermolide	>100	0.016±0.003	0.067±0.004	0.072±0.005	64±2
Paclitaxel	100	0.0024±0.0016	0.015±0.002	0.0092±0.0016	37±1

3.2.4. 11*S*, 17*S*, 19*S*-carbamoyloxy analogues

The stereochemistry at C17 in this set of analogues was inverted from *R* to *S* and the lactone ring substituted with simple esters. The biological evaluation data is represented in Table 3. The data suggests that inversion of the configuration at C17 decreased biological activity to a considerable extent (Minguez *et al*. 2003). The percent inhibition values from the binding assay and percent microtubule assembly from the polymerization assay were lower than the previously described analogues. The GI_{50} values against the three carcinoma cell lines were in mid-μM range for all the analogues except for the hydroxymethyl derivative that yielded GI_{50}s > 50 μM.

Table 3. Biological activity data for 11*S*, 17*S*, 19*S*-carbamoyloxy analogues

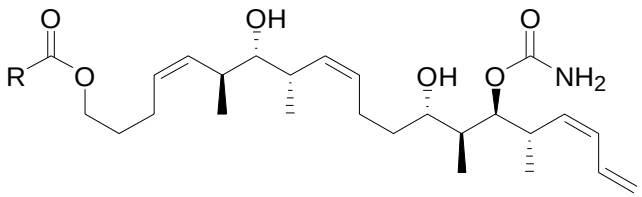

Analogue	**%MT Assembly**	**Antiproliferative activity - GI_{50}(μM); N=4**			**%Paclitaxel Inhibition N=6**
		MDA-MB-231	**PC-3**	**2008**	
JMM503 R=^{t}Bu	7	24±1	23±2	27±1	17±1
JMM504 R=Ph	179	20±2	23±2	21±3	11±2
JMM506 R=CH_2OH	15	>50	>50	>50	18±0
JMM508 R=2-Methylfuran	20	19±0	23±1	20±7	20±4
Discodermolide	>100	0.016±0.003	0.067±0.004	0.072±0.005	64±2
Paclitaxel	100	0.0024±0.0016	0.015±0.002	0.0092±0.0016	37±1

3.2.5. 11*S*, 17*R*-carbamoyloxy or 11*S*,17*R*-acetoxy analogues

These analogues had the carbamoyl or the acetoxy groups positioned at C17 instead of at C19 and the lactone ring of the parent molecule replaced with simple esters. The biological activity data is presented in Table 4. Data from the paclitaxel binding assay showed this set of analogues to have moderate inhibition properties. The analogues, except for JMM416 and JMM417, showed considerable microtubule-stabilizing activities as well (Minguez *et al*. 2003). Also, there was decreased antiproliferative activity with these analogues, but the structural manipulations done were not as detrimental as was the inversion of configuration at C17. The GI_{50} values for most of these analogues were in low to mid μM range. The analogues had lower antiproliferative and [^{3}H]paclitaxel inhibition activities than either paclitaxel or discodermolide. The methylester analogue had GI_{50}s greater than 50 μM in all the cell lines studied.

3.2.6. 11*R*,17*R*-carbamoyloxy and 11*R*,17*R*-acetoxy analogues

The next set of analogues had both the configuration of the C11 changed from *S* to *R* and also the carbamate or the acetoxy groups switched to the C17 position, along with the lactone ring replaced with simple esters. The paclitaxel site binding activity data for this set of analogues yielded moderate results (Table 5). Inversion of configuration at C11 proved highly detrimental for the biological activity of these analogues, with none showing microtubule-stabilizing properties (microtubule assembly < 5%) and very few of them having even very weak antiproliferative activities (Minguez *et al*. 2003). The GI_{50}s were higher (ranging from 20->50 μM) for this set of analogues than in the remainder of this library when compared with either discodermolide or paclitaxel.

Table 4. Biological activity data for 11*S*,17*R*-carbamoyloxy or 11*S*,17*R*-acetoxy analogues

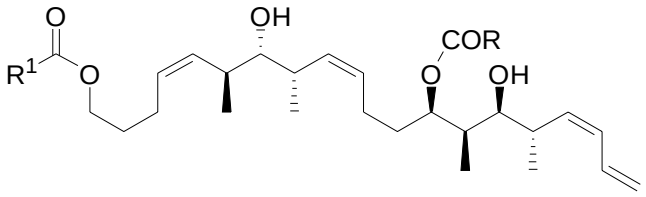

Analogue	%MT Assembly	Antiproliferative activity - GI_{50}(μM); N=4 MDA-MB-231	PC-3	2008	%Paclitaxel Inhibition N=6
JMM365 R=NH_2, R1=^{t}Bu	12	11±2	20±3	2.7±3.5	15±3
JMM416 R=NH_2, R1=Ph	13	15±0	15±1	21±2	12±5
JMM417 R=NH_2, R1=Me	18	>50	>50	>50	10±4
JMM369 R=Me, R1=^{t}Bu	10	20±4	20±3	5.8±2.2	21±3
JMM370 R=Me, R1=Ph	<5	25±6	>50	3±0.9	16±2
Discodermolide	>100	0.016±0.003	0.067±0.004	0.072±0.005	64±2
Paclitaxel	100	0.0024±0.0016	0.015±0.002	0.0092±0.0016	37±1

3.2.7. Discussion of the first library of discodermolide analogues

From the SAR studies of the first set of discodermolide analogues, it can be concluded that left display (lactone) of discodermolide can be simplified or modified without much loss of activity. The tertiary butanoyl ester analogue retained biological activity to a considerable extent suggesting that the lactone ring of discodermolide can be substituted with bulkier groups with retention of microtubule-targeting activities. However, the lactone seems to play a significant

Table 5. Biological activity data for 11*R*,17*R*-carbamoyloxy or 11*R*,17*R*-acetoxy analogues

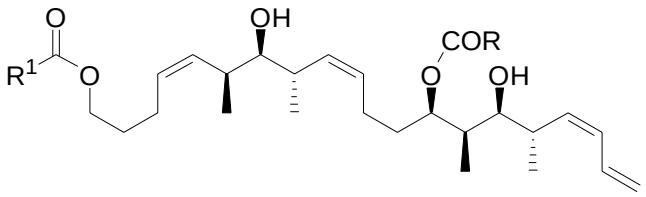

Analogue	**%MT Assembly**	**Antiproliferative activity - GI_{50}(µM); N=4**			**%Paclitaxel Inhibition N=6**
		MDA-MB-231	**PC-3**	**2008**	
SKY1 R=NH_2, R1=Me	<5	>50	>50	>50	21±2
SKY2 R=NH_2, R1=^{i}Pr	<5	>50	>50	31±4	19±2
SKY3 R=NH_2, R1=^{t}Bu	<5	22±2	33±1	33±1	17±1
SKY4 R=NH_2, R1=Ph	<5	25±6	20±1	26±4	18±1
SKY5 R=NH_2, R1=CH_2OMe	<5	>50	>50	>50	18±1
SKY-A1 R=Me, R1=Me	<5	>50	>50	>50	15±1
SKY-A2 R=Me, R1=^{i}Pr	<5	12±5	>50	>50	17±2
SKY-A3 R=Me, R1=^{t}Bu	<5	23±1	43±11	41±5	17±2
SKY-A4 R=Me, R1=Ph	<5	7±3	26±6	29±2	20±5
SKY-A5 R=Me, R1=CH_2OMe	<5	>50	>50	>50	16±2
Discodermolide	>100	0.016±0.003	0.067±0.004	0.072±0.005	64±2
Paclitaxel	100	0.0024±0.002	0.015±0.002	0.0092±0.002	37±1

role in the biological potency of the parent molecule. Stereochemistry at C11(*S*), C17(*R*), and C19(*S*) and the carbamate moiety at position C19 are important for activity. Switching the carbamate group to C17 or introducing an acetoxy group at C19 led to loss of microtubule binding activity but proved not to be as detrimental as was modifying the configuration at any of these two positions. These data correlate with the antiproliferative assay data wherein GI_{50} values greater than 20 μM were obtained for these analogues.

3.3. 4-*epi*-7-Dehydroxy-14,16-didemethyl-(+)-discodermolide

NMR analysis of discodermolide in acetonitrile showed that the molecule assumed a helical conformation and this observation was in congruence with the designated X-ray crystal structure (Smith *et al*. 2001; Ballone *et al*. 1999). Conformational analysis suggested that the major conformer seemed to assume a curved tilde (~) shape in which an elongated hydrophobic core was surrounded by polar groups projecting outward. The center part of the molecule adopted the U-turn shape to minimize *syn*-pentane interactions by the methyl groups in the main chain and to avoid A-1,2 strain by the vinyl groups projecting outward from the methyl-bearing stereocenters. It was assumed that the 3'-OH group of the lactone ring might be interacting with the nitrogen of the carbamate group via hydrogen-bonding interactions. The resulting hypothesis then explored by the Day and Curran laboratories was that analogues having an extended spacer that reduced the distance between the functional groups involved in hydrogen bonding interactions, thus stabilizing the overall conformation of the molecule, would be more potent or retain activity similar to the parent molecule. The solution conformational properties obtained for discodermolide was the basis for designing novel conformational analogues along the lines of rational drug design. Structural variants of left and right displays of discodermolide were synthesized and evaluated for further SAR analysis (Choy *et al*. 2003). Modifications that were

done included the introduction of a C4-*epi*-lactone on the left display, alterations on the right display, truncation of the C19 analogues, wholesale replacement of the diene on the right display and substitution of the C3-OH group with a methoxymethyl (MOM) protecting group for incorporating an extended H-bond acceptor. The analogues were synthesized by Drs. Nakyen Choy, Phu Qui Nguyen and Youseung Shin in the Curran laboratory, following a retrosynthetic methodology represented in Scheme 2 (Choy *et al*. 2003).

3.3.1. Biological evaluation of 4-*epi*-discodermolide analogues

This class includes 7-dehydroxy-14,16-didemethyl-(+)-discodermolides, C19-truncated analogues, diene-containing analogues with the C4-*epi*-lactone, C1 and C3 substituted analogues, and analogues with wholesale replacement of the diene.

The first set of analogues in this library consisted of compounds that had the C19-diene truncated and the configuration at C4 of the lactone modified with or without installment of a C3 MOM-protecting group. The biological activity data obtained with these analogues is presented in Table 6. Evaluation of the C19-truncated analogues (NC164, NC165, NC142 and NC112) showed that these compounds were all much less active than discodermolide in their ability to inhibit paclitaxel from binding to tubulin polymer (< 10%), to induce microtubule stabilization (<10%) and to exhibit antiproliferative action against human carcinoma cell lines (> 50 μM). Similar results were observed for the two C4 epimers. All the C4-*epi* analogues with C19 truncated dienes had similar, weak biological activities. The antiproliferative and % [^{3}H]paclitaxel inhibition values were lower than those observed for discodermolide and/or paclitaxel. This data underlines the significance of the diene group of discodermolides for microtubule-stabilizing activities. Hence, the next set of analogues was prepared with the diene

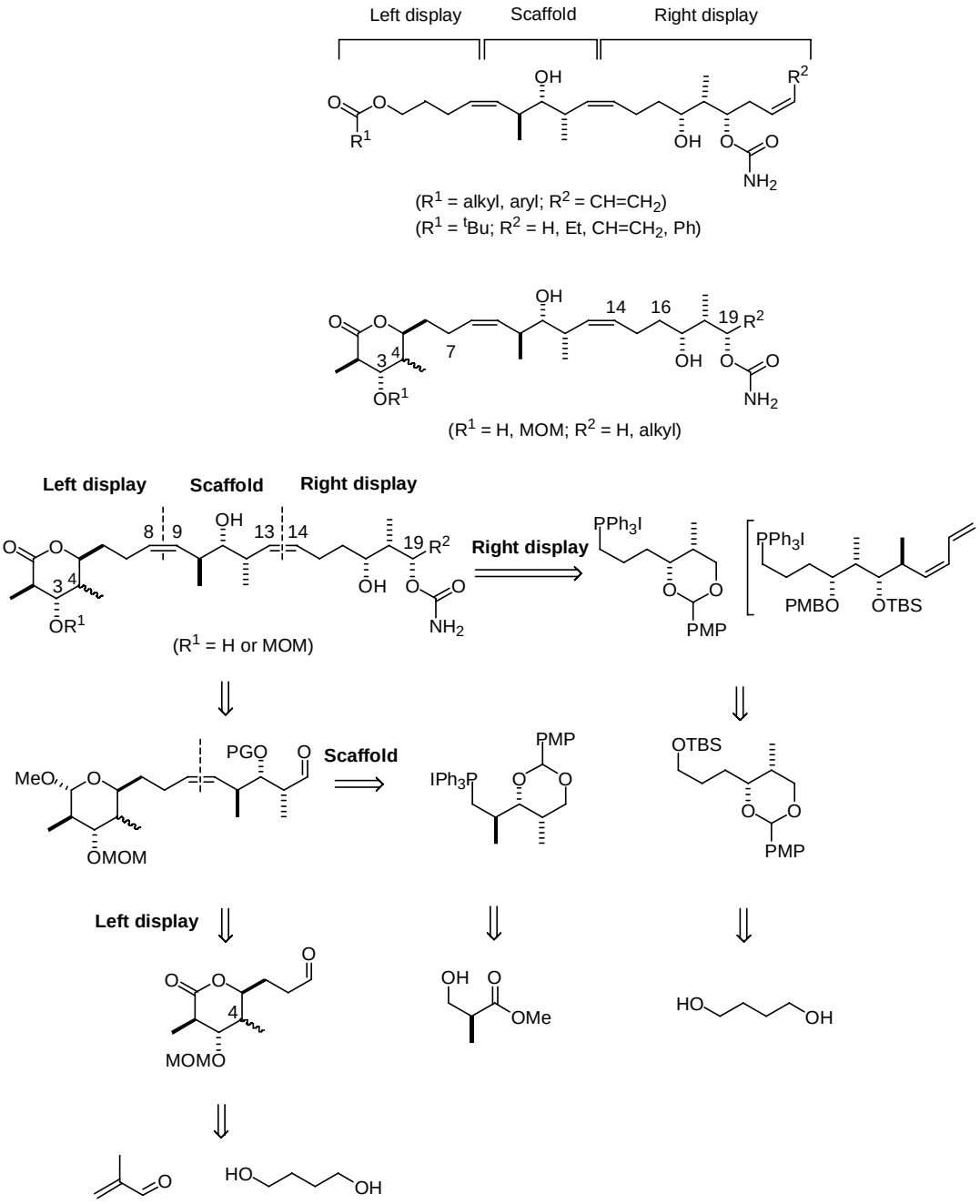

Scheme 2. Retrosynthetic strategy plan for the second library of analogues

Table 6. Biological activity data for 4-*epi*-discodermolides

This includes 4-*epi*-7-dehydroxy-14,16-didemethyl-(+)-discodermolides and C19-truncated analogues.

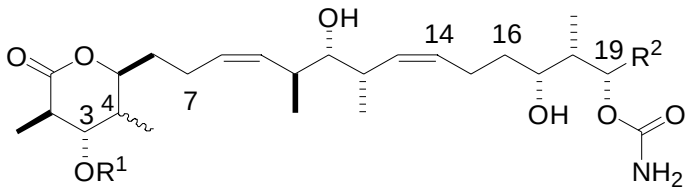

Analogue	%MT Assembly	Antiproliferative activity - GI_{50}(μM); N=4 MDA-MB-231	PC-3	2008	%Paclitaxel Inhibition N=6
NC164 4*R*,R1=MOM, R2=^{i}Pr	7	>50	>50	>50	10±1
NC165 4*R*,R1=H, R2=^{i}Pr	13	>50	>50	>50	10±3
NC142 4*S*,R1=MOM, R2=^{i}Pr	<5	46±1	>50	>50	3±10
NC112 4*S*,R1=MOM, R2=H	<5	30±8	>50	>50	13±1
Discodermolide	>100	0.016±0.003	0.067±0.004	0.072±0.005	64±2
Paclitaxel	100	0.0024±0.002	0.015±0.002	0.0092±0.002	37±1

intact but with a modified left display, namely, altered or natural configuration at C4 and introduction of a MOM group or a free hydroxyl group at C3 of the lactone.

The retrosynthetic strategy followed by the synthetic chemists yielded five analogues that had either a free hydroxyl group or a MOM substitution at the C3 position, and/or a methoxy group at C1 and a diene or an alkyl substituent at C19. The compound NC84 had the lactone, a free

hydroxyl group at C3 and an intact diene. NC86 had the lactone, a MOM group at C3 and an intact diene. NC85 is the lactol derivative of NC86. Derivatives of NC85 were made wherein the diene was totally replaced by an alkyl functionality (compounds PN1 and PN2). Biological evaluation of these analogues included paclitaxel site inhibition, microtubule stabilization and antiproliferative activities. The data are presented in Table 7.

The biological studies with these compounds showed that the lactone MOM ether NC86 was more potent than its closely related lactol NC85 or the free hydroxyl NC84 derivatives. NC86 inhibited the binding of tritiated paclitaxel to an extent of about 57%. In antiproliferative assays, NC86 showed activity in high nanomolar to low micromolar range against three different human carcinoma cell lines (GI_{50}~0.6-1.8 μM) and this compound induced microtubule stabilization (27%) to a considerable degree. Interestingly, at 40 μM, NC86 caused hypernucleation of tubulin assembly. Although the biological activity of NC86 was less potent than that of discodermolide and paclitaxel in all the three assays, the results were quite encouraging. NC84 and NC85 were not as biologically active as was NC86. The antiproliferative activity values were lower for NC84 and NC85 compared to that obtained for either discodermolide or paclitaxel. However, in 2008 cell line, the GI_{50} value was not different from the values observed for either discodermolide or paclitaxel. Their ability to inhibit paclitaxel from binding to tubulin polymer was about 20% and percent microtubule stabilization was about 11%, while their GI_{50} values were in the low micromolar range (GI_{50} ~ 2-15 μM). PN1 and PN2 had the diene replaced with a saturated alkyl group and the stereochemistry at C19 erased by either deleting or adding methyl groups, respectively. The biological activity data from these two compounds showed them to be less active than NC86, with antiproliferative

Table 7. Biological activity data for 4-*epi*-discodermolides

This includes C1- and C3-substituted and C19 diene intact or truncated analogues.

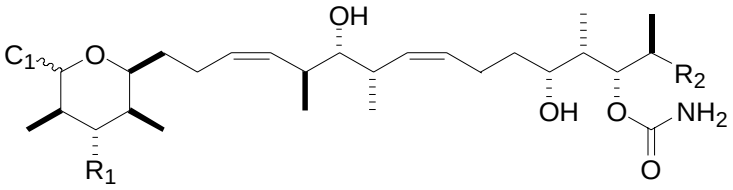

Analogue	**%MT Assembly**	**Antiproliferative activity - GI_{50}(µM); N=4**			**%Paclitaxel Inhibition N=6**
		MDA-MB-231	**PC-3**	**2008**	
NC84 C1:C=O, R1=OH, R2=diene	11	2.1±1.8	7.5±2	5.2±1	21±1
NC86 C1:C=O, R1=OMOM, R2=diene	27	0.87±0.21	1.8±0.9	0.65±0.25	57±2
NC85 C1:C=OMe, R1=OMOM, R2=diene	11	3.4±0.8	15±3	4.7±0.6	19±2
PN1 C1:C=OMe, R1=OMOM, R2= alkyl	6	24±1	>50	29±4	9±0
PN2 C1:C=OMe, R1=OMOM, R2= alkyl	9	23±0	38±1	42±5	15±5
Discodermolide	>100	0.016±0.003	0.067±0.004	0.072±0.005	64±2
Paclitaxel	100	0.0024±0.002	0.015±0.002	0.0092±0.002	37±1

values in 20-50 μM range and only modest abilities to stabilize microtubules or compete for paclitaxel site on microtubules. The GI_{50} and % [^{3}H]paclitaxel inhibition values were lower than those observed for either discodermolide or paclitaxel.

3.3.2. Discussion of the second library of discodermolide analogues

Biological activity data from the 4-*epi*-7-dehydroxy-14,16-didemethyl-(+)-discodermolides strongly supported the hypothesis that conformational analogues of discodermolide could yield compounds with potency comparable to the parent molecule. The data further supports the conformational analysis and pharmacophore studies on discodermolide that hypothesize a hydrogen bonding interaction between the C3 or C7 hydroxyl and the C19 carbamate moieties, and for this close proximity in space of the lactone and carbamate to playing a major role in the stabilization of the most biologically active conformer of discodermolide. Introduction of a hydrogen bond acceptor and a spacer like the MOM group at C3 seemed promising and one of these analogues (NC86) retained microtubule-targeting activity to a considerable extent. The right display (diene portion) was more sensitive to changes and changes there proved detrimental, yielding agents with very weak biological activity.

3.4. Design and biological evaluation of discodermolide/dictyostatin hybrids

Dictyostatin, like discodermolide, is a natural product derived from marine sources (Pettit *et al*. 1994). It was first isolated by Pettit and was assigned structure 7 or 1b (Figures 3 and 6, respectively). Cytotoxicity assays done in P388 leukemia cells have shown dictyostatin to be more potent than discodermolide with an ED_{50} of 0.38 nM. The Curran and Day groups proposed that, structurally, discodermolide and dictyostatin appear to be similar, assuming the theoretical cyclization of discodermolide's carbamate amino group with the lactone carbonyl

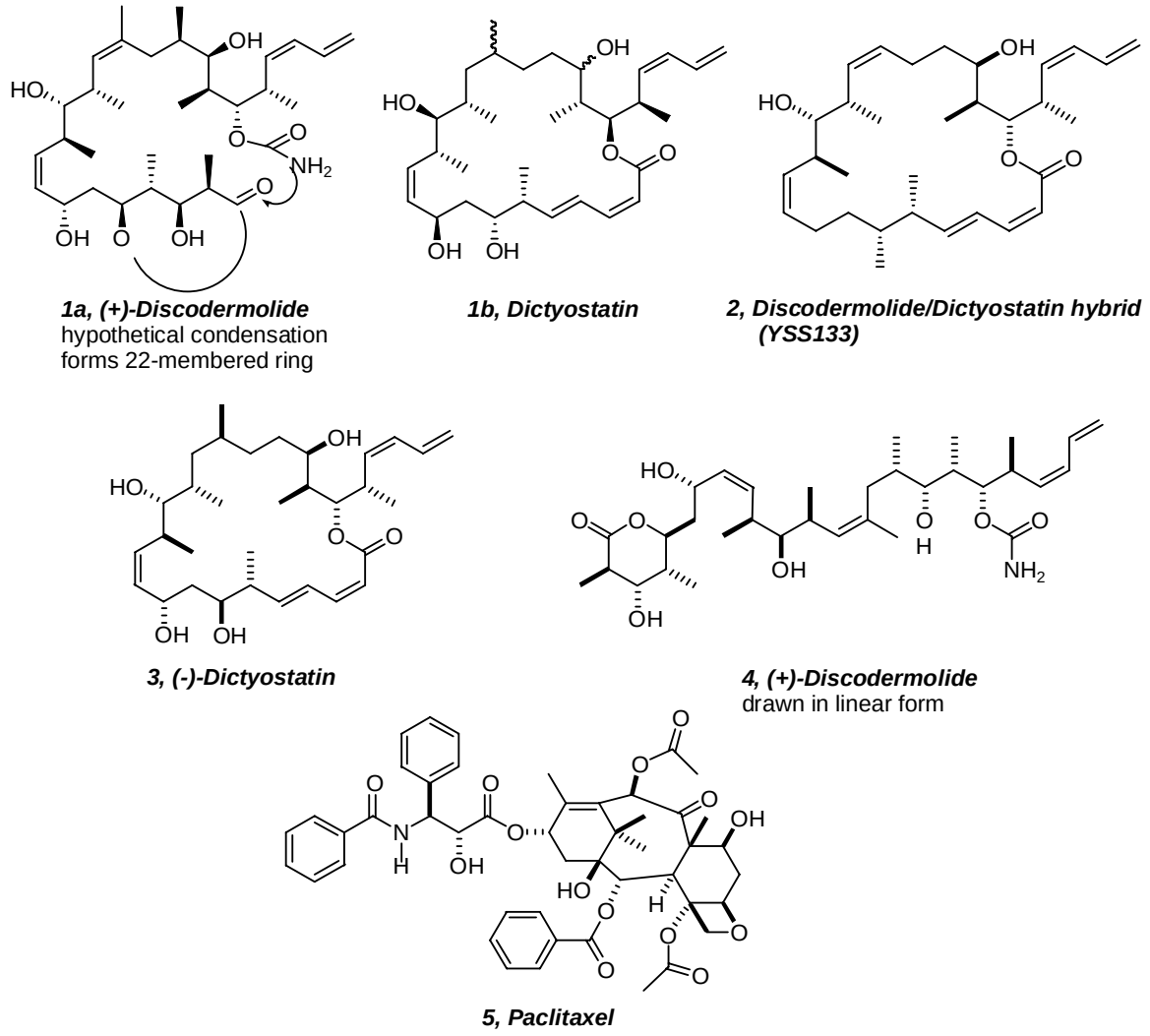

Figure 6. Representation of structural resemblances of discodermolide and dictyostatin

Pettit's original structure (1b) and Paterson's modified structure (3) of dictyostatin are shown. Also represented are structures for discodermolide, in its linear form (4), and paclitaxel (5). Adapted from: Pettit *et al*. 1984 and Paterson *et al*. 2004a.

(Shin *et al*. 2002). Dictyostatin has two additional carbon atoms and differs, at least in the structure originally proposed by Pettit, in stereochemistry with that of discodermolide (Figure 6).

Hence, it was hypothesized that macrocyclic analogues of discodermolide might have interesting biological activities. On the basis of these assumptions, discodermolide/dictyostatin hybrids were constructed and evaluated. for microtubule-targeting actions. Macrolactones of discodermolide were synthesized by Drs. Youseung Shin, Nakyen Choy, and Ms. Tiffany Turner in the Curran group. Following the convergent retrosynthetic strategy outlined for the synthesis of discodermolide analogues, the macrocyclic hybrids YSS072 and YSS133 were constructed using sequential Wittig coupling reactions (Shin *et al*. 2002). Acyclic analogues YSS083, YSS085 and YSS086 were also synthesized from the appropriate synthetic intermediates as reference molecules. This small library was evaluated for microtubule-targeting and antiproliferative activities, which revealed that the macrocyclic analogue YSS133 indeed had promising biological activity (Table 8). This compound had GI_{50} values in low micromolar range (1-1.4 μM) and competed with paclitaxel for binding to tubulin polymer (27% inhibition) to a reasonable extent. The GI_{50} values obtained for the other analogues tested against three different cancer cell lines showed that the macrolactone YSS072 and the acyclic analogues (YSS083, YSS085 and YSS086) had weak activity. The GI_{50} as well as % [^{3}H]paclitaxel inhibition values were similar for all the four analogues. The fact that one of the discodermolide/dictyostain hybrids showed considerable microtubule-stabilizing activity raised hope for the design of potent discodermolide and dictyostatin hybrids and, more importantly, the synthesis of dictyostatin itself and its synthetic analogues.

Table 8. Biological activity data for discodermolide/dictyostatin hybrids

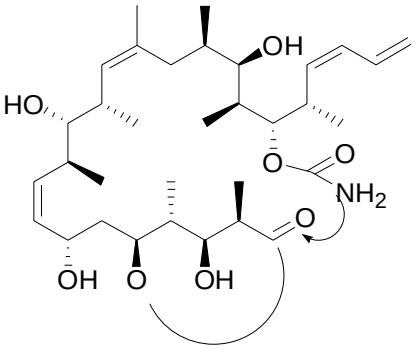

(+)-Discodermolide
GI_{50}: 0.016±0.003 μM
% Paclitaxel inhibition: 64±2

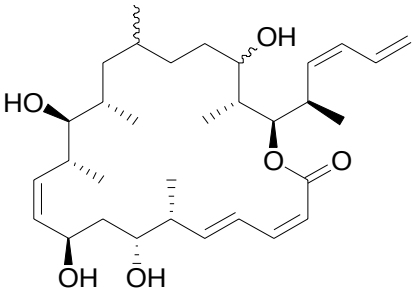

(-)-Dictyostatin
Pettit's proposed structure

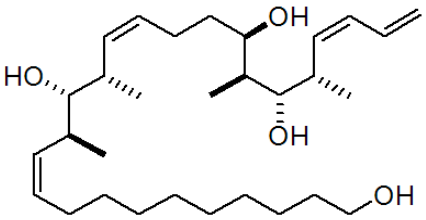

YSS083
GI_{50}: 18±1 μM
% Paclitaxel inhibition: 21±2

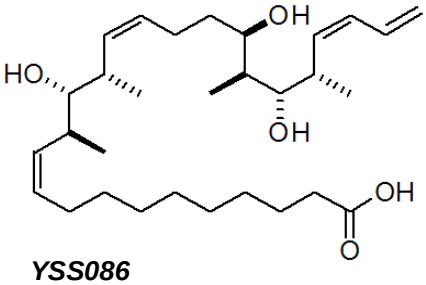

YSS086
GI_{50}: > 50 μM
% Paclitaxel inhibition: 16±3

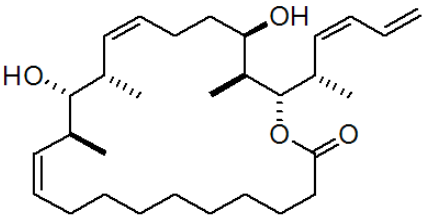

YSS072
GI_{50}: 27±1 μM
% Paclitaxel inhibition: 16±3

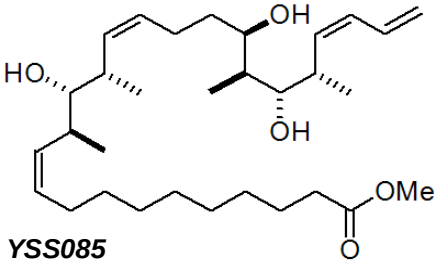

YSS085
GI_{50}: 26±3 μM
% Paclitaxel inhibition: 17±1

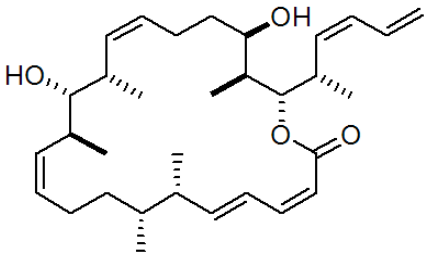

YSS133
GI_{50}: 1.4±0.1 μM
% Paclitaxel inhibition: 27±8

3.5. Discussion

Preliminary evaluation of discodermolide and discodermmolide/dictyostatin analogues for antiproliferative and tubulin polymerization activities helped establish a reasonable SAR. Earlier, it was shown that removal of the methyl groups at C14, C16 and the hydroxyl group at C7 led to analogues with some retention of activity. Schreiber's group observed that C16-normethyldiscodermolide was as active as the parent molecule in cytotoxicity assays (Hung *et al*. 1996b). Studies from Longley's group suggest that one of the hydroxyl groups at C3 or C7 is important for the activity of the parent molecule (Gunasekera *et al*. 2001; Isbrucker *et al*. 2001). It was found that the C3-dehydro and C3-dehydro/C7-deoxy analogues were approximately 2-fold more and 3-fold less cytotoxic than discodermolide. Smith's group reported that the geometry at C14 was important for biological activity of discodermolide (Martello *et al*. 2001). The C14-*cis*-normethyldiscodermolide was found to be only 2-fold less cytotoxic than discodermolide and C14-*trans*-normethyldiscodermolide had less cytotoxic activity. The first and second library set of analogues in the current studies lacked methyl groups at C14 and C16 and the hydroxyl at C7.

Biological evaluation data for the first and second libraries of discodermolide analogues suggested that the lactone moiety of discodermolide is amenable to modifications. Bulkier functional groups were well tolerated and this was shown to be the case with JMM452 wherein the lactone group was replaced with *tert*-butanoate ester. Nevertheless, the lactone is critical for biological activity of discodermolide. One of the 4-*epi*-7-dehydroxy-14,16-didemethyl-(+)-discodermolides, NC86, was the most promising (in drug discovery vernacular, "A Hit!") of all the discodermolide analogues studied for microtubule-targeting activities. NC86 was designed via a rational drug design standpoint based on the solution conformational properties of discodermolide. Conformational analysis of discodermolide suggests that a hydrogen bond

interaction between an acceptor like a hydroxyl group or a MOM group positioned at C3 of the lactone ring or the hydroxyl at C7 with the C19 carbamate would stabilize the tilde conformation of discodermolide. Intensive cellular profiling immunofluorescence experiments done with these analogues strongly suggest that JMM452 and NC86 caused: (i) microtubule perturbation with morphologies varying from normal bipolar to abnormal multipolar mitotic spindles; (ii) condensation of nuclear chromatin; and (iii) elevated levels of certain mitotic markers like phosphohistone H3 and stress pathway kinase downstream targets (phosphoRSK90). Noteworthy in these studies is the finding that JMM452 was more selective for mutated β-tubulin ovarian carcinoma cell lines than for the non-mutated parental cells (Minguez *et al*. 2003).

Following the intensive SAR analyses done by replacing the lactone moiety of discodermolide with a variety of esters which led to retention of biological activity to a considerable extent, Smith's group has recently made a series of 7-deoxy aryl discodermolide analogues wherein the lactone functionality is replaced with aryl substituents (Burlingame *et al*. 2004). The 2,3-anhydro analogue of discodermolide showed considerable cytotoxicity against all cell lines tested. Also, incorporation of a phenolic (*meta* to the ethylene linker) moiety in place of the lactone in discodermolide gives an analogue with increased cytotoxic action relative to the unsubstituted derivative. Introduction of another hydroxyl group, *meta* to the hydroxyl in the previous analogue, provided no change in the cytotoxicity. These results led to preparation by the Smith group of a library of 7-deoxy aryl discodermolide analogues having a range of functionalized phenyl rings and thiophene moieties. This set of analogues was evaluated for biological activity and most were active against various cancer cell lines in low micromolar range. The methylthiophene and *meta*-substituted aryl analogues exhibited greater cytotoxic

effects than the remaining analogues. Aryl analogues with *para*-substitution or difluoro derivatives and unsubstituted thiophenes had drastically decreased cytotoxic actions These results indicate that removal of five stereogenic centers and replacement of the entire 'C' region (as shown with phenylethylene substituent and derivatives of it) with various aryl and thiophene substituents gives analogues with promising biological activities.

Novartis chemists have synthesized discodermolide analogues wherein isosteric replacements of the C1-C5 lactone ring with aromatic groups, of the trisubstituted olefin with an *N*-methyl amide group, and of the C21-24 diene were done (Palermo *et al.* 2002; Weichun *et al*. 2002; Peng *et al*. 2002). A structurally diverse set discodermolide analogues was also synthesized. The biological activity studies for these analogues were performed against five different human carcinoma cell lines, three paclitaxel-sensitive -- A549, HCT 116, 1A9, and two paclitaxel-resistant -- MIP101, 1A9PTX22. 7-Acetyldiscodermolide was found to be the most potent of all the analogues tested for microtubule bundling and growth inhibition, and the truncated analogue was as potent as discodermolide in microtubule bundle formation but was less potent in inhibiting the growth of the cell lines studied. In the paclitaxel-resistant MIP101 cell line, the C14-demethylated analogue showed a drastic reduction in antiproliferative activity. Also, most of the C21-C24 modified analogues turned out to be less potent.

Smith's group has further explored the critical functional groups on the lactone ring that are important for activity (Shaw *et al*. 2005). In these studies, analogues with modifications done on the lactone ring showed greater antiproliferative activity (IC_{50}s in the range of 2-9 nM) than the parent molecule (IC_{50}s of 16-28 nM). The 2-normethyl-2,3-anhydro and 2,4-normethyl-2,3-anhydro analogues were quite active, suggesting that the 2- and 4- methyl groups and the 3-hydroxyl group of the discodermolide lactone have no significant role in the biological potency

of the parent molecule. The α,β-unsaturated carbonyl was found not to be important. The unsubstituted lactone showed greater activity in all the cell lines except the NCI/ADR cell line, known to overexpress P-gp. 4,5-*Bis*-*epi*-2,3-anhydrodiscodermolide turned out to be active as well. A five-membered unsubstituted butyrolactone showed marked improvement in biological activity as compared to the parent molecule. These studies are on par with the data discussed in this dissertation that suggest that the lactone moiety of discodermolide is flexible for modification and analogues with the correct conformation, as reported in the NMR solution structure of discodermolide analysis, yielded promising results. Later studies from Smith also evaluated analogues with alterations of the carbamate group (Smith *et al*. 2005). Derivatives of 2,3-anhydrodiscodermolide and 14-normethyldiscodermolide that were made and of interest are the analogues having the *N*,*N*-dimethylaniline substituent on the nitrogen of the carbamate. These two analogues had greater antiproliferative potencies than discodermolide.

Structure-activity relationship evaluations of discodermolide analogues suggest that the structural framework of the parent molecule is amenable for modifications. Based on our observations and findings in the literature the SAR for discodermolide can be represented as shown in Figure 7. The future holds promise for developing conformationally active and less toxic variants of discodermolide as novel microtubule-stabilizing agents. Interesting amongst all the libraries of compounds is the one consisting of macrocyclic analogues of discodermolide. One of the macrolactones, YSS133, which was designed based on the stereochemistry of discodermolide, showed promising activity in paclitaxel site inhibition, microtubule stabilization, and antiproliferative experiments. This result paved way for the total synthesis of dictyostatin, a macrocycle and a structural congener of discodermolide, and laid the foundation for future scope of the project.

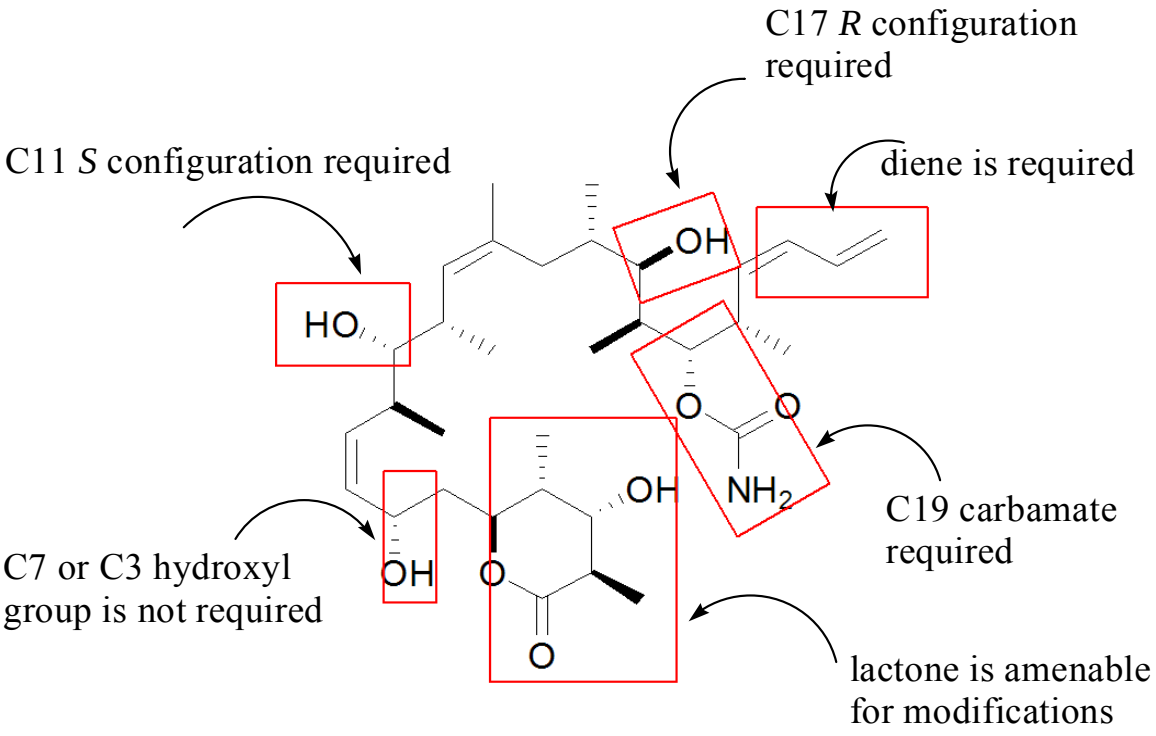

Figure 7. Representation of SAR for (+)-discodermolide

4. TUBULIN ASSEMBLY, PACLITAXEL SITE BINDING, AND CELLULAR EFFECTS OF DICTYOSTATIN AND DICTYOSTATIN ANALOGUES

4.1. Introduction and literature cited

(–)-Dictyostatin is a 22-membered macrolactone with 11 stereocenters, an endocyclic *Z*,*E*-dienoate and a pendant *Z*-diene (3 in Figure 6, Chapter 3). It was first isolated from a marine sponge of the genus *Spongia* collected in the Republic of Maldives and found to be a potent antiproliferative agent of nanomolar potency (Pettit *et al*. 1994). Cytotoxicity assays done in P388 leukemia cells showed dictyostatin to be a potent molecule with an ED_{50} 0.38 nM. NMR experiments revealed dictyostatin to be a polyketide that was assigned structure 1b (Chapter 3, Figure 6). Several questions remained as to the proposed structure of this compound. Even with the first structural assignment, it was clear that the compound had great similarities to that of (+)-discodermolide (Shin *et al*. 2002). A hypothetical cyclization of the sp^3-hybridized oxygen in the carbamate group with the lactone carbonyl group of discodermolide gives a structure resembling that of dictyostatin, although the latter has two additional carbon atoms. If one does this hypothetical cyclization with the carbamate nitrogen and the lactone carbonyl, the macrocycles would be the same size. Before knowing the true relative and absolute stereochemistry of dictyostatin, the macrocyclic hybrids of discodermolide/dictyostatin structures discussed earlier were designed and evaluated for microtubule-targeting actions. One of the analogues, YSS133, shown also in Table 8 of Chapter 3, indeed caused assembly of tubulin, exhibited a GI_{50} potency in the low micromolar range (~1 μM) and competed, albeit weakly, with paclitaxel for binding to tubulin polymer.

During this time, dictyostatin was again isolated from a *Lithistida* sponge of the family *Corallistidae* harvested near Jamaica (Isbrucker *et al*. 2003). In that study, the natural product was further evaluated in biological assays and found to promote tubulin assembly in the presence of GTP but in the absence of MAPs at temperatures (4 ^{o}C) where paclitaxel is inactive, to enhance tubulin assembly much more potently than paclitaxel at 37 ^{o}C, and to form microtubule polymer that is, unlike that formed by paclitaxel, cold-stable. Antiproliferative potencies against various human tumor cell lines (A549, MCF7, MES-SA) were found to be in the 1-5 nM range, comparable to, or even lower than those observed for paclitaxel. Even the NCI/ADR-RES cell lines that overexpress the ABC1 drug efflux transporter (a.k.a. the P-glycoprotein pump) were susceptible to the antiproliferative effects of natural dictyostatin (GI_{50} ~20 nM). Flow cytometric analyses of A549 cells treated with 10 nM natural dictyostatin showed induction of G2/M block and the effect was more extensive than that seen with cells treated with 10 nM paclitaxel. Immunofluorescence studies of treated cells revealed that natural dictyostatin caused microtubule rearrangement and bundling at very low concentrations (10-100 nM). Natural dictyostatin also promoted nuclear degradation characteristic of apoptosis and induced aneuploidy.

The relative stereochemistry of dictyostatin was proposed after high field NMR experiments and molecular modeling (Paterson *et al*. 2004a). Shortly thereafter, simultaneous publications describing full syntheses of the compound gave unequivocal evidence for the structure and its absolute stereochemistry as shown in Figure 6 of Chapter 3 (Paterson *et al*. 2004b, Shin *et al*. 2004). These full syntheses and our previous approaches to dictyostatin/discodermolide hybrids opened the door for detailed biological evaluations of this rare natural product and for building analogues of the parent structure. The total syntheses of

dictyostatin and its analogues were done by Drs. Youseung Shin, Jean-Hugues Fournier, Yoshikazu Fukui and Arndt Brückner in Prof. Curran's laboratory.

Hypothesis II: Synthetic dictyostatin, like its structural congener discodermolide, hypernucleates tubulin assembly more potently than paclitaxel in the presence and absence of MAPs and/or GTP, binds to taxoid site on tubulin polymer with greater affinity and is active against paclitaxel-resistant cells.

Rationale: Discodermolide binds to taxoid site on tubulin polymer with high affinity, competes with paclitaxel for binding on tubulin polymer, and hypernucleates tubulin assembly more potently than paclitaxel in the presence and absence of MAPs and/or GTP (ter Haar *et al*. 1996b; Kowalski *et al*. 1997). It would be of interest then to investigate if dictyostatin binds to tubulin polymer and nucleates microtubule assembly much more potently than paclitaxel by direct evaluation of its polymerization ability as well as polymer morphology. Also important would be to evaluate the role of MAPs and GTP in modulating the interaction of dictyostatin with tubulin. Previous reports on breast carcinoma cell lines have shown that discodermolide potently induced microtubule bundle formation than paclitaxel, in spite of these two compounds having almost equivalent IC_{50} values (Kowalski *et al*. 1997; Balachandran *et al*. 1998). Microtubule bundle formation was seen in cells treated with 10 nM discodermolide as opposed to paclitaxel, which required 1 μM to show this same effect. It would be important to study if dictyostatin, like discodermolide, promotes microtubule bundle formation and mitotic aberrations more potently than paclitaxel in human carcinoma cell lines. Therefore, in-depth pharmacological investigations were undertaken to study tubulin assembly, paclitaxel site binding, and cellular effects of synthetic dictyostatin and to obtain comparison profiles against paclitaxel, discodermolide and epothilone B. Dictyostatin analogues were synthesized for structure-activity

relationship evaluation. Synthesis of the analogues was done by Drs. Youseung Shin and Jean-Hugues Fournier in Prof. Curran's laboratory. The structures of the analogues are presented in Figure 8. Modifications done on the parent molecule for SAR evaluation are listed below.

1. YSS631 is dictyostatin.

2. YSS629 is an open-chain methyl ester of dictyostatin.

3. YSS479 has the configuration of the methyl groups at C6 and C16 epimerized. The functional groups at C6 and C7 are *syn* to each other.

4. YSS133 is a previously reported macrocyclic hybrid of discodermolide/dictyostatin.

5. YSS652 is an epimer of dictyostatin wherein the configuration of the hydroxyl group at C19 was changed from *R* to *S*.

6. YSS665 has the configuration at C6 and C14 modified and also the geometry of C4:C5 was changed from (*E:Z*) to (*E:E*).

7. YSS675-1 has the configuration of the methyl groups at C6, C14, and the hydroxyl group at C19 modified.

8. YSS675-2 has the configuration of the methyl groups at C6, C14, the hydroxyl group at C19, and also the geometry of C4:C5 was changed from (*E:Z*) to (*E:E*).

9. YSS698-2 is C16-normethyldictyostatin.

Structural analogues of dictyostatin were also evaluated for microtubule-targeting activities. The goal was to establish a reasonable SAR for dictyostatin and analogues. The biological activity data for this library is discussed below.

4.2. Experimental approach and results

Cell-based *in vivo* and isolated protein-based *in vitro* experiments were performed to evaluate dictyostatin and its analogues for their effects on microtubule binding and microtubule

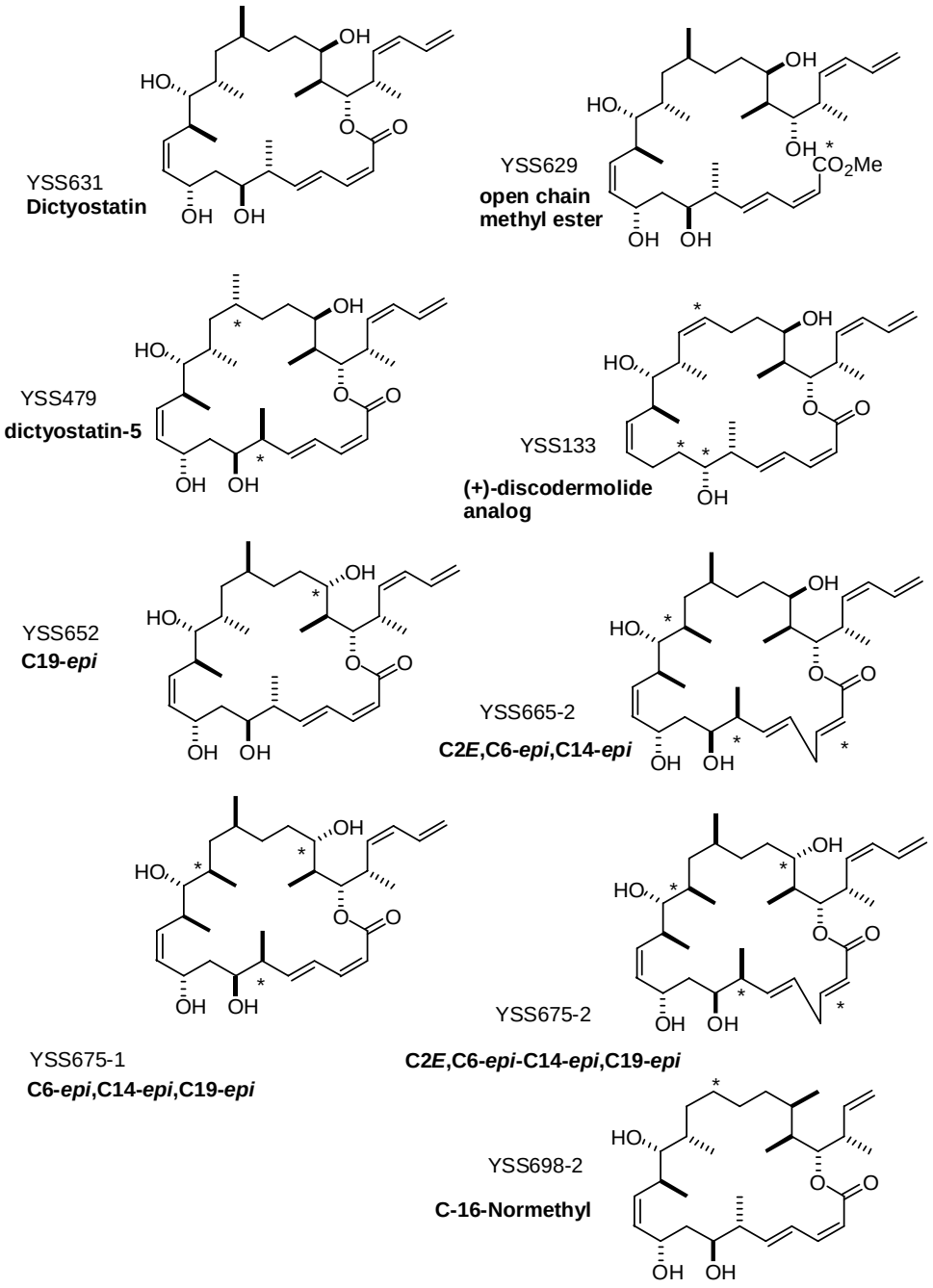

Figure 8. Structural analogues of dictyostatin for SAR and pharmacological evaluation

perturbing activities. *In vivo* experiments included antiproliferative and immunofluorescence assays. *In vitro* studies included the radiolabeled, microtubule stabilization, critical concentration and pelleting assays. A brief description of those experiments is given below. Details are given in Chapter 2 for all the assays employed for this study. In addition, experimental details considered important for the studies aimed for this set of analogues are described in the results section for each assay.

Antiproliferative assay: The ability of dictyostatin and its synthetic analogues to inhibit cell growth was studied in three different ovarian cancer cell lines and two breast cancer cell lines. 1A9 is a parental ovarian cancer cell line. 1A9PTX10 and 1A9PTX22 are the mutated ovarian carcinoma cells derived from the parental cell line. The generation of mutated paclitaxel-resistant cell lines is as described in Chapter 2. The former has phenylalanine at position 270 on β-tubulin mutated to valine, the latter has alanine at 364 on β-tubulin mutated to threonine. Two breast cancer cell lines included in the experiment were the MDA-MB-231, an estrogen receptor alpha negative breast cancer cell line and T47D, a cell line expressing substantial levels of estrogen receptor beta. The experimental protocol is the same as described in Chapter 2 except that T47D cell line was grown in DMEM medium. The assay was done in RPMI medium supplemented with 10% FBS for all the cell lines. The GI_{50} values were calculated in the presence of all the test agents.

Multiparameter immunofluorescence experiments: Immunofluorescence technique was employed to investigate the microtubule bundling and mitotic effects of dictyostatin and its analogues. An advanced robot technology in tandem with array scan equipment was used for the study. The description of the experimental protocol is as described in Chapter 2.

Paclitaxel site inhibition assay: The abilities of test agents to displace radioligands from binding to tubulin polymer were determined following the procedure described in Chapter 2. Monosodium glutamate at pH 6.6 and ddGTP were used for reasons as described previously (Chapter 3). The radioligands used for the inhibition study included [^{3}H]paclitaxel, [^{3}H]discodermolide, and [^{14}C]epothilone B. Radioactive counts from the supernatant (50 μL) were determined by scintillation spectrometry. Bound tracer was calculated from the amount of total tracer added to each reaction mixture minus the amount of tracer found in the supernatant. Percent inhibition values were determined with respect to control experiments.

Microtubule stabilization assay: Tubulin polymerization assays were done in Gilford 250 and Beckman-Coulter DU7400 spectrophotometers as described in Chapter 2 for different reaction conditions. The percent microtubule stabilization was calculated for each analogue with respect to the turbidity readings obtained for positive (in the presence of 10 μM paclitaxel) and negative controls (in the presence of DMSO). Electron microscopic analysis of the microtubule polymer formed in the presence of test agents was done following 1% v/v uranylacetate staining procedure as described in Chapter 2.

Critical concentration was performed to determine the hypernucleating ability of dictyostatin in comparison with discodermolide. The ability of dictyostatin and its analogues to induce polymerization was given a quantitative estimation by calculating the EC_{50} values from the pelleting assay. The experimental details for these two experiments are as described in Chapter 2.

4.3. *In vivo* cell-based experiments

4.3.1. Antiproliferative activity studies

Parental (1A9 cell line) and β-tubulin mutated (1A9/PTX10 and 1A9/PTX22) ovarian cancer cell lines were used for studying antiproliferative activity of dictyostatin and its synthetic analogues. In addition, two breast cancer cell lines, T47D and MDA-MB-231, were also investigated for microtubule perturbing effects in the presence of test agents. The paclitaxel-resistant cells were maintained in RPMI/10% FBS medium containing 17 nM paclitaxel and 10 μM of MDR1 reversal agent verapamil. Experiments with test agents were done in paclitaxel- and verapamil-free RPMI/10% FBS medium. Antiproliferation experiments were done following the protocol described in Chapter 2. The experimental results are presented in Table 9. The GI_{50} values determined show that dictyostatin was active in the very low nanomolar range and was the most potent growth inhibitory agent of all the compounds studied. Dictyostatin and paclitaxel exhibited comparable GI_{50} values against the parental 1A9 cells (0.69 nM vs. 0.71 nM). The mutant β-tubulin-expressing cells showed about 90- and 70-fold resistance to paclitaxel, while their cross-resistance to dictyostatin was only 2- to 4-fold. Against the mutated cell lines, the GI_{50} values observed for dictyostatin were 3.2 and 1.3 nM, respectively. Dictyostatin had over a two-fold lower GI_{50} value than that of discodermolide against 1A9 cell line (0.69 versus 1.7 nM, respectively). The mutated β-tubulin cell line 1A9/PTX10 retained its sensitivity to both dictyostatin and discodermolide, but the GI_{50} value for dictyostatin was lower than for discodermolide (3.2 vs. 6.2 nM, respectively). Against 1A9/PTX22 cells, dictyostatin was over 5-fold more active than discodermolide (1.3 vs. 7 nM, respectively). Comparison of the relative resistance values for 1A9/PTX22 cell line revealed that the fold-resistance observed in the presence of dictyostatin was about 2-fold lower than that with discodermolide. The relative

resistance values for 1A9/PTX10 cell line in the presence of these two compounds were comparable.

The analogues were also examined for their antiproliferative activities against 1A9, PTX10 and PTX22 cell lines. Although less active than the parent compound, the GI_{50} values were in mid-nM range for all the analogues, except for the C6-*epi*/C16-*epi* analogue YSS479 (for which the GI_{50} was >500 nM), against the three cell lines (Table 9). It should also be noted that the fold-resistance values for these compounds against PTX10 and PTX22 cell lines were much lower than that observed for paclitaxel. Of interest is the antiproliferative activity of 16-normethyldictyostatin, YSS698-2. The GI_{50} values for this compound ranged from 0.5-2 nM. While this compound showed potency equivalent to that of the parent molecule against parental 1A9 cells as well as against one of the mutated β-tubulin cell lines (PTX22), its GI_{50} was close to 500 nM in the other mutated cell line, PTX10. The open-chain methyl ester analogue, YSS629, and the C19 epimer, YSS652 had activities in mid-nM range. Likewise, YSS652, with the C19 configuration inverted, showed preferential antiproliferative activity against one mutated β-tubulin cell line over the other. The PTX22 cell line exhibited a 2-fold resistance vs. that seen with the PTX10 cell line, which was about 6-fold resistant to YSS652 in comparison to the activity observed in the parental cell line. This demonstrates the importance of C16 and C19 position for binding of the parent molecule to the biological target. The C2-*E*/C6-*epi*/C14-*epi* alterations in analogue YSS665-2 led to a loss of antiproliferative activity, with GI_{50} values in the range of 300-800 nM. However, analogues with C19 epimerized and with retention of C6-*epi* and C14-*epi* (YSS675-1) or C2-*E*, C6-*epi* and C14-*epi* (YSS675-2) configurations were quite active and had better antiproliferative activity profiles in all the cell lines studied than did YSS665-2 (GI_{50}s ~ 25 nM). Nevertheless, the activity was far less than seen for the parent

molecule, thus indicating the significance of *E:Z* geometry of the diene and the configuration of C14 and of C19 for biological activity. Noteworthy is the observation that dictyostatin-like compounds, with an exception noted for the C16-normethyl analogue, retained their sensitivity against mutated paclitaxel-resistant cell lines.

Table 9. Antiproliferative activities of dictyostatin and its analogues

Fifty percent growth inhibitory concentrations (GI_{50}) of dictyostatin, discodermolide and paclitaxel against human ovarian cancer cell lines after 72 h in continuous presence of the agents. 1A9 cells express wild-type β-tubulin, whereas the 1A9PTX10 and 1A9PTX22 cells express, respectively, the Phe270→Val and Ala364→Thr mutant forms of the protein.

	GI_{50} ± S.D., nM (fold-resistance) (N=4) Cell line		
Compound	**1A9**	**1A9/PTX10 (Phe270→Val)**	**1A9/PTX22 (Ala364→Thr)**
Discodermolide	1.7±1.2	6.2±3.6 (3.6)	7.0±8.4 (4.1)
Paclitaxel	0.71±0.11	64±8	51±9
Dictyostatin	0.69±0.80	3.2±2.4 (4.6)	1.3±1.0 (1.9)
YSS479	> 500	> 500	> 500
YSS629	56±16	79±13 (1.4)	85±2 (1.5)
YSS652	21±14	120±60 (5.7)	43±12 (2.0)
YSS665-2	310±40	780±200 (2.5)	790±560 (2.5)
YSS675-1	28±1	26±0	30±1
YSS675-2	25±2	25±1	30±1
YSS698-2	0.41±0.52	470±70	5.6±4.7

Antiproliferative activities of dictyostatin and its 16-normethyl analogue were determined in breast cancer cell lines. The data is presented in Table 10. These results suggest that in T47D cell lines, epothilone B and dictyostatin were the most potent of all agents studied. The GI_{50} value observed for dictyostatin (0.5 nM) was over 3-fold and 7-fold lower than that observed for paclitaxel and discodermolide, respectively. In MDA-MB-231 cell line, dictyostatin showed activity comparable to that of paclitaxel. Epothilone B turned out to be the most potent of all, although the fold-difference in GI_{50} values for all the test agents. 16-Normethyldictyostatin (YSS698-2) showed lower GI_{50} values compared to dictyostatin in the two cell lines.

The SAR determined include: the macrolactone is important, but not a full requisite, for MT stabilization; the configuration of the hydroxyl at C19 has an important role; the configuration of the C6 and C14 methyls are important; *anti* positioning of the C6 and C7 functional groups seems mandatory for MT stabilization; the natural *E:Z* geometry of the diene seems crucial; and the C16 methyl is not a factor in antiproliferative activity.

Table 10. Antiproliferative activities of dictyostatin and its analogues

Fifty percent growth inhibitory concentrations (GI_{50}) of dictyostatin, discodermolide and paclitaxel against human breast cancer cell lines after 72 h in continuous presence of the agents.

	GI_{50} ± S.D., nM (N=4) Cell line	
Compound	**T47D**	**MDA-MB-231**
Discodermolide	3.6±5	9.8±8
Paclitaxel	1.5±1	5.5±6
Dictyostatin	0.5±0	5.3±6
Epothilone B	< 0.2	1.2±1
YSS698-2	76±14	57±5

4.3.2. Multiparameter fluorescence analysis of cellular effects.

A high-throughout and high-content screening (HTS and HCS) methodology was employed to study the cellular effects of dictyostatin and its analogues. HCS defines the effects that test agents have on the temporal and spatial regulation of multiple cell functions and has been adopted by the pharmaceutical industry as a standard platform for compound screening (Giuliano *et al*. 2003a; Abraham *et al*. 2004). The multiplexed HCS assay described here provides measurements of nuclear morphology, microtubule stability, and histone H3 phosphorylation, which is a marker of cells at the G_2/M cell cycle boundary, was previously validated and used to generate results for several reports (Wipf *et al*. 2000; Minguez *et al*. 2002; Giuliano *et al*. 2003b; Giuliano *et al*. 2004). The procedure is described in Chapter 2.

Briefly, HeLa cells were plated on collagen-coated 384-well microtiter plates, allowed to attach, and then treated for 24 h with DMSO or test agents. Test agent concentrations began at 1 μM and two-fold dilutions were made down the plate to levels below 1 nM. After the treatment period, the cells were fixed with formalin and their chromatin stained with Hoechst 33342. Cells were permeabilized and treated with primary antibodies for α-tubulin and phosphohistone H3, and then with fluorophore-labeled secondary antibodies (tubulin - FITC; phosphohistone H3 - Cy3). The three fluorescent channels were then examined on an ArrayScanII® after scanning the plate using either target activation or compartmental analysis bioapplications which gives quantitative pixel distribution and density information in each channel on a per cell basis. An Omega XF93 filter set at excitation/emission wavelengths of 350/461 nm (Hoechst), 494/519 nm (FITC), and 556/573 nm (Cy3) was used for scanning and 1000 cells/well were imaged at these wavelengths. The BioApplications portion of the software was used to perform automated image acquisition, characterization and classification of the cell population according to response

relative to controls. The concentration-response curves were plotted for four parameters that were normalized to control values using PRISM 4.0 software version 4.0 (GraphPad Software, Inc., San Diego, CA USA). The parameters include objects per field (refers to cell density), average tubulin polymer mass (a measure of microtubule stabilization), percent condensed nuclei (a measure of DNA content), and percent histone H3 phosphorylation (a measure of mitosis). The data were quantified and compared based on minimum detectable effective concentrations (MDECs) of each test agent required for initiating a cellular response (Wipf *et al*. 2000; Minguez *et al*. 2002). Concentration-response data, MDECs for each parameter, representative composite immunofluorescent images and cell cycle data are presented and described below.

The fluorescence intensity values detected on a per cell basis for a given subpopulation of cells are presented as concentration of test agent versus response normalized to control in Figure 9A-E. Test agents included in the graphs are dictyostatin (squares), paclitaxel (triangles), discodermolide (inverted triangles), and 16-normethyldictyostatin (diamonds). Objects per field data (Figure 9A) suggested that dictyostatin more potently inhibits the growth of HeLa cells than all the other test agents. The intensity of microtubules stabilized in the presence of paclitaxel seemed to be greater than that observed with dictyostatin or discodermolide (Figure 9B). The phosphohistone H3 (mitotic marker) and condensation of nuclear chromatin responses were comparable in the presence of all the test agents (Figure 9C-E). However, dictyostatin yielded greater cellular response than other test agents. The data were quantified and compared based on minimum detectable effective concentrations (MDECs) of each test agent required for initiating a cellular response (Wipf *et al*. 2000; Minguez *et al*. 2002). MDECs were determined for each test agent for a given parameter by interpolating the linear portion of concentration-response curve,

shown in Figure 9A-D, to the upper limit of the error in the measurements made in control cells. The data is presented in Table 11.

The results showed that HeLa cells were most sensitive to the microtubule stabilization and mitosis-blocking effects of dictyostatin, closely followed by paclitaxel. Discodermolide was ca. 10-fold less potent. MDECs for increases in tubulin polymer mass with dictyostatin, paclitaxel and discodermolide were 3.6 nM, 5 nM and 40 nM, respectively; for the phosphohistone H3 response, 5.6, 6.0 and 89 nM; and for nuclear condensation, 6.1, 7.9 and 56 nM (Table 11). Of interest was the data for YSS698-2, the C16-normethyl analogue of dictyostatin. The MDECs for tubulin polymer, phosphohistone H3, and Hoechst intensities were 22.4, 27 and 22.4 nM, respectively. This data correlates with the relative antiproliferative activities observed in the 1A9 parental ovarian cancer cell lines in the presence of the above test agents.

The concentrations of YSS698-2 required for initiating a response were lower than that observed for discodermolide. This C16-normethyl analogue was over 2-fold and about 3-fold more potent than discodermolide in causing condensation of nuclear chromatin and in causing elevation of phosphohistone H3 levels, respectively, but was over 4-fold less potent than dictyostatin or paclitaxel. Nevertheless, the fact that YSS698-2 is synthetically simpler than dictyostatin, plus showed potent and promising cellular effects, make this analogue a very interesting lead compound. These results suggest that MDECs for tubulin polymer, phosphohistone, and Hoechst intensities were comparable for dictyostatin, discodermolide, paclitaxel, and 16-normethyl dictyostatin. The open-chain methyl ether YSS629 and the C19-epimer YSS652 were less active than YSS698-2 or the parent molecule in initiating the cellular responses. YSS665-2, YSS675-1, and YSS675-2 were about 40- and 80-fold less active than the

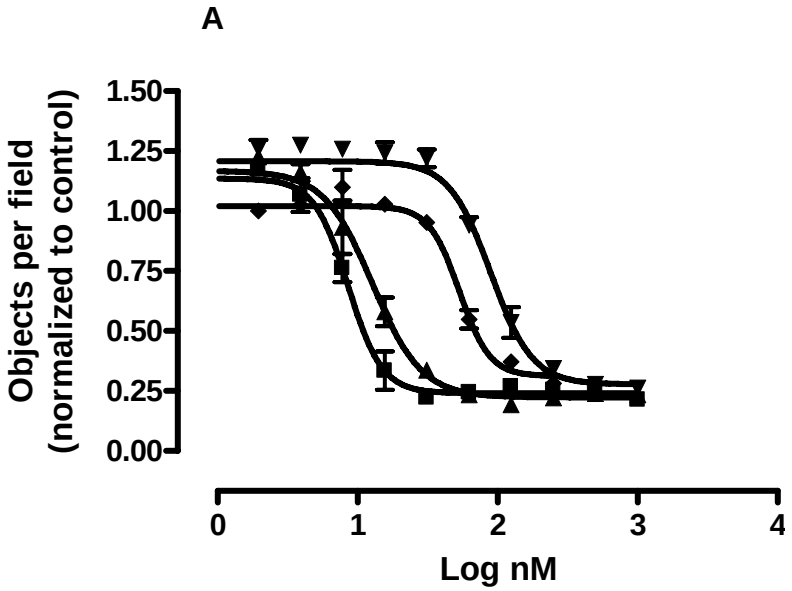

Figure 9. Sigmoidal profiles of multiparameter immunofluorescence analyses.

The effects are from 24 h treatment over a range of test agent concentrations. Each point represents the mean ± S.D. of fluorescence intensity values obtained from at least 1000 cells in three independent experiments. Experiments were conducted on HeLa cells.

Figure 9A. Objects per field data in the presence of microtubule stabilizers

Test agents: dictyostatin (squares), paclitaxel (triangles), discodermolide (inverted triangles), and normethyldiscodermolide, YSS698-2 (diamonds).

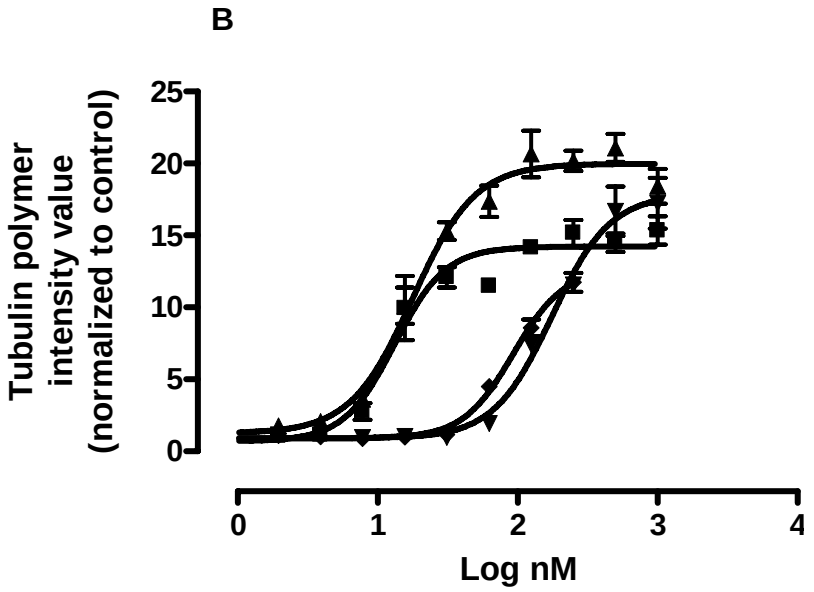

Figure 9B. Tubulin polymer intensities in the presence of microtubule stabilizers

Test agents: dictyostatin (squares), paclitaxel (triangles), discodermolide (inverted triangles), and normethyldiscodermolide, YSS698-2 (diamonds).

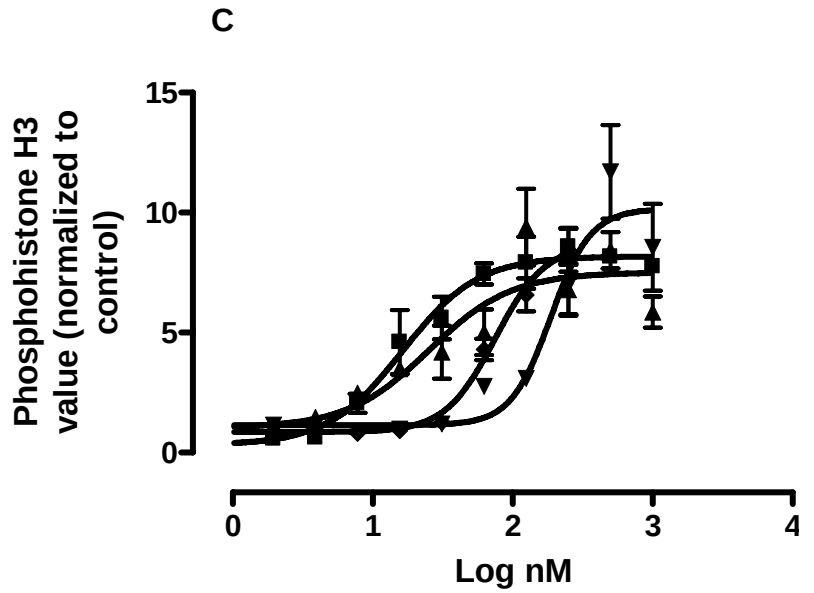

Figure 9C. Nuclear phosphohistone H3 levels in the presence of microtubule stabilizers

Test agents: dictyostatin (squares), paclitaxel (triangles), discodermolide (inverted triangles), and normethyldiscodermolide, YSS698-2 (diamonds).

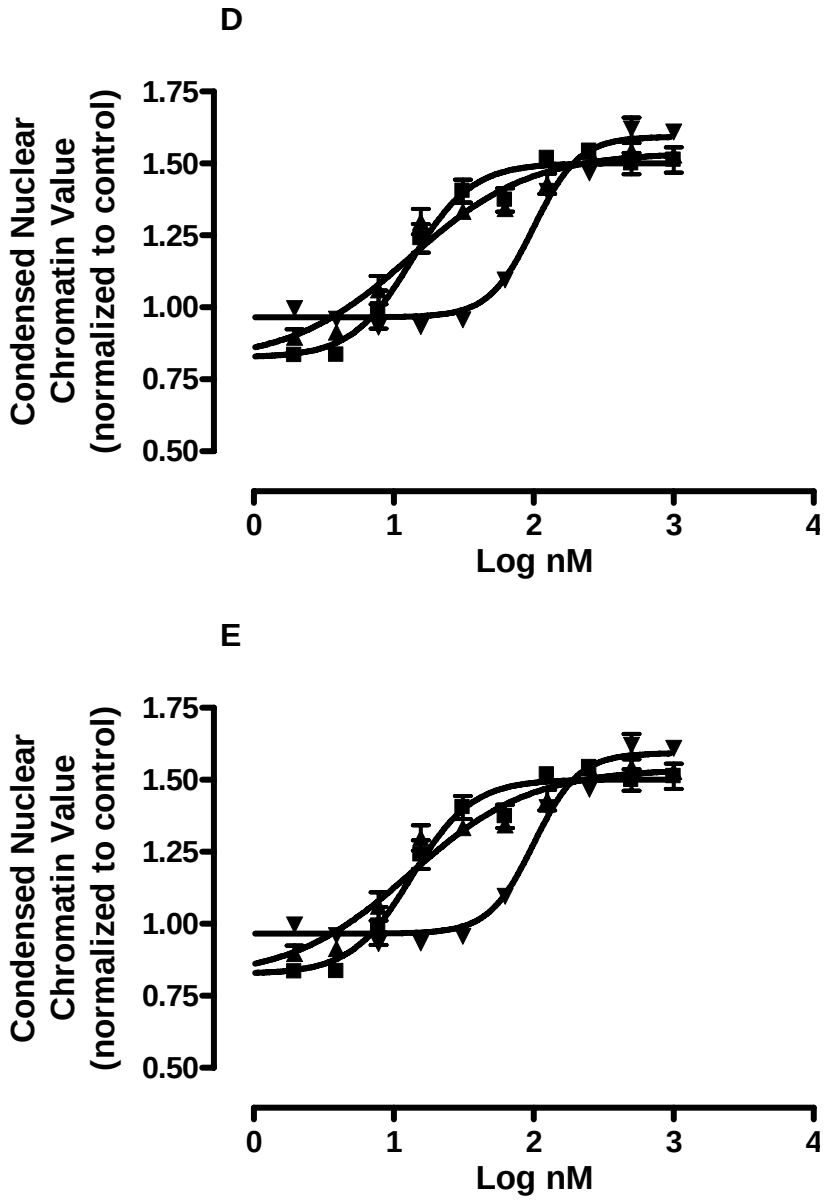

Figure 9D. Condensed nuclear chromatin values in the presence of microtubule stabilizers

Figure 9E. Condensed nuclear chromatin values in the presence of microtubule stabilizers

D, E. Condensed nuclear chromatin value normalized to control. Test agents: dictyostatin (squares), paclitaxel (triangles), discodermolide (inverted triangles, *D*), and normethyldiscodermolide, YSS698-2 (inverted triangles, *E*) on HeLa cells.

Table 11. Minimum detectable effective concentrations

Compound	Minimum detectable effective concentration (nM) (mean±SD., N=4)		
	Average tubulin polymer intensity	**Phosphohistone H3 response**	**Hoechst 33342 intensity**
Dictyostatin	3.6±0.6	5.6±0	6.1±1.5
Paclitaxel	5±1.9	6.0±0.9	7.9±0
Discodermolide	39.8	89.1	56.2
YSS698-2	22.4±0	27±6.5	22.4±0
YSS629	178.7±64	175.6±107	277.2±110
YSS652	531.8±43	398±0	474±39

parent molecule. The C2-*E*, C6-*epi*/C14-*epi* analogue (YSS665-2) and analogues with C19 epimerized and with C6- and C14-*epi* configurations (YSS675-1) or C2-*E*, C6-and C14-*epi* configurations (YSS675-2) were all inactive, yielding flat concentration-response curves. All the dictyostatin analogues, except for the 16-normethyldictyostatin, had higher MDECs when compared with either paclitaxel or dictyostatin.

Representative immunofluorescent images depicting tubulin polymer (FITC: green), condensed nuclear chromatin (Hoechst 33342: blue), and phosphohistone H3 (Cy3: red) intensities are shown in Figure 10A-F. The images depict the quantitative data described above. Dictyostatin induced microtubule bundling and formation of either round or elongated cells having needle-like microtubule morphology (FITC, green). Most of the cells exhibited elevated phosphohistone H3 levels (Cy3, red) and had a rounded shape, indicating that most of the dictyostatin-treated cells were arrested in the G2/M phase of the cell cycle (Figure 10A). The

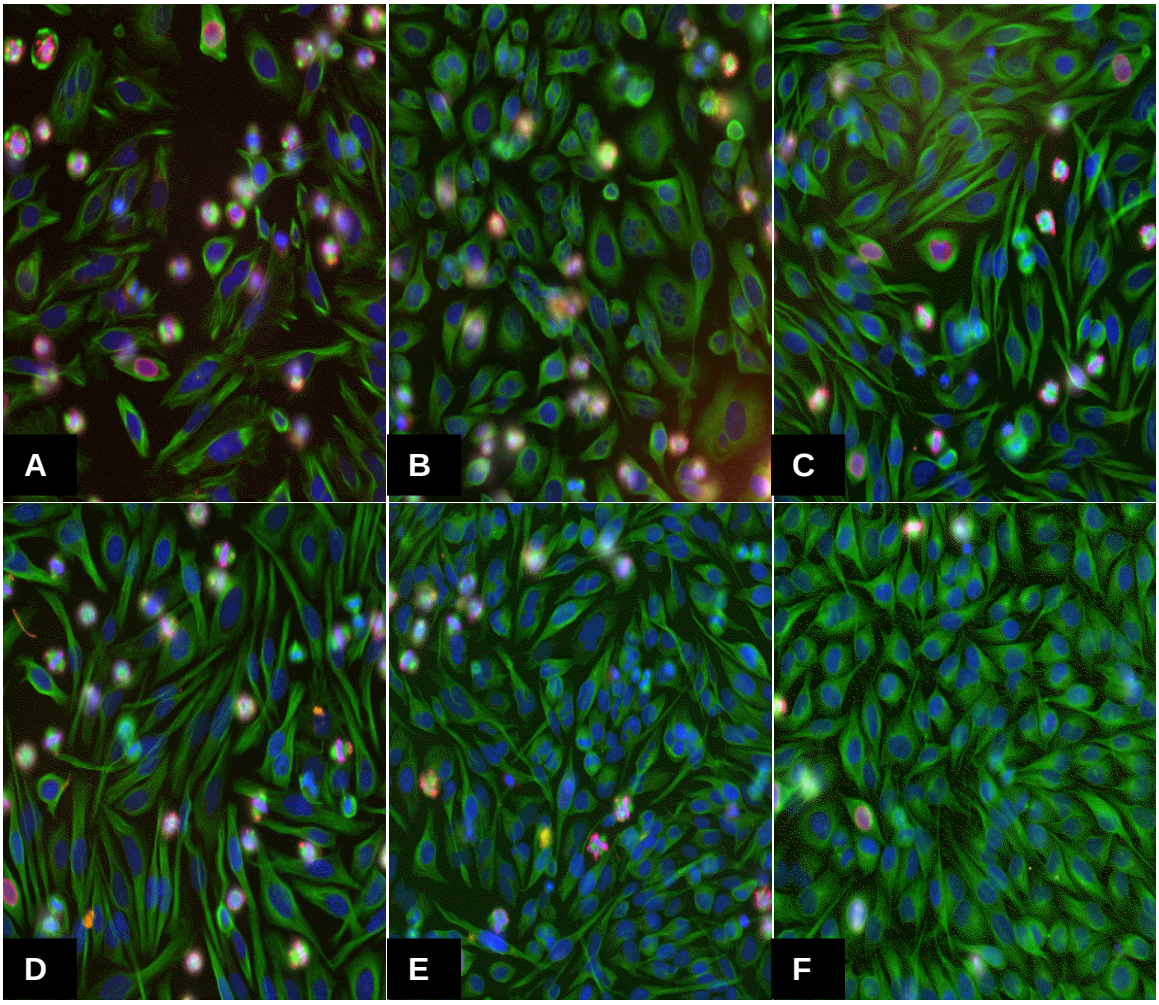

Figure 10. Representative composite immunofluorescent images

A. Dictyostatin (8.5 nM). ***B***. Paclitaxel (12.8 nM). ***C***. Normethyldictyostatin (53 nM). ***D***. YSS629 (250 nM). ***E***. YSS652 (250 nM). ***F***. 4% v/v DMSO. Each image represents FITC: green), condensed nuclear chromatin (Hoechst 33342: blue), and phosphohistone H3 (Cy3: red) fluorescence intensities in the presence of test agents at concentrations corresponding to the EC_{50} values obtained from the objects (i.e., cell nuclei) per field data for each compound. The values in parenthesis next to each test agent represent the EC_{50} values observed for the test agent. Paclitaxel and vehicle (DMSO) are the positive and negative controls, respectively.

cells lost their original architecture, plus attained abnormal subcellular morphology as evidenced by nuclear condensation (Hoechst, blue staining) and membrane blebbing, characteristic of apoptosis. Similar observations were made from discodermolide-treated cells (images not shown, see Balachandran *et al*. 1998). The cells were quite distinct from control (DMSO-treated) cells (Figure 10F). All the above features were also seen upon treatment with paclitaxel (Figure 10B), with the major differences being that the cells had more rounded than elongated features and binucleated or multinucleated cells were more prominent. The analogues YSS698-2, YSS629 and YSS652 elicited similar features with cells showing more elongated microtubule morphology and cells were seen arrested at mitotic and cytokinesis phases (Figure 10C-E). These effects were similar to dictyostatin treated cells, but the intensity to which the analogues exerted cellular response in each case was less than the parent molecule.

Cell cycle distribution data was obtained in order to determine the qualitative and quantitative information about the effects of each compound on cell cycle distribution. Cell cycle profiles for quantification of DNA content were obtained from total Hoechst staining intensity with respect to the cell density (valid cell count/field parameter was used) using S-Plus statistical software. A normal bimodal (first node G1, second node G2/M) distribution pattern of cell cycle is shown in Figure 11. Representations of various distribution patterns of cell cycle upon treatment with an agent that caused cell cycle arrest in a time-dependent manner are given in Figure 11. One of these patterns was observed in the presence of microtubule perturbing agents. Cell cycle analysis and comparison of the cell cycle distribution upon various treatments, shown in Figure 12, were done primarily by examining the shifts in the bimodal distribution pattern with respect to control (DMSO-treated cell). The cell cycle profiles were quantified by taking the ratio of distributions of a given sub population of cells in G2/M and G1 phases.

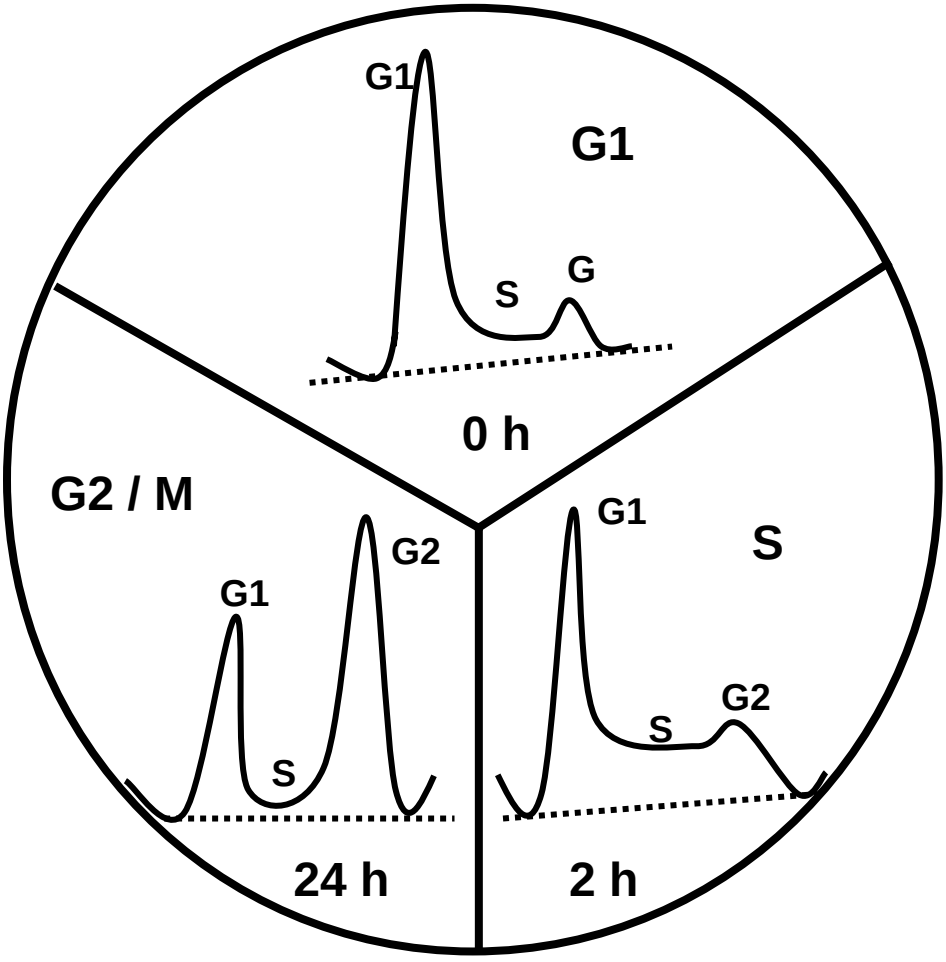

Figure 11. Representation of cell cycle profile during different phases of cell cycle

This image also represents cell cycle distribution in the event of mitotic arrest at G2/M phase.

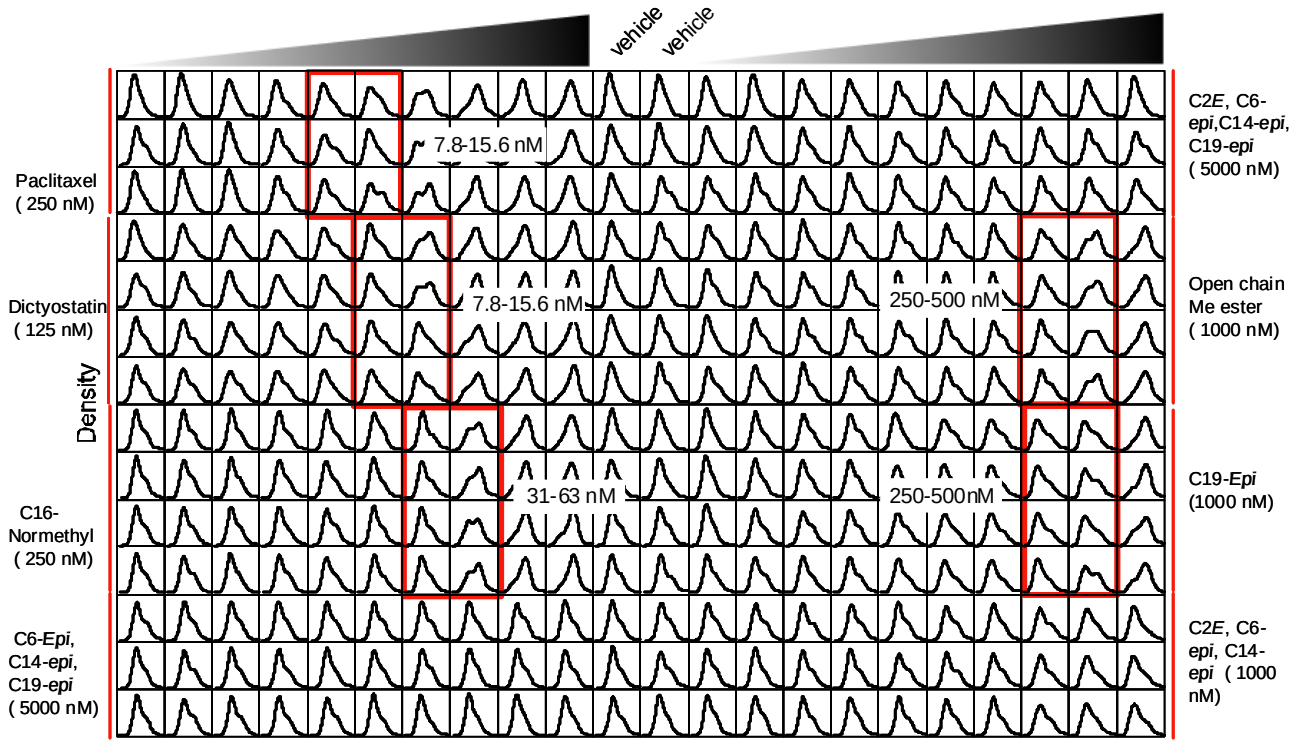

Figure 12. Cell cycle analysis of dictyostatin and synthetic dictyostatin analogues

The starting concentrations for each test agent are represented in parenthesis and concentration of each test agent increased from left to right. Boxes represent the range of concentrations within which the EC_{50}s, calculated from objects per field data, are for each test agent. Each test agent is studied either in triplicate or in quadruplicate (N=3 or N=4). Paclitaxel and vehicle (4% v/v DMSO) are the positive and negative controls, respectively.

Numerical values for distribution of a given sub-population of cells were obtained by estimating the area under each distribution phase of the cell cycle, namely G1 and G2/M phases (data not shown). Vehicle (DMSO)-treated cells had normal cell cycle distribution, meaning that the population histogram of cells was biased to the left due to distribution of the majority of cells in the G1 phase of the cell cycle (Figure 12). Cells that received microtubule stabilizer treatment exhibited a shift in the distribution of cells to the right, indicating an increased number of cells in the G2/M phase of cell cycle. This pattern was observed to be concentration- as well as test agent-dependent, with higher concentrations and more potent compounds showing a strong bias towards G2/M. However, in the presence of inactive compounds, the cell cycle profiles were similar to the negative (DMSO only) controls. Dictyostatin, like paclitaxel, caused extensive changes in the distribution profiles starting from 3-7 nM upward. This data correlates with the EC_{50} values obtained from the objects (i.e., cell nuclei) per field data for each compound.

These values were in the range of 7.8-15.6 nM for dictyostatin and paclitaxel. Concentrations at and higher than 3 nM caused extensive shift towards the right of the cell cycle profiles, suggesting test agent-induced G2/M phase arrest of the cells. C16-Normethyldictyostatin, YSS698-2, was the most potent of the dictyostatin analogues, giving G2/M arrest at around 30-60 nM. The open-chain analogue and the C19-epimer caused G2/M phase arrest in the range of 250-500 nM. All other analogues showed profiles similar to DMSO-treated cells. Analysis of dictyostatin and dictyostatin analogues by this approach suggest that the configurations of the C6 and C14 methyls are important, *anti* positioning of the C6 and C7 functional groups seems mandatory for cellular response, and the natural *E:Z* geometry of the diene seems crucial. The configuration of the C19 and intact macrolactone are also important.

4.4. *In vitro* isolated protein-based experiments

Previous studies have shown that dictyostatin, like discodermolide, promotes tubulin assembly (without MAPs but in the presence of GTP) at lower temperatures (4 ^{o}C), enhanced tubulin assembly much more potently than paclitaxel at 37 ^{o}C, and the microtubule polymer that is formed in the presence of discodermolide was known to be stable under cold conditions as well (Isbrucker *et al*. 2003). It was therefore of interest to determine if dictyostatin and dictyostatin analogues nucleate microtubule assembly much more potently than paclitaxel by direct evaluation of tubulin polymerizing ability. Also important was the evaluation of the effect of MAPs and GTP in modulating the interaction of these agents with tubulin.

4.4.1. Tubulin polymerization activities of dictyostatin

Sequential incubation studies.

Tubulin assembly reactions under various conditions were performed to compare 10 μM dictyostatin, paclitaxel and discodermolide. Polymer development was determined in temperature-controlled spectrophotometers by measuring turbidity at 350 nm. The experimental procedure is described in Chapter 2. Briefly, reaction mixtures consisting of tubulin (1 mg/ml), heat-treated MAPs (0.75 mg/ml, if present), GTP (100 μM, if present), and 0.1M Mes, pH 6.9, were prepared. Baselines were established after addition of all reaction components, except the compounds, to the cuvettes held at 0 ^{o}C. Compounds predissolved in DMSO were added and each reaction mixture (0.25 mL final volume) was subjected to the sequential temperature change studies at the indicated temperatures. The positive controls were either paclitaxel or GTP. The negative control was 4% v/v DMSO. The hypernucleating potencies of the test agents were evaluated by turbidimetry and the morphologies of resulting polymer were evaluated by electron microscopy by simultaneously preparing grids prepared

from aliquots withdrawn from each sample in the cuvette. Polymerization reactions were carried out under four different conditions: tubulin with heat-treated MAPs and with GTP (complete system); tubulin with MAPs (no GTP); tubulin with GTP (no MAPs); and tubulin with no MAPs and with no GTP (tubulin-only system). Tubulin polymerization activity of dictyostatin under various reaction conditions are described in the following paragraphs.

Tubulin with MAPs and with GTP (complete system)

Test agent-induced turbidity profiles in the complete system are shown in Figure 13A. Dictyostatin rapidly initiated polymer formation at 0 ^{o}C. An increase in temperature to 10 ^{o}C resulted in a more extensive assembly reaction as shown by the rapid rise in turbidity readings. A further increase in temperature to 20 ^{o}C showed a slight increase in turbidity, and when temperature was increased from 20 ^{o}C to 30 ^{o}C the assembly reaction reached a plateau. When the temperature was rapidly dropped from 30 ^{o}C back to 0 ^{o}C, the turbidity reading remained unchanged (i.e., the dictyostatin-induced tubulin polymer was completely cold-stable). A similar turbidimetry profile was observed with discodermolide except that at the initial 0 ^{o}C incubation temperature assembly reaction was slightly more vigorous. This pattern has been previously reported (ter Haar *et al*. 1996b). The polymer was also completely cold-stable in the presence of discodermolide. With paclitaxel, as also reported previously, polymer was not observed at 0 ^{o}C but was at 10 ^{o}C. The assembly was not as brisk as that induced by dictyostatin or discodermolide, however. At 20 ^{o}C, the paclitaxel-induced assembly reaction was very vigorous and this continued at 30 ^{o}C, where polymer formation rapidly reached a plateau. When the temperature was dropped to 0 ^{o}C, the paclitaxel-induced polymer was not completely cold-stable. At 30 ^{o}C, all three of the compounds caused similar turbidity readings and that at the initial 0 ^{o}C, dictysostatin, like discodermolide, showed hypernucleation of tubulin assembly. Paclitaxel

lacked this hypernucleating ability at lower temperatures. Although the vehicle (4% DMSO) allowed for GTP-induced polymer formation at 30 ^{o}C, the reaction was far less extensive than that seen with the test agents. The percent microtubule stabilization values relative to that of paclitaxel at 30 ^{o}C were calculated for dictyostatin and discodermolide, after subtraction of the control, GTP-induced values (Table 12).

Tubulin with MAPs (no GTP)

Polymerization reactions carried out with tubulin in the presence of MAPs showed that dictyostatin induced polymer formation at 0 ^{o}C, although the extent of assembly was slightly lower than that seen in the complete system (Figure 13B). Rapid assembly occurred when the temperature was increased stepwise from 0 ^{o}C to 10 ^{o}C to 20 ^{o}C to 30 ^{o}C. The assembly induced at 10 ^{o}C by dictyostatin and discodermolide was nearly identical. At 20 ^{o} and 30 ^{o}C, the reaction was more vigorous with dictyostatin than with discodermolide, and a decrease in the temperature from 30 ^{o} to 0 ^{o}C did not destabilize the polymer induced by dictyostatin nor that induced by discodermolide. In reactions containing paclitaxel, assembly was induced only when the mixture reached 20 ^{o}C, after which polymer formation increased rapidly but the reaction was considerably less vigorous than that observed in the complete system and also as compared with dictyostatin in this system. The polymer formed by paclitaxel was also less cold-stable. DMSO caused some assembly, but only at 30 ^{o}C. The percent microtubule stabilization values for this reaction condition are also presented in Table 12.

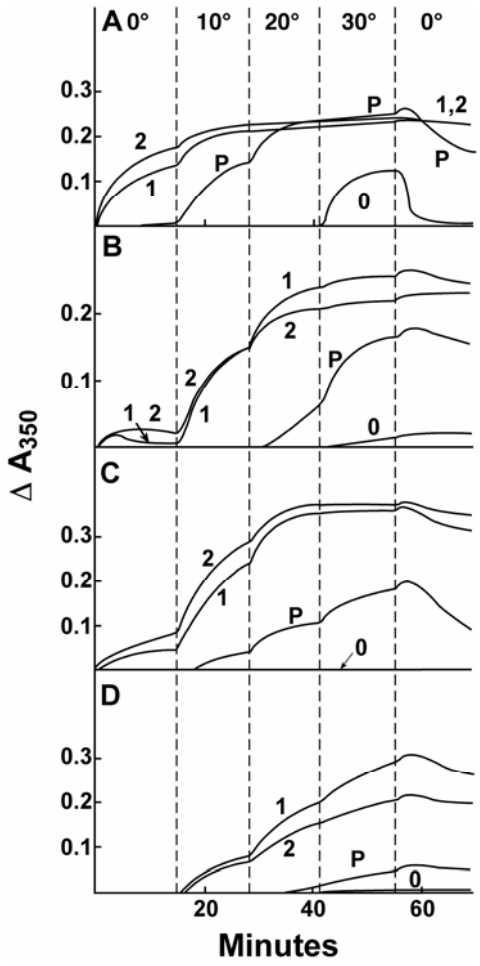

Figure 13. Turbidity profiles of tubulin polymerization assays

Reaction mixtures contained 1.0 mg/mL (10 μM) tubulin, 0.1 M Mes (pH 6.9), 4% (v/v) DMSO, 10 μM test agent, and further additions as indicated. ***A***, Complete system: 0.75 mg/mL MAPs, 100 μM GTP. ***B***, MAPs-only system: 0.75 mg/mL MAPs. ***C***, GTP-only system: 100 μM GTP. ***D***, Tubulin-only system: no further additions. In each panel: ***1***, dictyostatin; ***2***, discodermolide; ***P***, paclitaxel; ***0***, No test agent. Reaction temperatures were as indicated, with the temperature set on the temperature controller at the time indicated by the vertical dashed line to the left of the temperature. Test agents were added to the reaction mixtures at zero time at 0 °C. Temperature in the cuvettes rose at about 0.5 °C/s and fell at about 0.1-0.15 °C/s.

Tubulin with GTP (no MAPs)

Polymer formation occurred more vigorously when the reaction was performed in the presence of tubulin plus GTP than what was seen in the previous two systems (Figure 13C). Dictyostatin, like discodermolide, caused hypernucleation of tubulin assembly at 0 ^{o}C. Stepwise increases in temperature from 0 ^{o}C to 10 ^{o}C to 20 ^{o}C, led to greater turbidity changes with time because of the more extensive assembly reactions. The turbidity changes reached a plateau at 30 ^{o}C. Polymer formed in the presence of dictyostatin and discodermolide was again cold-stable. At all incubation temperatures, the assembly reactions were more vigorous in the presence of dictyostatin than in the presence of discodermolide. Paclitaxel did not induce assembly until the reaction mixture reached 10 ^{o}C. Sequential increases in temperature thereafter caused a gradual increase in turbidity. The paclitaxel-induced assembly was less vigorous than that observed with dictyostatin, and the polymer formed in the presence of paclitaxel was not cold-stable. DMSO (4% v/v) did not cause detectable assembly. Percent microtubule stabilization values for this condition are given in Table 12.

No MAPs, no GTP (tubulin-only system)

In the tubulin-only system, none of the test agents initiated polymerization at 0 ^{o}C (Figure 13D). Turbidity increases were observed for dictyostatin and discodermolide beginning at 10 ^{o}C. Polymer formation induced by these agents was rapid and vigorous when the temperature was raised from 10 ^{o}C to 20 ^{o}C and to 30 ^{o}C. As in the other systems, the polymer induced by dictyostatin and by discodermolide was cold-stable. During the time period analyzed, the turbidity developed in the presence of dictyostatin was greater than that in the presence of discodermolide. With paclitaxel, assembly reactions were slower and polymer formation was observed only from 20 ^{o}C onward, and an increase in the reaction temperature to 30 ^{o}C caused

only a slight increase in turbidity. The paclitaxel-induced polymer formed under these conditions was less cold-labile than the polymer formed by paclitaxel under the three previously discussed reaction conditions. Little or no polymer formed in the presence of DMSO only. Percent microtubule stabilization values are given in Table 12.

Temperature jump studies

The sequential incubation studies performed in the complete and tubulin-only reaction conditions described above revealed turbidity profiles that were quite different. Temperature-jump studies (incubation at 0 ^{o}C followed by a rapid jump in temperature to 30 ^{o}C) were therefore performed to detect any differences in the test agent activities. Polymer morphologies were also examined. Aliquots, withdrawn from each sample at the initial 0 ^{o}C, after the temperature reached 30 ^{o}C and when the temperature was returned to 0 ^{o}C, were placed on grids, stained with uranyl acetate and polymer morphology was examined by electron microscopy.

Complete system.

Dictyostatin, like discodermolide, caused extensive tubulin assembly at 0 ^{o}C (Figure 14A) in the presence of MAPs and GTP. However, discodermolide caused slightly greater increases in turbidity readings than did dictyostatin. At 30 ^{o}C, assembly reactions continued and then reached a plateau. The polymers induced by both dictyostatin and discodermolide were cold-stable. Paclitaxel initiated tubulin assembly at 0 ^{o}C to a slight extent. When the temperature was increased to 30 ^{o}C a very vigorous assembly reaction ensued that rapidly reached a plateau. The ultimate turbidity values caused by paclitaxel at 30 ^{o}C were comparable to those observed with dictyostatin and discodermolide. The paclitaxel-induced polymer was less cold-stable, however. The DMSO control caused some polymer formation at 30 ^{o}C, but the solvent-induced polymer was cold-labile.

Table 12. Percent microtubule stabilization values in the presence of test agents

Percent microtubule stabilization values in all the four reaction conditions studied are presented below. Each reaction mixture consisted of 1 mg/mL tubulin, 0.1M MeS (pH 6.9), 4% DMSO, 10 μM compound, and/or MAPs, and/or GTP. Percent microtubule stabilization is a measure of the polymer-inducing property of a compound.

Reaction Condition/ Compound (Test agent)	% MT Stabilization with respect to Paclitaxel	% MT Stabilization with respect to Discodermolide
A. MAPs+GTP system (complete system)		
Dictyostatin	83	91
Discodermolide	92	100
Paclitaxel	100	>100 (109)
B. MAPs only system		
Dictyostatin	>100 (160)	>100 (120)
Discodermolide	>100 (133)	100
Paclitaxel	100	75
C. GTP only system		
Dictyostatin	>100 (226)	97
Discodermolide	>100 (232)	100
Paclitaxel	100	43
D. No MAPs + No GTP (tubulin only system)		
Dictyostatin	> 100 (800)	>100 (155)
Discodermolide	>100 (569)	100
Paclitaxel	100	18

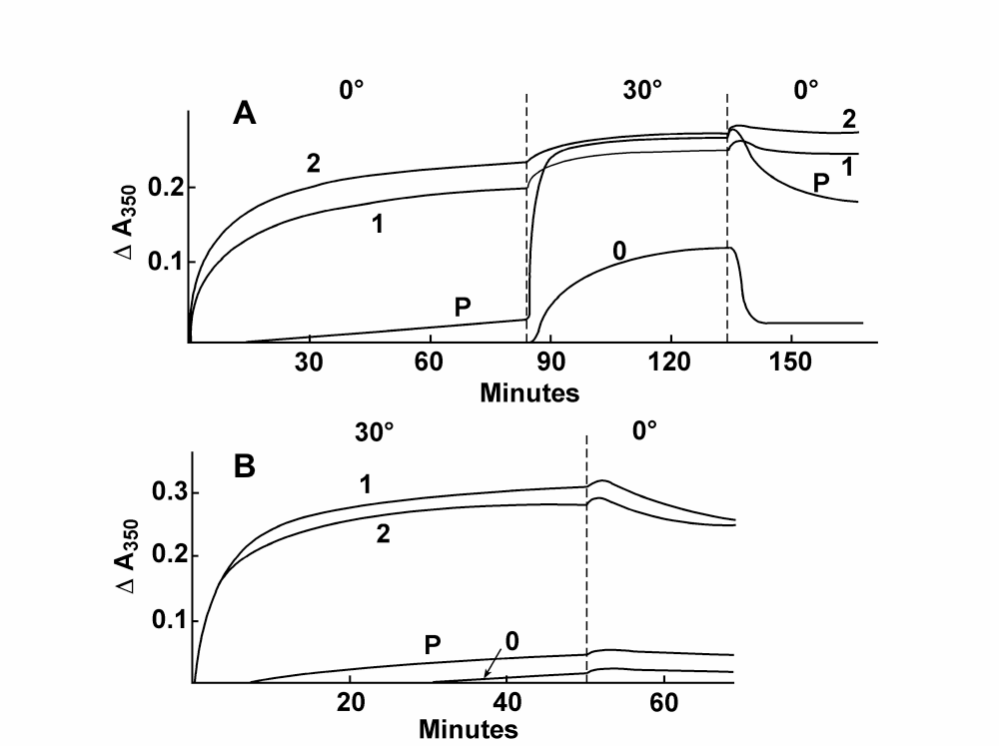

Figure 14. Turbidity profiles of tubulin polymerization assays

Each reaction mixture contained 1.0 mg/mL (10 μM) tubulin, 0.1 M Mes (pH 6.9), 4% DMSO, 10 μM test agent and further additions as indicated. ***A***, Complete system: 0.75 mg/mL MAPs, 100 μM GTP. ***B***, Tubulin-only system: no further additions. In each panel: ***1***, dictyostatin; ***2***, discodermolide; ***P***, paclitaxel; ***0***, No test agent. Reaction temperatures were as indicated by the vertical dashed line to the left of the temperature. See legend of Figure 7 for further details. For panel ***A***, test agents were added to reactions at zero time at 0 ^{o}C. For panel ***B***, test agents were added to reaction mixtures at 0 ^{o}C, and the temperature controller was set at 30 ^{o}C at zero time.

Tubulin-only system.

With tubulin only, none of the compounds induced assembly at 0 ^{o}C. When the temperature was increased to 30 ^{o}C, dictyostatin and discodermolide induced rapid and brisk assembly (Figure 14B). Turbidity values observed with dictyostatin were greater than those observed with discodermolide. Paclitaxel caused a slight but considerably lower induction of polymer formation at 30 ^{o}C. Polymer induced by dictyostatin and by discodermolide was stable at 0 ^{o}C. Paclitaxel-induced polymer was less cold-stable, but more so than paclitaxel-induced polymer formed in the complete system. DMSO caused very little, if any, polymer formation.

4.4.2. Tubulin polymerization activities of dictyostatin analogues

Tubulin polymerization activity was determined under complete reaction conditions consisting of tubulin (1 mg/mL), MAPs (0.75 mg/ml), GTP (100 μM), and dictyostatin analogues at either 10 or 40 μM. Turbidity profiles show that the open-chain and the C19-*epi* analogues, YSS629 and YSS652, although less active than the parent molecule, induced tubulin polymerization even at lower temperatures (<30 ^{o}C). Under the reaction condition studied, at 10 μM, YSS629 induced tubulin assembly from 10 ^{o}C onward and the reaction was vigorous at 20 ^{o}C and 30 oC. However, the microtubule polymer formed was not cold-stable (Figure 15B). YSS652 also induced polymer formation at 20 ^{o}C onward, but the polymer mass as read from turbidity readings was lower than that observed in the presence of YSS629 (Figure 15A). The assembly reaction was less vigorous at 30 ^{o}C and the polymer was not cold-stable. YSS133 (previous chapter) induced tubulin assembly from 20 ^{o}C onward, the reaction was rapid at 30 ^{o}C and the polymer formed was also cold-stable (Figure 15C). Tubulin polymerization assays done with the other analogues did not give promising results. YSS479, YSS665, YSS675-1 and YSS675-2 when studied at 10 μM, were very weak in inducing tubulin assembly even at 30 ^{o}C

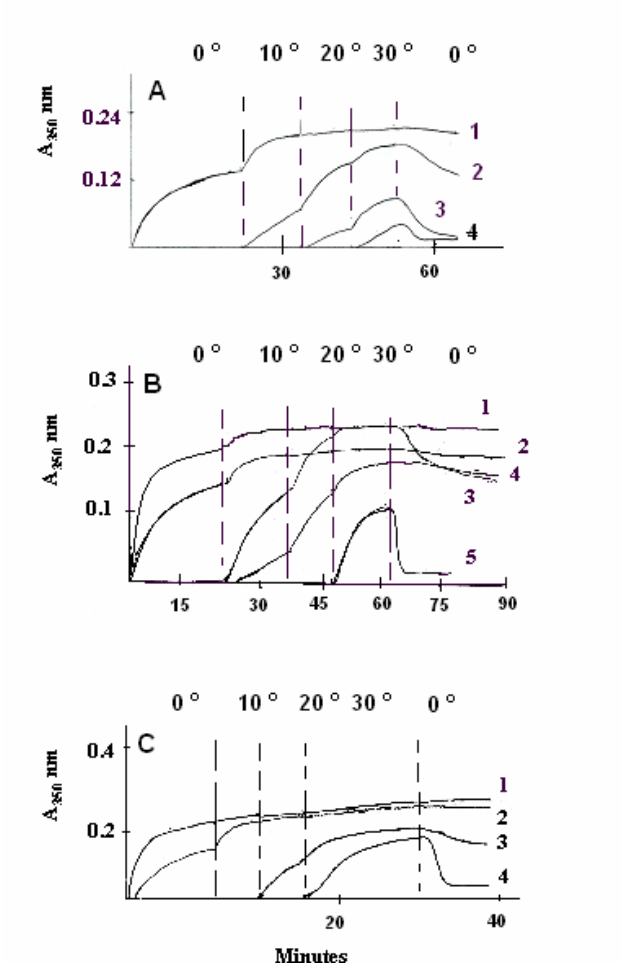

Figure 15. Turbidity profiles in the presence of dictyostatin analogues

Reaction mixtures contained 1.0 mg/mL (10 μM) tubulin, 0.1 M Mes (pH 6.9), 4% (v/v) DMSO, 10 μM test agent, 0.75 mg/mL MAPs, and 100 μM GTP. Reaction temperatures were as indicated, with the temperature set on the temperature controller at the time indicated by the vertical dashed line to the left of the temperature. Test agents were added to the reaction mixtures at zero time at 0 °C.

Panel *A*: ***1***, dictyostatin; ***2***, paclitaxel; ***3***, YSS652; ***4***, No test agent.

Panel *B:* ***1***, dictyostatin; ***2***, discodermolide; ***3***, paclitaxel; ***4***, YSS629; ***5***, No test agent.

Panel C: ***1***, dictyostatin; ***2***, discodermolide; ***3***, YSS133; ***4***, No test agent.

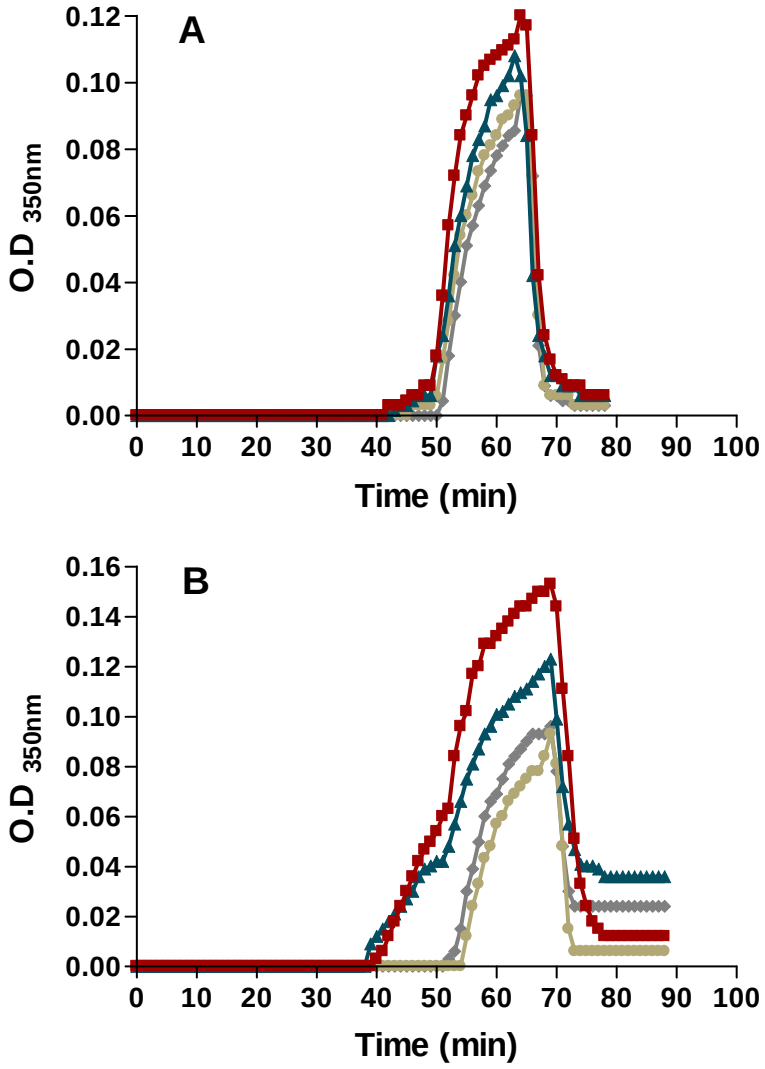

Figure 16. Turbidity profiles for dictyostatin analogues

Reaction mixtures contained 1.0 mg/mL (10 μM) tubulin, 0.1 M Mes (pH 6.9), 4% (v/v) DMSO, 10 μM or 40 μM test agent, 0.75 mg/mL MAPs, and 100 μM GTP. Reaction temperatures were as indicated, with the temperature set on the temperature controller at the time indicated by the vertical dashed line to the left of the temperature. Test agents were added to the reaction mixtures at zero time at 0 °C. **A**: 10 μM dictyostatin analogues. YSS675-2 (brown); YSS675-1 (rust/brick red); YSS665 (blue); no test agent (gray). **B**: 40 μM dictyostatin analogues. YSS675-2 (brown); YSS675-1 (rust/brick red); YSS665 (blue); no test agent (gray).

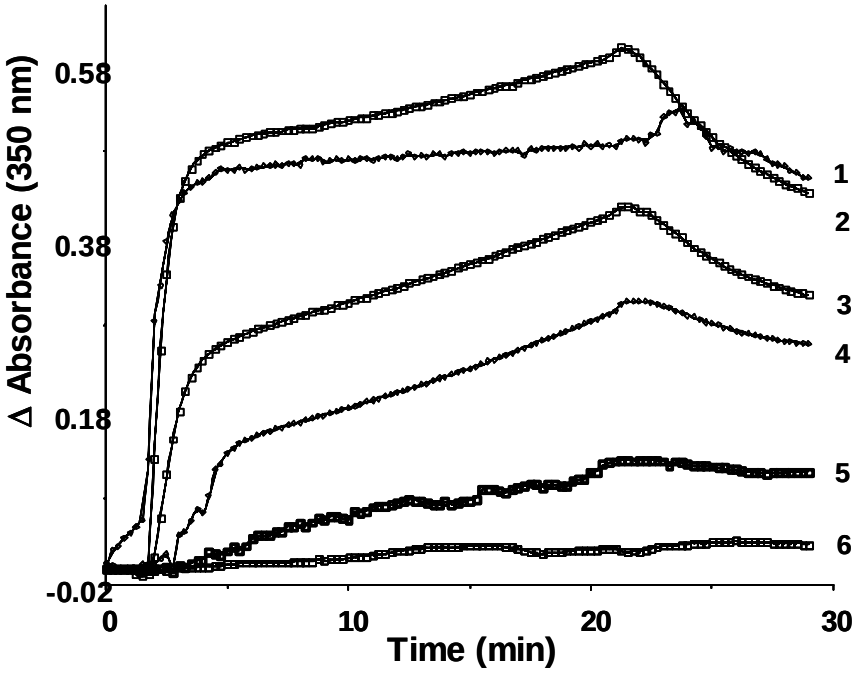

Figure 17. Turbidity profiles of tubulin polymerization assays for 16-normethyldictyostatin
Each reaction mixture contained 1.0 mg/mL (10 μM) tubulin, 0.75 M MSG (pH 6.6), 4% DMSO, test agent as indicated. ***6***, No test agent; ***1***, 10 μM discodermolide; ***5***, 5 μM 16-normethyldictyostatin; ***4***, 10 μM 16-normethyldictyostatin; ***3***, 20 μM 16-normethyldictyostatin; ***2***, 40 μM 16-normethyldictyostatin. Test agents were added to reaction mixtures at 0 ^{o}C (set for 1 min), and the temperature controller was set at 30 ^{o}C starting from 1 min until 20 minutes after which the temperature was dropped back to 0 ^{o}C.

and the polymer formed was cold-labile (Figure 16A). When YSS665, YSS675-1 and YSS675-2 were studied at 40 μM, although the turbidity values were slightly greater than that seen with

compounds at 10 μM concentration at 30 ^{o}C, the overall assembly reactions were weak and polymer formed was not cold-stable (Figure 16B). Figure 17 represents the tubulin polymerization activity of the normethyl analogue, YSS698-2, showing it to be an interesting compound. It potently induced tubulin polymerization at lower concentrations (5 μM) as well as lower temperature and showed a concentration-dependent increase in polymer formation. However, MAPs were replaced by 0.75 M MSG in the experiment with this analogue. This data suggests that YSS698-2 might hypernucleate tubulin assembly like the parent molecule.

4.4.3. Electron microscopy studies

Electron microscopic evaluation of test agent-induced polymer morphology.

The immunofluorescence studies that demonstrated mitotic arrest (*vide supra*), are consistent with the enhanced turbidity development observed with dictyostatin representing drug-induced MT assembly. Nevertheless, it was important to demonstrate this by electron microscopic observation. Tubulin polymer formed in the presence of small molecule test agents and detected by turbidimetry can appear in a variety of forms. "Normal" polymer is microtubules, but near-normal (e.g., sheets) and abnormal (e.g., spirals, crystals, amorphous solid) polymers have been observed. Previous experiences in the Day laboratory with discodermolide and paclitaxel showed that these agents induce polymer largely in the form of microtubules, so it was of interest to evaluate the differences, if any, of the polymer morphologies caused by dictyostatin in complete and tubulin-only systems.

Complete system.

Electron microscopic analysis of polymer induced by dictyostatin and discodermolide at 0 ^{o}C showed it to be largely in the form of microtubules. In the presence of dictyostatin, microtubules were shorter in length than those observed from the discodermolide sample (Figure

18C *versus* 18D, Table 13). As expected, since the hypernucleating ability of paclitaxel at this temperature is low, very few microtubules were seen in any given electron microscopic field (Figure 18B). At 30 ^{o}C, all three of the compounds caused extensive microtubule polymer formation as seen in the EM images (Figure 18F-H). However, the lengths of the polymer measured, in each case, was an approximate estimation since full length polymer couldn't be measured accurately. This is because at 30 ^{o}C, abundant polymer formation occurred unlike that observed at 0 ^{o}C. Polymer formed in the presence of either dictyostatin or discodermolide was mostly in the form of either short microtubules or ribbons (Figure 18G-H). The majority of the microtubules formed by paclitaxel at this temperature had curved ends, and the polymer showed some morphology in the form of ribbons (Figure 18F). Many of the paclitaxel-induced microtubules also showed characteristic peeling of apparent protofilaments at their ends. The polymer morphology observed at 30 ^{o}C in the presence of dictyostatin or discodermolide was retained when the temperature was decreased to 0 ^{o}C (data not shown). In agreement with the turbidity profile, EM analysis of the polymer in the paclitaxel sample after it was returned to 0 ^{o}C showed a large decrease in the microtubule mass as compared to the sample taken at 30 ^{o}C (data not shown). Under both temperature conditions, 0 ^{o} and 30 ^{o}C, no polymer formed in the absence of test agent (Figure 18A & E).

Tubulin-only reaction condition.

Dictyostatin and discodermolide at 30 ^{o}C both caused formation of tubulin polymer, although not as extensive as that observed with the complete system. Interestingly, mostly ribbon-like structures along with microtubules were noted (Figure 18K-L). Discodermolide- and dictyostatin-induced polymer showed ring-like morphology (abnormal polymer) that was not

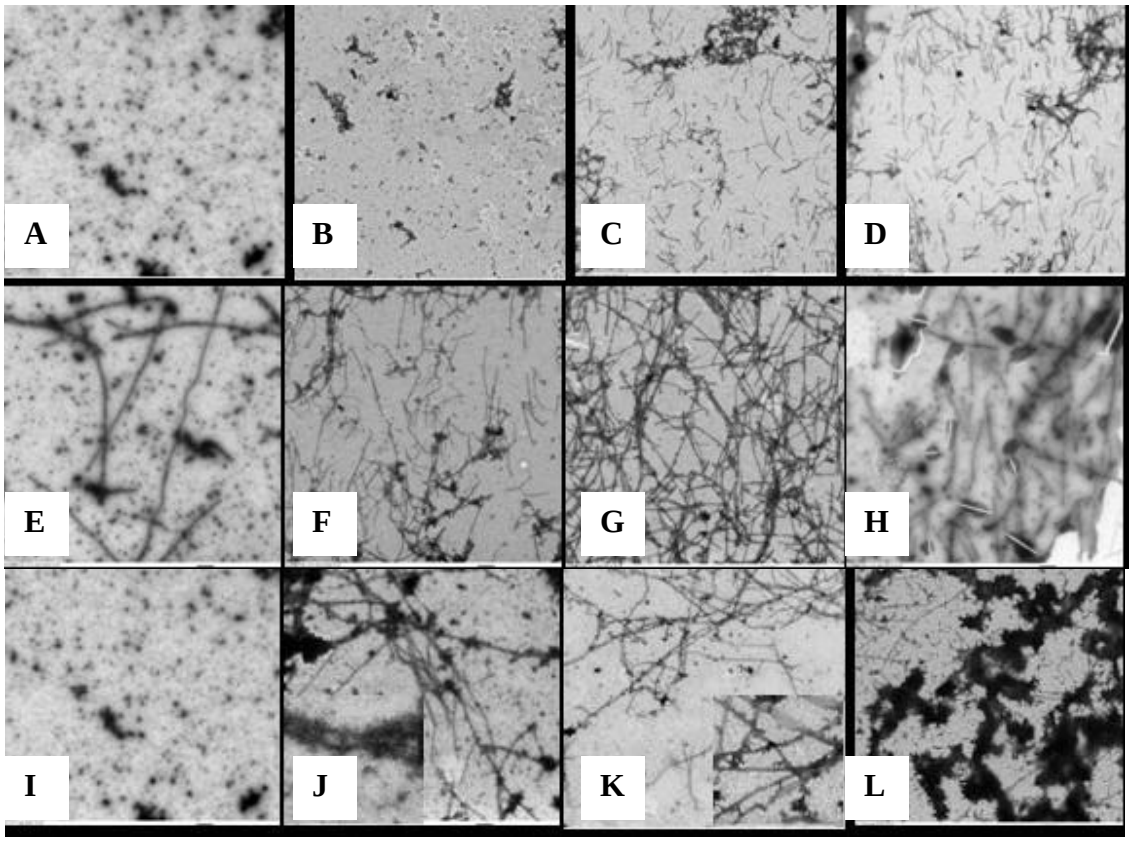

Figure 18. Electron microscopy images from complete and tubulin-only systems

Images A-D: Electron microscopic observation of the polymer formed in the presence of microtubule stabilizers under complete reaction conditions at 0 ^{o}C. A: 4% DMSO; B: 10 μM Paclitaxel; C: 10 μuM Dictyostatin; D: 10 μM Discodermolide.

Images E-H: Electron microscopic observation of the polymer formed in the presence of microtubule stabilizers under complete reaction conditions at 30 ^{o}C.

E: 4% DMSO; F: 10 μM Paclitaxel; G: 10 μM Dictyostatin; H: 10 μM Discodermolide.

Images I-L: Electron microscopic observation of the polymer formed in the presence of microtubule stabilizers under tubulin-only reaction conditions at 30 ^{o}C. I: 4% DMSO ; J: 10 μM Paclitaxel; K: 10 μM Dictyostatin; L: 10 μM Discodermolide.

Table 13. Microtubule polymer lengths in the presence of microtubule stabilizers

Each reaction mixture consisted of 1 mg/mL tubulin, 0.1M MeS (pH 6.9), 4% DMSO, 10 μM compound, and/or 0.75 mg/mL MAPs, and/or 100 μM GTP.

Reaction condition/ Compound (Test agent)	**Microtubule length (μm)** 0 °C	30 °C
A. MAPs+GTP system (complete system)		
Dictyostatin	0.34 ± 0.02(70)*	1.1 ± 0.2(87)
Discodermolide	0.42 ± 0.07(78)	0.9 ± 0.1(51)
Paclitaxel	-	0.8 ± 0.02(3)
B. No MAPs + No GTP (tubulin-only system)		
Dictyostatin	-	2.0 ± 0.8(4)
Discodermolide	-	1.2 ± 0.7(3)
Paclitaxel	-	3.4 ± 0.9(4)

* number of microtubules measured is indicated in parenthesis.

seen with paclitaxel-induced polymer. These subtle differences could be accounted for MAPs and/or GTP in the reaction system, since in the complete system ring-like structures were not

observed. Paclitaxel at 30 ^{o}C induced formation of ribbons mostly and also some microtubules, though not as extensive as that seen in the complete system (Figure 18J). When the temperature was dropped to 0 ^{o}C, paclitaxel-induced polymer lost this morphology (since the paclitaxel-induced polymer is more cold-labile). The polymer induced by dictyostatin and discodermolide was, however, cold stable. DMSO treated protein did not show polymer formation under these conditions (Figure 18I).

To summarize the current studies, for any given reaction condition, there was little overall difference in morphology of the polymer formed with any of the test agents in that microtubules and ribbon polymers were seen under all conditions. While relative proportions seemed to vary, this was difficult to quantitate. Under both reaction conditions chosen, no polymer formed in the absence of test agent. Figure 19A shows the short MTs and ribbons, observed in the complete system after 1 h at 0 ° and 30 ^{o}C in the presence of dictyostatin. Figure 19B shows the polymer, mostly in the form of short ribbons, observed in the tubulin-only system after 1 h at 30 °C in the presence of dictyostatin.

4.4.4. Relative polymer-inducing potencies of dictyostatin and discodermolide

The turbidimetry studies presented in Figures 13 and 14 indicated dictyostatin and discodermolide to have similar potencies as inducers of tubulin assembly. A more quantitative measurement of their relative activities were desired; to achieve this, two types of experiments were performed. 1) critical concentration 2) centrifugation or pelleting assay.

Critical concentration experiments.

The hypernucleating ability of a microtubule-stabilizing agent can be quantitatively evaluated/assessed by determining the critical concentration (Cc) of tubulin required for initiation of polymer formation in the presence of the agent (Grover *et al*. 1995). The Cc of a

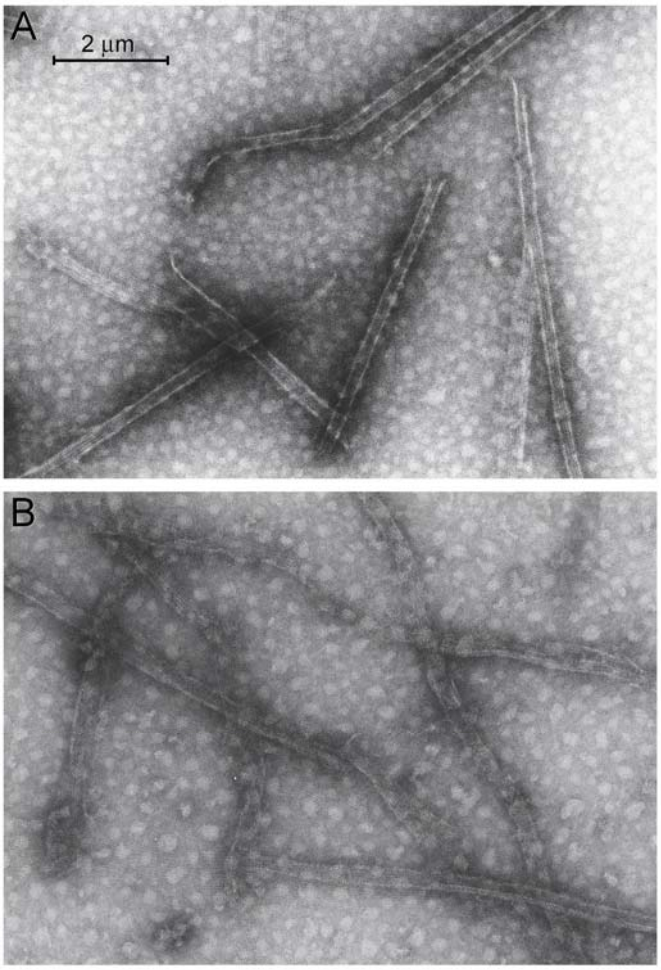

Figure 19. Electron micrographs of dictyostatin-induced polymer

Microtubules formed in the complete system (*A*) and in the tubulin-only system (*B*).

The reaction mixtures were followed spectrophotometrically and prepared as described in Figure 5, with aliquots removed from the cuvettes either at the end of the 0 ^{o}C incubation (***A***) or the end of the 30 ^{o}C incubation (***B***).

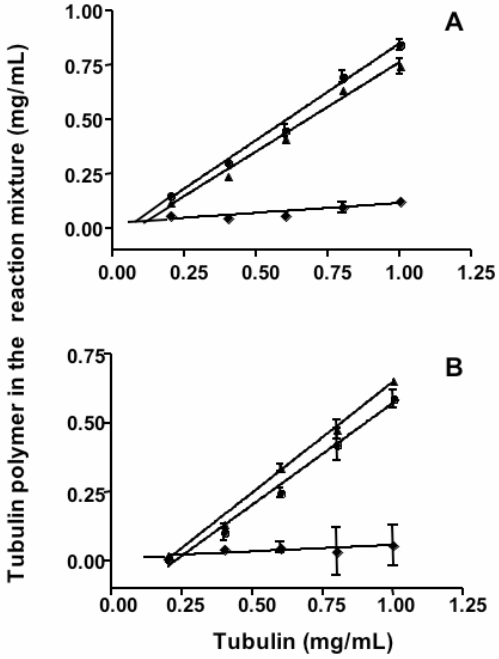

Figure 20. Tubulin critical concentration determinations

A, Complete system. ***B***, Tubulin-only system. In both panels: no test agent, diamonds; dictyostatin, circles; discodermolide, triangles. The critical concentration was the intersection of the interpolated control and test agent regression lines. The abscissa shows the concentrations of tubulin (mg/mL), while the ordinate values show the polymerized tubulin (mg/mL) present in the reaction mixture. Each data point was determined in triplicate. The concentration of dictyostatin or discodermolide was 10 μM. Critical concentration values in the complete system were 0.06 μM (0.006 mg/mL) for dictyostatin and 1.0 μM (0.1 mg/mL) for discodermolide. In the tubulin-only system, the critical tubulin concentrations were 2.5 μM (0.25 mg/mL) for dictyostatin and 2.1 μM (0.21 mg/mL) for discodermolide.

test agent is a function of both its nucleation properties and its binding affinity to the polymer. Experiments to determine Cc were performed under complete and tubulin-only reaction conditions to help explain if there is a difference in the nucleation reactions between dictyostatin and discodermolide. The details of the experiment are described in Chapter 2. Reaction mixtures contained tubulin (1 mg/mL), MAPs and GTP (0.75 mg/mL and 100 μM, respectively), if required, in 0.1M Mes, pH 6.9. Reaction mixtures with test agent or 4% v/v DMSO were incubated at 37 ^{o}C for 30 min following which the samples were centrifuged at 14,000 rpm for 15 min at RT. The supernatants were collected and assayed by the Lowry method for protein quantitation. The results showed that in the complete system the tubulin Cc was 0.6 μM for dictyostatin and 1.0 μM for discodermolide (Figure 20A). In the tubulin-only system, the critical concentrations increased to 2.5 μM for dictyostatin and to 2.1 μM for discodermolide (Figure 20B). These studies further demonstrated that the nucleation properties and polymer-inducing abilities of dictyostatin were slightly greater than those of discodermolide in the complete system, and in the tubulin-only reaction conditions these properties were nearly identical for the two compounds. In an earlier study (Kowalski *et al*. 1997) utilizing the tubulin-only system, Cc values of 1.5 and 5.9 μM were obtained for discodermolide and paclitaxel, respectively. This data suggests that MAPs and/or GTP play a very important role in the nucleation step during the polymerization reaction. Probably, these regulatory elements stabilize the nucleation centers as well as the microtubules in the presence of paclitaxel. The Gibb's free energy calculations were done from critical concentration values for dictyostatin and discodermolide in order to determine the energetics of the nucleation process. The data is presented in Table 14. This data shows the difference in free energetics between the complete system and tubulin-only system. MAPs and GTP lower the energetics required for nucleation

and promote microtubule stabilization. The Gibb's free energy values also underline the fact that MAPs and GTP play a crucial role in the energetics of binding in the presence of dictyostatin or discodermolide. In the complete system, dictyostatin had lower Gibb's free energy for hypernucleation (-14.5 Kcal/mol) than discodermolide (-14.2 Kcal/mol). The free energies for hypernucleation were quite low for complete system than for tubulin-only system. This is true for dictyostatin as well as discodermolide.

Pelleting Assay.

Centrifugation experiments were designed to quantitatively compare the tubulin polymerizing effectiveness of dictyostatin against those of discodermolide and paclitaxel. The

Table 14. Summary of critical concentration and Gibb's free energy calculations

Critical concentrations for dictyostatin and discodermolide for complete and tubulin-only systems are tabulated below. Gibb's free energy calculations were done for 37 ^{o}C reaction condition.

System/Compound	Critical concentration (μM) (N=3)	Gibb's free energy (Kcal/mol)
	Complete system	
Dictyostatin	0.6	-14.5
Discodermolide	1.0	-14.2
	Tubulin-only system	
Dictyostatin	2.5	-13.7
Discodermolide	2.1	-13.6

assay was performed under the reaction condition that employed 0.2 M MSG, 10 μM nucleotide-free tubulin, 5% v/v DMSO and varying drug concentrations. The protein concentrations in supernatants from each centrifugation run were determined by the Lowry method. Data is

presented in Table 15. The quantitative measure chosen to compare the polymer-inducing properties of these compounds was the EC_{50} value, the concentration of test agent required to polymerize 50% of tubulin with respect to the control incubation. This assay exploits the interaction of MSG and tubulin in assembly reactions. In the absence of GTP, tubulin assembly will not occur in MSG unless a taxoid-mimetic agent is present. In the case of paclitaxel, detailed studies show that the lower the MSG concentration the higher the EC_{50} value. Thus, the assay can be modulated to study taxoid site drugs both less active and more active than paclitaxel. In the studies summarized in Table 15, a low concentration of MSG (0.2 M) was used because of the potent activity of dictyostatin and discodermolide. Dictyostatin seemed slightly more active than discodermolide. The EC_{50} for dictyostatin (3.1 μM) was slightly lower than that observed for discodermolide (3.6 μM). Paclitaxel was less active and yielded a 7-fold higher EC_{50} (25 μM) than that observed for dictyostatin. Along with dictyostatin, its synthetic analogues were also evaluated for their ability to promote tubulin polymerization. The centrifugation assay for the analogues was performed under three different reaction conditions. Reaction condition 1 was similar to the one described for analyzing dictyostatin. The activity of percent tubulin polymerized was assessed under other two reaction conditions, 2 and 3, to see if there would be any enhancement in the tubulin polymerization activity of the analogues. The MSG and GTP percent in reaction conditions 2 and 3 are varied and are described in Table 15. Quantitative analysis of the data showed that all the analogues had EC_{50} values greater than 50 μM under reaction condition 1 (Table 15). These values were higher than that observed for dictyostatin. The EC_{50} value observed for dictyostatin under these conditions was 3.1±0.2 μM.

Table 15. Tubulin polymerization abilities of dictyostatin analogues

Compound	[a]Reaction condition 1		[b]Reaction condition 2	[c]Reaction condition 3
	EC_{50} (μM) ± S.D (N)	**% of Control at 50 μM**	**% of Control at 10 μM**	**% of Control at 10 μM**
Dictyostatin	3.1 ± 0.2 (3)	N/D	38	16
Discodermolide	3.6 ± 0.4 (3)	N/D	37	14
Taxol	25 ± 3 (3)	N/D	42	20
YSS-629	> 50 (2)	71 ± 7	51	34
YSS-652	> 50 (2)	70 ± 2	71	67
YSS-133	> 50 (2)	95 ± 4	66	53
YSS-665	> 50 (2)	99 ± 1	96	100
YSS-675-1	> 50 (2)	95 ± 1	100	97
YSS-675-2	> 50 (2)	95 ± 4	94	100

[a]:reaction condition 1 is 0.2M MSG, 10 μM tubulin, and 5% DMSO; [b]:reaction condition 2 is 0.8M MSG, 400 μM GTP, 10 μM tubulin, and 5% DMSO; [c]:reaction condition 3 is 0.6M MSG, 200 μM GTP, 10 μM tubulin, and 5% DMSO.

Under the other two reaction conditions there was very little improvement in the polymerization ability of the analogues. The percent tubulin polymerized with 10 μM test agent with respect to control is reported for these two conditions as well. From this data, it appears thatYSS629, YSS133 and YSS652 had moderate activity with percent unpolymerized values (with respect to control) of 51, 66 and 71 respectively, under reaction condition 2. In the presence of dictyostatin, the percent tubulin unpolymerized with respect to control was about 40. The percent unpolymerized values were 34, 53, and 67, for compounds YSS629, YSS133 and YSS652, respectively, studied at 10 μM with reaction condition 3. Dictyostatin had a percent unpolymerized value of 16 under these reaction conditions. This data also shows that YSS479, YSS665, YSS675-1 and YSS675-2 had weak tubulin polymerizing ability. The EC_{50} value for

the normethyl analogue, YSS698-2, was estimated from the turbidity readings (Figure 17) and the value was around 14±7.

4.4.5. Paclitaxel-site binding experiments

Binding experiments with dictyostatin

Previous work shows that discodermolide strongly inhibited the binding of radiolabeled paclitaxel to tubulin polymer (ter Haar *et al*. 1996b), while paclitaxel has little ability to inhibit the binding of radiolabeled discodermolide to polymer (Hung *et al*. 1996b). Epothilone B also binds the taxoid site and potently inhibits paclitaxel from binding to tubulin polymer (Kowalski *et al*. 1997). Moreover, studies with radiolabeled paclitaxel at 37 °C have indicated the following order of affinity of taxoidmimetic drugs for the taxoid site: paclitaxel/epothilone A < docetaxel/epothilone B < discodermolide (Hamel *et al*. 1999). More precise measurements of K_a values for the taxoids and epothilones, obtained by measuring inhibition of binding of a fluorescent taxoid to MTs (Buey *et al*. 2004), show the affinity of epothilone B to be significantly greater than the affinities of paclitaxel, docetaxel, and epothilone A (the K_a values at 37 °C for the four compounds were reported to be, respectively, 61, 1.1, 3.1, and 2.9 x 10^7 M^{-1}). Since the structure of dictyostatin so closely resembles that of discodermolide, we anticipated that it would inhibit [^{3}H]paclitaxel, [^{3}H]discodermolide and [^{14}C]epothilone B from binding to tubulin polymer.

Dictyostatin, paclitaxel, discodermolide, epothilone B and docetaxel were examined for their abilities at 4 μM to displace these radioligands at 2 μM from polymer induced by ddGTP from 2 μM tubulin. The percent inhibition values for dictyostatin and the other compounds are shown in Table 16. Dictyostatin potently displaced [^{3}H]paclitaxel bound to tubulin polymer (75% inhibition). Discodermolide yielded a similar value (76% inhibition). When

[^{3}H]discodermolide was used as the tracer, dictyostatin displaced less than 50% of the radioligand. None of the test agents studied were as potent as dictyostatin at displacing bound [^{3}H]discodermolide: epothilone B, paclitaxel and docetaxel only weakly displaced [^{3}H]discodermolide, yielding inhibition values of ca. 10% (Table 16). The data also suggests that discodermolide has a stronger affinity for tubulin polymer than does paclitaxel and epothilone B, and that dictyostatin has a similar affinity. The value for dictyostatin found with polymer bound [^{14}C]epothilone B (88% inhibition) was again essentially identical to that obtained for discodermolide (90%).

Epothilone A and docetaxel had negligible inhibitory effects on the binding of [^{3}H]discodermolide, intermediate effects on the binding of [^{14}C]epothilone B, and their greatest inhibitory effects on the binding of [^{3}H]paclitaxel to tubulin polymer. However and for unknown reasons, the maximum inhibitory effect observed with the tritiated ligands (paclitaxel and discodermolide) is 70-80%, while total inhibition of [^{14}C]epothilone B binding could be observed. This provided further evidence that the activity of dictyostatin is comparable to that of discodermolide in this assay and that the two compounds have the same or very similar binding sites on tubulin polymer. Displacement of 2 μM [^{3}H]discodermolide by 20 μM dictyostatin, paclitaxel and epothilone was also examined. Dictyostatin was by far the most effective of the three in displacing discodermolide. The effects of lower concentrations of dictyostatin and discodermolide on paclitaxel and epothilone B binding were also examined, and again little difference was observed between the two compounds. These competition experiments provided conclusive evidence that dictyostatin binds the taxoid site on tubulin polymer, and that it is the most effective of the test agents in displacing discodermolide from this site.

Table 16. Percent radioligand inhibition by test agents.

Percent inhibition values are expressed as mean±S.D (N).

Inhibitor	% Inhibition of [^{3}H]discodermolide binding	% Inhibition of [^{14}C]epothilone B binding	% Inhibition of [^{3}H]paclitaxel binding
4 μM discodermolide	nd[a]	90 ± 1 (3)	76 ± 6 (4)
4 μM dictyostatin	40 ± 3 (3)	88 ± 1 (3)	75 ± 5 (3)
20 μM dictyostatin	70 ± 1 (2)	nd	nd
4 μM epothilone B	14 ± 3 (3)	nd	71 ± 5 (4)
20 μM epothilone B	31 ± 6 (2)	nd	nd
4 μM paclitaxel	6 ± 5 (3)	26 ± 1 (3)	nd
20 μM paclitaxel	3 ± 4 (2)	nd	nd
4 μM docetaxel	8 ± 6 (3)	36 ± 1 (3)	63 ± 8 (4)
4 μM epothilone A	6 ± 6 (3)	25 ± 3 (3)	53 ± 4 (4)

[a]: not determined

Binding experiments for dictyostatin analogues

Since dictyostatin displaced paclitaxel from binding to tubulin polymer, it was anticipated that analogues of dictyostatin would also possess similar property. Dictyostatin analogues were examined for their abilities to displace [^{3}H]paclitaxel from binding to microtubule polymer induced by ddGTP and 2 μM tubulin. The percent inhibition values for dictyostatin analogues are shown in Table 17. All the analogues had lower [^{3}H]paclitaxel inhibition values when compared to dictyostatin. Two of the six analogues studied for this activity showed inhibition values >40%. All other analogues turned out to be weak inhibitors. The data for the open-chain analogue YSS629 correlates with tubulin polymerization data which also suggested this analogue to be moderately active. The C19 epimer, YSS652, was less active. The interesting analogue is the C16-normethyl analogue YSS698-2. Although the normethyl analogue of dictyostatin showed potent tubulin polymerizing activity (Figure 17), its ability to inhibit [^{3}H]paclitaxel from binding to tubulin polymer was less than 50%. In antiproliferative assays this compound also

showed differential sensitivities towards two mutated β-tubulin cell lines, 1A9PTX22 (Ala364→Thr) and 1A9PTX10 (Phe270→Val). While the former cell line was sensitive to YSS698-2 the latter showed over a 1000-fold resistance to the normethyl analogue. This might be an indication that the C16 methyl group is in orientation towards Phe270 in the paclitaxel-binding site on β-tubulin.

Table 17. Percent inhibition by test agents of [^{3}H]paclitaxel binding to tubulin polymer

Inhibitor Added	% Paclitaxel Inhibition (Mean±S.D) (N)
Discodermolide	80 ± 2 (4)
Dictyostatin	78 ±2 (6)
YSS629	42+1 (6)
YSS652	7±2 (6)
YSS665-2	0±0.4 (6)
YSS675-1	0±1 (6)
YSS675-2	0±1 (6)
YSS698-2	48±3 (6)
Paclitaxel	20±1 (6)
Podophyllotoxin	3±1 (6)
Laulimalide	0±0.4 (6)

4.5. Discussion

Cellular assays showed dictyostatin to be a potent antiproliferative agent, a property unaffected by mutations in the taxoid binding site that confer resistance to paclitaxel. Multiparameter cell-based fluorescence analyses also provided good evidence that dictyostatin caused massive polymerization of cellular tubulin, which correlated well with its *in vitro* effects on isolated

bovine tubulin. The effects of dictyostatin on cellular markers of mitotic block were also well correlated with its antiproliferative and cellular MT-stabilizing activity.

Experiments using radiolabeled paclitaxel, discodermolide and epothilone demonstrated that dictyostatin binds the taxoid site on microtubules with avidity very close to that of discodermolide, which has one of the most potent known affinities for this site (ter Haar *et al*. 1996b, Kowalski *et al*. 1997). When 2 μM [^{3}H]discodermolide was used as the radioligand in this assay, 4 μM dictyostatin inhibited the binding of the former by less than 50%. It is impossible to determine accurately the ability of normoisotopic discodermolide to inhibit the binding of [^{3}H]discodermolide to tubulin polymer, but as a point of reference the theoretical isotope dilution with 4 μM unlabeled compound competing with 2 μM of bound radiolabeled compound would give an apparent inhibition of 67%. It should be noted, that 4 μM unlabeled paclitaxel inhibited only ca. 33% of 2 μM polymer-bound [^{3}H]paclitaxel in such experiments (Hamel *et al*. 1999).

Assuming that the four microtubule stabilizers examined here all bind to the taxoid site, the present data suggests that discodermolide and dictyostatin have the strongest and similar affinities for binding to this site on tubulin polymer. When the inhibitory effects of dictyostatin on [^{3}H]discodermolide binding were examined, the first impression was that dictyostatin bound somewhat less well than discodermolide, since only 40% inhibition was observed with both compounds at 4.0 μM. However, a nearly identical effect was obtained when 4.0 μM nonradiolabeled discodermolide was mixed with 4.0 μM [^{3}H]discodermolide, reflecting the apparent inability to completely inhibit binding of the tritiated ligands to tubulin noted above. This suggests that the affinities of dictyostatin and discodermolide for tubulin polymer are nearly identical. The only other test agent that showed significant ability to inhibit discodermolide

binding at the concentrations examined was epothilone B. However, the inhibitory effect of 20 μM epothilone B was less than that of 4.0 μM dictyostatin or 4.0 μM nonradiolabeled discodermolide. This indicates that the affinity of dictyostatin and discodermolide for the taxoid site is at least 5-fold greater than that of epothilone B. Thus, it can be predicted, based on the earlier work of (Buey *et al*. 2004), that the K_a value for dictyostatin and discodermolide will be greater than 3×10^9 M^{-1}.

While the inhibitory effects of dictyostatin have not been evaluated simultaneously, all studies to date with inhibitors of [^{3}H]paclitaxel binding to tubulin polymer have yielded competitive patterns – for epothilones A and B (Kowalski *et al*. 1997), for eleutherobin (Hamel *et al*. 1999) and for discodermolide (Kowalski *et al*. 1997). Even though such a finding with discodermolide implies that it and paclitaxel bind at essentially the same site on tubulin polymer, cytotoxicity studies (Martello *et al*. 2000) have demonstrated synergism between the two agents that has not yet been demonstrated with other combinations of agents that bind at the taxoid site. Earlier reports have hypothesized overlapping, but not identical, binding sites for paclitaxel and discodermolide (Hung *et al*. 1996b). The possibility of two mutually exclusive binding sites on tubulin polymer for discodermolide has been suggested to be a reason for the synergistic cytotoxicity of combined paclitaxel and discodermolide (Hung *et al*. 1996b; Martello *et al*. 2000). The synergism was attributed to the presence of a minimum overlapping binding site on tubulin polymer for these two compounds. This distinct feature was recently hypothesized to be one of several possible mechanisms that could contribute to the synergistic suppression of microtubule dynamics observed with paclitaxel and discodermolide (Honore *et al*. 2004). Such synergism appeared to occur between discodermolide and paclitaxel when intracellular microtubule dynamics are examined, but no such synergy occurs in tubulin assembly reactions

between paclitaxel, discodermolide and dictyostatin (unpublished data). In contrast, assembly synergy can be readily demonstrated when laulimalide, which binds at a site on tubulin polymer distinct from the taxoid site (Gapud *et al*. 2004), is combined with paclitaxel (Dabydeen *et al*. 2004), or with discodermolide or dictyostatin (unpublished data). A potential explanation for this puzzling discrepancy between the cytological and biochemical findings with discodermolide may lie in the recent report that discodermolide, but not paclitaxel, induces accelerated senescence in cells in culture (Klein *et al*. 2005). However, it was also recently reported that paclitaxel and epothilone A bind to taxoid site on tubulin polymer but have minimum overlapping binding sites that explains the sensitivity of paclitaxel-resistant ovarian cancer cell lines to epothilone A. These subtle differences in binding sites might reflect in either synergistic cytotoxicities and/or differences in polymer morphology. However, these differences do not quite reflect in tubulin polymerization experiments when combinations of test agents are studied. This could be because the change in polymer mass is insignificant to be revealed as a big difference in turbidity profile. Nevertheless, the possibility of higher affinity for tubulin polymer, hypernucleating ability, and minimum overlapping binding sites for discodermolide as compared to paclitaxel on microtubule polymer might help explain the accelerated mitotic response induced by discodermolide over paclitaxel and hence the synergism observed in cytotoxicity studies.

These results correlate to some degree with the results from antiproliferative assays. Dictyostatin, like discodermolide, was unaffected by the mutations expressed in the β-tubulin of the paclitaxel-resistant cells. The antiproliferative activity of dictyostatin was comparable to that of paclitaxel in parental 1A9 cell lines. On the other hand, dictyostatin was more slightly potent than discodermolide as an antiproliferative agent in all three ovarian cell lines, and definitely

much more potent in HeLa cells. Noteworthy is the biological activity of the normethyl dictyostatin. Considering that the normethyl analogues, YSS698-2, is as potent as parent molecule in antiproliferative assays and that it inhibited only 50% of the tracer from binding to tubulin polymer, it is very likely that there could an overlapping binding site at the taxoid site on tubulin polymer on which YSS698-2 binds. This data substantiates the antiproliferative data obtained for YSS698-2 with paclitaxel-resistant cell lines 1A9PTX22 and 1A9PTX10. While the former cell line almost completely retained sensitivity for the 16-normethyl analogue, the latter was quite resistant. This data suggests that the C16-methyl group in dictyostatin is oriented towards Phe270. In addition, Ala364 mutation had no effect on the antiproliferative activity suggesting YSS698-2 does not interact with this residue. The data from [^{3}H]paclitaxel inhibition (that showed ~ 50% inhibition) and antiproliferative assays for YSS698-2 lead to a possibility of a site partially different from the binding site of paclitaxel on β-tubulin subunit. It could also be possible that β-tubulin subtype selectivity might have a role to play. Efforts are underway to understand the binding orientation of YSS698-2. Also of interest would be to use YSS698-2 as a probe to investigate the differences in protein-ligand interactions between the two paclitaxel resistant cell lines.

Many regulatory elements in the cell are known to have a significant role in the assembly/disassembly processes of tubulin polymer. The primary regulatory factors include MAPs and GTP (Soifer 1986; Grover *et al*. 1995; Weisenberg and Deery 1976; Weisenberg *et al*. 1976). *In vitro* polymerization experiments done under various reaction conditions can in part explain the differences observed in the antiproliferative activity profile of these compounds against parental and mutated β-tubulin cell lines. Tubulin polymerization experiments done under conditions ranging from a system consisting of tubulin alone to its combination with

MAPs and/or GTP demonstrated that dictyostatin, like discodermolide, enhanced nucleation reactions at low temperatures, 0 ^{o}-10 ^{o}C. The hypernucleating ability of paclitaxel was far less potent than that of dictyostatin and there was a considerable lag time in the paclitaxel-induced polymerization reaction. Not only were the reactions more vigorous in the presence of dictyostatin, the dictyostatin-induced polymer was completely cold-stable. In all these reaction conditions, greater polymer mass formation was observed with dictyostatin than with paclitaxel. In the complete system, polymer mass was greater in the presence of dictyostatin than with either paclitaxel or discodermolide. This might help explain the slightly greater antiproliferative activity observed with dictyostatin in 1A9 cell lines, as cells contain MAPs and GTP. This might also account for the lower Cc value observed with dictyostatin over that seen with discodermolide in the complete reaction conditions. The energetics of binding and initiation of polymer formation were lower for dictyostatin than that observed for discodermolide.

The qualitative differences observed between the turbidity profiles of paclitaxel and dictyostatin were consistent with the electron microscopic analyses. Abundant microtubule bundling was observed with dictyostatin as well as with discodermolide under all reaction conditions. When individual microtubules in a given field were quantified for microtubule lengths, it was apparent that dictyostatin forms microtubules shorter in length than does discodermolide or paclitaxel. Dictyostatin, similar to discodermolide, formed sheets of microtubule polymer. Paclitaxel at 37 ^{o}C in the presence of MAPs and GTP formed abundant polymer that consisted of both sheets and ribbons. These morphological differences were highly dependent on the presence or absence of MAPs and/or GTP in the reaction mixture. Dynamic events during polymerization of tubulin are known to be regulated to a greater extent by the presence of GTP (Weisenberg and Deery 1976). GTP is known to be localized in the

exchangeable (with GDP) site on β-tubulin and in a non-exchangeable site on α-tubulin. Tubulin heterodimer containing GTP bound to β-tubulin is therefore termed GTP-tubulin, and tubulin with GDP bound at the exchangeable site is termed GDP-tubulin. GTP-tubulin is competent for assembly and a cap of GTP-tubulin on MTs maintains their stability. Although GTP is not necessary for tubulin polymerization, its presence enhances the assembly process. MAPs are known to shift the equilibrium of the tubulin polymerization process to the right of the polymer (Hamel *et al*. 1999). Polymer induced by paclitaxel in the presence of GTP consisted of MTs with their ends curved or containing loops/ribbons, which appeared to be peeled protofilaments. The number of such MTs with curved ends was low in polymer induced by paclitaxel in the tubulin-only system. This data suggests that MAPs and/or GTP play a very crucial role in paclitaxel-induced assembly. Although the presence of these two regulatory elements seems not to be crucial for dictyostatin- and discodermolide-induced polymerization reactions, the turbidity profiles do indicate their critical role in the abilities of these agents to hypernucleate tubulin assembly. As mentioned earlier, the intracellular role of MAPs and GTP is important in explaining the near-identical GI_{50} values obtained for these three agents in the ovarian carcinoma cells, which correlated with the similar turbidity profiles observed in the reactions carried out with the complete system.

Turbidimetric assays done under restricted reaction conditions showed dictyostatin to cause a greater extent of assembly than caused by discodermolide. However, electron microscopic analyses of discodermolide-induced tubulin polymer in these experiments showed an apparently more abundant polymer mass than that observed for dictyostatin-induced polymer. Abnormal polymer in the form of rings was also observed under these conditions in the presence of discodermolide and dictyostatin. This correlated with the lower Cc value obtained for

discodermolide compared to that for dictyostatin under these conditions. EM images from the complete system showed more abundant polymer in the presence of dictyostatin than in the presence of discodermolide. This might account for the lower Cc value observed for dictyostatin than for discodermolide in complete system. Also, the lengths of MTs in dictyostatin-induced polymer were shorter than in the discodermolide-induced polymer under this reaction condition. The EC_{50} values for dictyostatin and discodermolide obtained from pelleting assay were similar, although dictyostatin appeared to be slightly more potent. The free energies calculated from Cc values also suggest that in the presence of MAPs and GTP and dictyostatin, the Gibb's free energy value for hypernucleation was lower than that observed in the presence of discodermolide.

The results show dictyostatin to have *in vitro* properties essentially equivalent to those of the potent MT hypernucleating and taxoid binding site agent discodermolide. Both compounds cause tubulin to polymerize at low temperatures and at low concentrations, and the polymer formed by both is cold stable. These strikingly similar qualitative and quantitative results strongly suggest that the bioactive conformation of discodermolide is mapped by that of dictyostatin, which matches the compact, tilde-shaped conformation present in the discodermolide X-ray crystal structure as well as the NMR structure determined in deuterated acetonitrile (Gunasekera *et al*. 1990, Smith *et al*. 2001) versus the more open, extended structures suggested by the NMR analyses done with discodermolide dissolved in deuterated DMSO (Monteagudo *et al*. 2001). Interestingly, dictyostatin was the more potent antiproliferative agent of the two, especially in HeLa cells. This could be due to several reasons, including the fact that the carbamate moiety on discodermolide, lacking in dictyostatin, is known to be labile but also necessary for biological activity (Hung *et al*. 1996a), pointing to a potential

cellular (or culture medium) solvolytic or metabolic instability of discodermolide. This might explain the toxicity shown with discodermolide upon dose escalation during trials clinical trials and led to this molecule being kept on hold for further clinical trials (Novartis 2005). Alternatively, dictyostatin could simply enter cells more readily than discodermolide and hence could be a promising clinical drug candidate.

Evaluation of dictyostatin analogues for SAR based on biological assays show that of all the analogues, the 16-normethyldictyostatin, YSS698-2 was the most active analogue identified. It was shown previously that 14-normethyldiscodermolide was as active as the parent molecule. 16-Normethyldictyostatin, in antiproliferative, tubulin polymerization, and immunofluorescence experiments had shown biological activity comparable to the parent molecule. The C16 methyl group, although not crucial for antiproliferative activity, however was shown to be important for paclitaxel site binding. This analogue also showed preferential antiproliferative activity in β-tubulin mutated cell lines suggesting that C16-methyl group orients towards Phe270 of paclitaxel binding site on tubulin polymer. The open-chain methyl ester of dictyostatin, YSS629 and the epimer of dictostatin, YSS652, seem to be moderately active. YSS629 and YSS652 induced polymer formation at lower temperatures, assembly reactions at all temperatures were moderate compared to dictyostatin, and the polymer formed was not cold-stable. In antiproliferative assays, the GI_{50} values were higher than that observed with the parent molecule but paclitaxel-resistant cells retained their sensitivity for these analogues. Based on these findings, a summary of SAR for dictyostatin was drawn out and can be represented as in Figure 21.

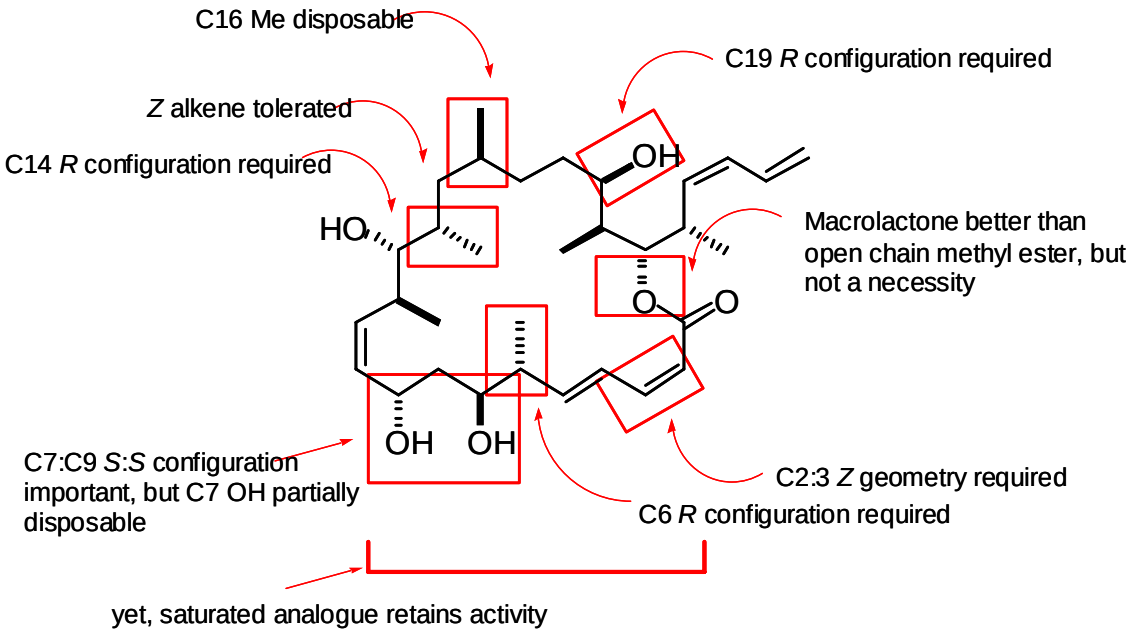

Figure 21. Representation of SAR for (-)-dictyostatin

5. BINDING KINETICS

5.1. Introduction and literature cited

Previous studies have shown that discodermolide competed with [^{3}H]paclitaxel from binding to MTs with an inhibition constant (K_i) of 0.4 μM (Kowalski *et al*. 1997). When [^{3}H]discodermolide was used as the tracer it was observed that the stoichiometry of binding to tubulin polymer was 1:1 (Hung *et al*. 1996b). It was also reported that the binding of discodermolide and paclitaxel was mutually exclusive and that paclitaxel bound to discodermolide-induced polymer very weakly. Other MT stabilizers like the epothilones, the eleutherobins and the sarcodictyins, when studied for binding kinetics were known to bind to paclitaxel site in a competitive manner (Kowalski *et al*. 1997; Hamel *et al*. 1999). However, the affinities with which these ligands bound to the polymer were lower than discodermolide. The reported K_i value for epothilone A and B were 0.6 μM and 0.4 μM, respectively as against the 0.4 μM value obtained for discodermolide when [^{3}H]paclitaxel was used as the tracer.

Modeling studies suggest that discodermolide fits into the common pharmacophore model hypothesized for MT-stabilizing agents including paclitaxel, docetaxel, epothilones, eleutherobins and sarcodictyins (Ojima *et al*. 1999). However, studies performed using the X-ray crystal structure of discodermolide onto the taxol binding site on MTs suggest two binding modes (Martello *et al*. 2001). From SAR studies, the model that was favored was the one that had the lactone of discodermolide overlapping with the C13-side chain of paclitaxel and the C19 portion of discodermolide matching with the C2-benzoyl of paclitaxel rather than *vice-versa.*

Recently, X-ray crystallography, modeling, and NMR studies done on epothilone A bound to tubulin polymer suggested a binding model for epothilone A that differed from that proposed for paclitaxel (Nettles *et al*. 2004). The results from this study help explain the sensitivity of paclitaxel-resistant cell lines towards epothilones A and B.

Recent evidence of synergism observed in MT polymer dynamics in the presence of both discodermolide and paclitaxel draws our attention to the possibility of overlapping but not entirely superimposable binding sites for discodermolide and paclitaxel (Honore *et al*. 2004). Earlier, it also was shown that in A549-T12 paclitaxel-resistant human lung adenocarcinoma cell line no cross-resistance was observed with discodermolide (Martello *et al*. 2000). Epothilone B-resistant cells having mutations in β-tubulin were sensitive upon treatment with discodermolide. These observations strongly support the proposed minimum overlapping binding model for discodermolide and paclitaxel (and may be epothilone B) that would account for synergistic effect of these two molecules in the cells. It was also hypothesized that the accelerated senescence that was recently reported for discodermolide might be one of the possible mechanisms contributing to the synergistic microtubule perturbation and cytotoxicity between discodermolide and paclitaxel (Madiraju *et al*. 2005).

Preliminary findings in this work that dictyostatin inhibits [^{3}H]paclitaxel from binding to tubulin polymer indicate that dictyostatin binds to the taxoid binding site on tubulin polymer (Chapter 4). Since dictyostatin structurally resembles discodermolide one would anticipate an inhibition pattern against [^{3}H]paclitaxel, similar to that of discodermolide, for binding to tubulin polymer. Antiproliferative activity studies show that dictyostatin, like discodermolide, is active in paclitaxel-resistant ovarian cancer cell lines (Chapter 4). This data suggests dictyostatin,

similar to discodermolide, might have a minimum overlapping binding site at the taxoid site on tubulin polymer.

Hypothesis III: Dictyostatin, discodermolide, and the 4-*epi* analogue of discodermolide will have similar inhibitory effects on [^{3}H]paclitaxel binding kinetics on tubulin polymer.

Rationale: It is of interest to investigate the mode of binding and to determine the inhibition kinetics for discodermolide, dictyostatin and their analogues. The rapid mitotic effects seen with discodermolide in comparison with paclitaxel could be attributed to the potent hypernucleating ability of discodermolide over paclitaxel. There must be subtle differences in binding models between discodermolide and paclitaxel that could account for the high-affinity binding, hypernucleation, and stabilization effects of discodermolide on microtubule polymer characteristically different from that of paclitaxel. These features could have an effect on the synergistic suppression of microtubule dynamics between discodermolide and paclitaxel. Hence, it is of importance to obtain clues about the binding kinetics for discodermolide and paclitaxel that aid in understanding the differences in their microtubule perturbing effects. Preliminary data with [^{3}H]paclitaxel and [^{14}C]epothilone B as tracers show a convincing evidence that dictyostatin is equivalent to discodermolide in binding to tubulin polymer with very high affinity (*vide supra*, Chapter 4). The cellular effects of dictyostatin are similar to discodermolide. Since, dictyostatin is a novel molecule, there are no studies done yet that report any sort of synergism between paclitaxel and dictyostatin on microtubule polymerization dynamics. Nevertheless, dictyostatin is comparable to discodermolide in its ability to bind tubulin polymer with greater affinity, to hypernucleate tubulin assembly, and to retain potency in paclitaxel-resistant cell lines. These features set dictyostatin on par with discodermolide. Hence, it would be of interest to understand

the subtle differences in binding modes, if any, between dictyostatin and paclitaxel. The quantitative estimation of binding data could help rationalize the *in vivo* findings.

Therefore, a detailed kinetic study was undertaken to investigate the mode of binding and to obtain apparent inhibition constant values (K_is). The K_i value could stand as a good parameter estimate for assessing the test agent's potential as a taxoid site binding agent. On par with these studies, the binding kinetics of the 4-*epi* analogue of discodermolide (NC86) was also determined. This compound is one of the first library discodermolide analogues that showed interesting biological activity. It inhibited [^{3}H]paclitaxel from binding to tubulin polymer to an extent of 57% and had μM GI_{50} values in antiproliferative assays (Chapter 3). Radioligand binding and fluorescent anisotropy techniques were employed for determining binding kinetics. [^{3}H]paclitaxel was used as the tracer for radioligand binding experiments and Flutax-2, having a difluorocarboxyfluorescein as the fluorophore linked to C-7 of paclitaxel was used as the tracer in fluorescent anisotropy experiments. Along with inhibition studies, saturation binding kinetics experiments were also done to derive the dissociation constant (K_D) and binding affinity of [^{3}H]paclitaxel itself, in an effort to re-establish the binding kinetic parameters for [^{3}H]paclitaxel using the tubulin aliquot that we had. The K_D parameter is also necessary for determining the K_i values for the inhibitors. Studies done earlier using radiolabeled as well as fluorescent-labeled paclitaxel show that paclitaxel binds to tubulin polymer with a 1:1 stoichiometry indicating only one binding site for paclitaxel. The K_D values reported were 0.01 μM and ~ 0.06-0.1 μM, respectively (Caplow *et al*. 1994; Ye *et al*., Diaz *et al*. 2000). Following the approach of radioligand binding assay, fluorescence anisotropy methodology described earlier (Diaz *et al*. 2000; Andreu and Barasoain 2001; Diaz *et al*. 2003*)* was also employed to obtain binding kinetic parameters and to provide conclusive evidence for stoichiometry of binding. This study was

done based on the reason that fluorescence anisotropy is a more sensitive technique to decipher the optimum binding characteristics for a molecule since a wide range of protein and ligand concentrations could be studied in a single experiment. Glutaraldehyde-fixed microtubules render stable polymer upon dilution and/or change in temperature (Andreu and Barasoain 2001). Additionally, work in the direction of determining the thermodynamics of ligand binding to MT polymer using Flutax-2 is in progress. Anisotropy experiments were employed to understand the binding energetics of the ligands on tubulin polymer. In this section, a portion of the work will only be presented since the studies are still on-going.

5.2. Experimental procedures and results

Paclitaxel saturation binding kinetics using tubulin aliquots and [^{3}H]paclitaxel as the tracer were determined to establish the equilibrium dissociation constant and the concentration of binding sites. A structural analogue of paclitaxel, docetaxel, was used to determine the effect non-specific binding would have on the binding kinetics. Docetaxel concentration required for doing non-specific binding experiments was first determined in the concentration range of 0.25-20 μM. The experimental procedure for determining saturation binding data is described in Chapter 2. The concentration of docetaxel was graphed against disintegrations per minute (dpm) for the tracer observed. Saturation binding studies were performed with [^{3}H]paclitaxel incubated at different concentrations (0.25-6 μM) with preformed MT polymer (2 μM) to determine the stoichiometry of binding following the protocol described in Chapter 2. Stoichiometry experiments were performed in the presence and absence of docetaxel. Nonspecific binding of [^{3}H]paclitaxel in the presence of docetaxel (12 μM) was determined. Specific binding of [^{3}H]paclitaxel was determined from the difference of total and nonspecific bound values.

Inhibition studies were performed with radiolabeled paclitaxel and different inhibitors. Different concentrations of [^{3}H]paclitaxel (ranging from 0.025-4.0 μM) were studied against different concentrations of discodermolide (in the concentration range of 0.25-4 μM). The experimental protocol was similar to the preliminary studies done with [^{3}H]paclitaxel and inhibitors studied at a single concentration. The procedure for [^{3}H]paclitaxel inhibition study is explained in Chapter 2. The 4-*epi* analogue of discodermolide (NC86) was also studied for inhibition kinetics. The experimental procedure was exactly similar to the one described for discodermolide except that the inhibitor concentrations ranged from 0.25-10 μM. Inhibition studies with dictyostatin were also studied following similar procedure as described above**.**

Saturation binding kinetic parameters were determined from the plots of free concentration of [^{3}H]paclitaxel (μM) versus number of moles of [^{3}H]paclitaxel bound per mole tubulin polymer. The latter term was either total or specific bound value of the tracer. Saturation binding parameters (K_D, B_{max}, and Hill slopes) were determined based on Langmuir binding isotherm equation using the non-linear regression program in PRISM software version 4.0 (GraphPad Software, Inc., San Diego, CA, USA) based on best-fit modeling strategy and are expressed in terms of mean+/-SEM. The inhibition study with discodermolide was quantitated and data analysis done with PRISM software version 4.0 (GraphPad Software, Inc., San Diego, CA, USA).

5.3. Docetaxel inhibition study

The concentration of docetaxel that almost completely inhibited [^{3}H]paclitaxel binding was determined from the graphical plot of docetaxel shown in Figure 22. At 8-16 μM docetaxel seemed to have a plateau-effect on [^{3}H]paclitaxel bound to tubulin polymer. This concentration

of 12 μM docetaxel was used to determine non-specific binding for all the saturation binding and inhibition experiments.

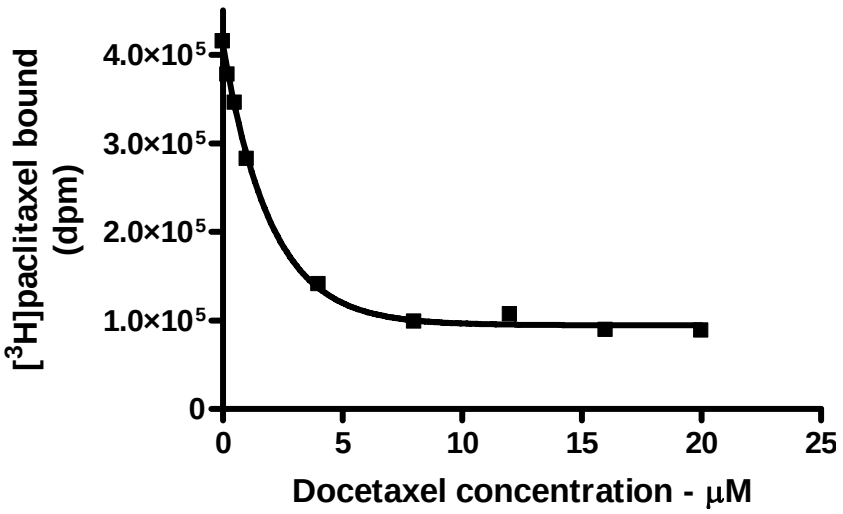

Figure 22. Determination of docetaxel concentration for non-specific binding experiments
Reaction mixtures consisted of 0.74M MSG (pH 6.6), ddGTP-induced microtubule polymer, and 2 μM [^{3}H]paclitaxel in the presence of docetaxel in the concentration range studied. Data is expressed as mean±S.D (N=3). Each data point represents total [^{3}H]paclitaxel bound at any single concentration of docetaxel. Abcissa (*X*-axis): docetaxel concentration (μM); Ordinate (*Y*-axis): total [^{3}H]paclitaxel bound (dpm).

5.4. Saturation binding experiments with [^{3}H]paclitaxel

Saturation binding experiments done with tubulin polymer and [^{3}H]paclitaxel revealed that 0.8 mol of total [^{3}H]paclitaxel bound per mol of tubulin polymer. Figure 23A represents the stoichiometry data obtained for total [^{3}H]paclitaxel bound per mol of tubulin polymer. The B_{max} and K_D values expressed as mean ± SEM were 0.8±0.014 and 0.0587±0.0048 μM, respectively.

In this set of experiments, the total [^{3}H]paclitaxel bound values were observed to be greater than 10% of the total radioligand added at concentrations less than the observed K_D value. The percent bound values were greater than 25% for the concentration range studied. The sigmoidal equations employed for calculating binding parameters assume that the free concentration of the radioligand measured is almost equal to the concentration of the radioligand added to the samples. When >10% of the added radioligand binds to the receptor the free concentration is less than the added concentration of the radioligand and this phenomenon is referred to as 'ligand depletion'. A parameter estimate that indicates whether a simple bimolecular reaction would explain the data, or not, is the Hill slope (nH) (Morton *et al*. 2002). A Hill slope of one indicates a one-site binding for the radioligand. Hill slope less than unity meaning the tracer has a shallow affinity for the site. A Hill slope greater than one suggests that the tracer or that the inhibitor have two active sites or equilibrium condition has not been reached or that the inhibitor has a positive co-operativity for radioligand binding to its active site. In our studies, the Hill slope obtained for total binding was nH ~ 1.6, suggesting more than one binding site (nH ~ 1.56). This indicates that paclitaxel binds to some nonspecific sites that might give an overestimation of the stoichiometric ratio if not corrected for. Hence, the standard saturation binding equation based on Langmuir isotherm is modified to account for non-specific binding that largely contributes to ligand depletion and greater Hill coefficient. Non-specific binding was accounted by using docetaxel as the non-specific inhibitor of [^{3}H]paclitaxel binding to the polymer. Specifically bound values were calculated form total bound minus non-specifically bound values from which the binding kinetic parameters were again determined. When specifically bound values were taken into consideration, the stoichiometry value obtained was around 0.6 mol of the radiolabeled tracer bound to 1 mol of MT polymer (Figure 23B).

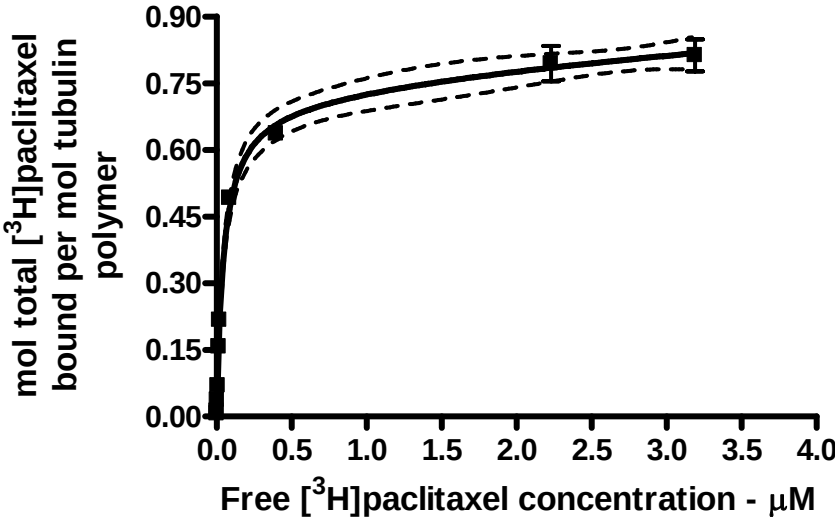

Figure 23. Stoichiometry data from [^{3}H]paclitaxel binding experiments

Figure 23A. Stoichiometry of total [^{3}H]paclitaxel bound per mol microtubule polymer

Stoichiometry experiments were conducted at concentrations that ranged from 0.01 μM-5.0 μM. Reaction mixtures consisted of 0.74M MSG (pH 6.6), ddGTP-induced microtubule polymer, and [^{3}H]paclitaxel in the concentration range studied. Data is expressed as mean±SEM (N=3). Each data point represents total [^{3}H]paclitaxel bound per mol tubulin polymer at a free [^{3}H]paclitaxel measured in the reaction mixture. Abcissa (*X*-axis): Free [^{3}H]paclitaxel (μM); Ordinate (*Y*-axis): total [^{3}H]paclitaxel bound per mol tubulin polymer.

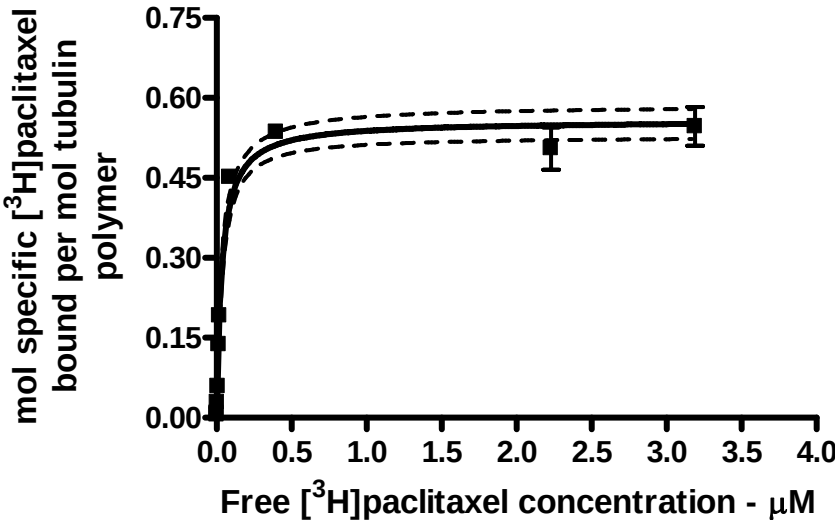

Figure 23B. Stoichiometry of specific [^{3}H]paclitaxel bound per mol microtubule polymer. Stoichiometry experiments were conducted at concentrations that ranged from 0.01 μM-5.0 μM. Non-specific binding was accounted from docetaxel containing sample set. Reaction mixtures consisted of 0.74 M MSG (pH 6.6), ddGTP-induced microtubule polymer, and [^{3}H]paclitaxel in the concentration range studied. Data is expressed as mean±SEM (N=3). Each data point represents [^{3}H]paclitaxel bound per mol tubulin polymer at a free [^{3}H]paclitaxel measured in the reaction mixture. Abcissa (*X*-axis): Free [^{3}H]paclitaxel (μM); Ordinate (*Y*-axis): specific [^{3}H]paclitaxel bound per mol tubulin polymer.

The B_{max} and K_D values obtained from specifically bound values expressed in terms of mean±SEM were 0.6±0.0143 and 0.0353±0.0041 μM, respectively. The specific binding data yielded a Hill slope of ~ 1.0. This correlates with the stoichiometry determined for total and specific binding of paclitaxel to tubulin polymer.

5.5. Radioligand inhibition studies

Inhibition studies were performed to understand the inhibition pattern and to demonstrate the relative potency of the agents for binding to tubulin polymer. The data were quantified to obtain the inhibition constant (K_i value) from the inhibition data profiles. Both classical pharmacological inhibition approach and modified Michaelis-Menten kinetics were employed for data analysis and interpretation (Dixon 1978; Edler *et al*. 2005). Figure 24 shows the inhibition profile obtained by plotting log concentration of discodermolide (μM) against percent inhibition. The model chosen for this set of data was one-site competition since the data best fit to this model. The equation for two-site model was tried, but the data did not converge. Percent inhibition values were obtained after normalizing the [^{3}H]paclitaxel bound values, in the presence of inhibitor, with respect to set of vehicle-only controls that had no inhibitor. The inhibition plot in Figure 24 suggests that discodermolide competitively inhibited [^{3}H]paclitaxel from binding to tubulin polymer at concentrations ranging from 0.5-2.0 μM. Sigmoidal concentration-response curves generated from nonlinear regression analysis of the log inhibitor concentration versus percent inhibition data using PRISM 4.0 yielded series of sigmoidal curves. The model with different Hill slopes fit the data the best. The Hill slopes for the set of [^{3}H]paclitaxel concentrations included in this study were greater than 1.0, regardless of whether the data was corrected for specific binding or not. Hill slopes greater than 1.0 could be because of several reasons which will be discussed in the next section. In addition, when data was transformed to the one based on modified Hanes equation and redrawn (free concentration of [^{3}H]paclitaxel versus free/bound concentration of [^{3}H]paclitaxel, S vs. S/V, respectively), the slopes of the lines at different inhibitor concentrations were not truly 1.0. The Hanes plot for

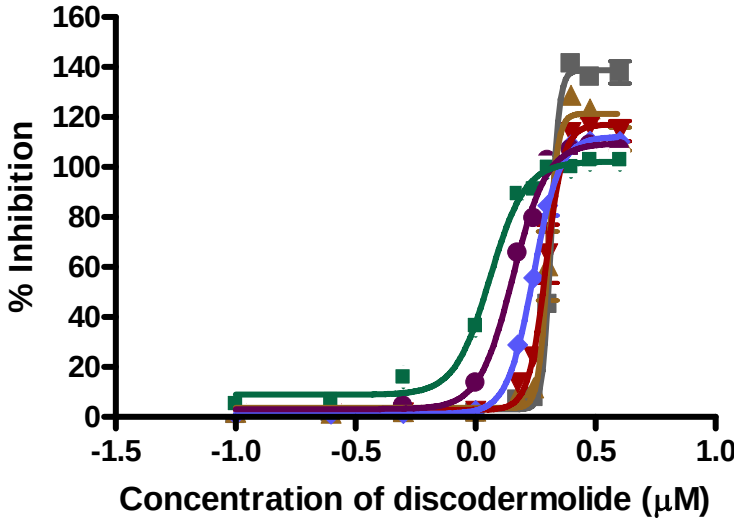

Figure 24. Graphical representation of discodermolide inhibition kinetics

Inhibition experiments were performed at concentrations of [^{3}H]paclitaxel that ranged from 0.01 to 5.0 μM and discodermolide concentrations ranging from 0.25 to 4.0 μM. Reaction mixtures consisted of 0.74 M MSG (pH 6.6), ddGTP-induced microtubule polymer, [^{3}H]paclitaxel and discodermolide in the concentration range studied. Percent inhibition was determined as described in Chapter 2. Data is expressed as mean±SEM (N=3). Each data point represents percent inhibition values plotted against concentration of discodermolide in log scale for each concentration of [^{3}H]paclitaxel: 0.1 μM (gray); 0.25 μM (rust); 0.5 μM (brown); 1.0 μM (blue); 1.5 μM (purple); 2.0 μM (green). Abcissa (*X*-axis): μM discodermolide (log scale); Ordinate (*Y*-axis): % inhibition.

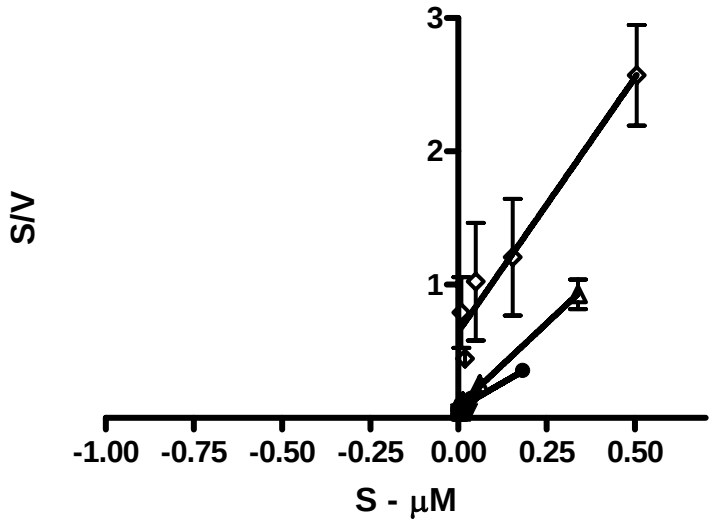

Figure 25. Hanes plot of discodermolide inhibition kinetics

Inhibition experiments were performed as described in Figure legend 24. Data is expressed as mean±SEM (N=3). Each data point represents free [^{3}H]paclitaxel (μM) plotted against free [^{3}H]paclitaxel over [^{3}H]paclitaxel bound both in μM. Abcissa (*X*-axis): Free [^{3}H]paclitaxel (μM); Ordinate (*Y*-axis): free [^{3}H]paclitaxel over [^{3}H]paclitaxel bound to tubulin polymer, both in μM. Discodermolide was studied at 1.5 μM (circles); 1.75 μM (open triangles); 2 μM (open squares). *Note:* slopes not equal, depicts mixed inhibition.

discodermolide is shown in Figure 25. It is known that for competitive inhibitors, Hanes analysis should yield lines with slopes more or less equal to 1.0 (Edler *et al*. 2005). The profiles shown in Figures 24 and 25 suggest one of the following:

The inhibitor might have two affinity sites for binding and/or the inhibitor must be exerting a mixed inhibition for binding to tubulin polymer. The equilibrium dissociation constant (K_D) of the radioligand as well as the molar ratio of the bound radioligand and tubulin protein (B_{max}) are known to be altered when a mixed inhibition occurs. Hence, calculation of the two inhibition constants seemed necessary in the present situation. The apparent inhibition constant values (K_i values) for high and low affinity sites were 34 nM and 178 nM, respectively. These values seemed quite reasonable for a potent molecule like discodermolide. The K_D value for [^{3}H]paclitaxel was 35 nM.

Non-linear regression analysis of the log concentration versus percent inhibition data for the 4-*epi* analogue of discodermolide (NC86) yielded sigmoidal concentration-response curves with variable slopes. Data accounted for non-specific binding resulted in nH values greater than 1.0 at lower concentrations (0.025, 0.05, 0.1 μM inhibitor concentrations) and about 1.0 at higher concentrations (0.25, 0.5, 1.0, and 2.0 μM). The data however, did not show a complete plateau effect and needs higher concentrations. Hanes analysis of the data was done by plotting free [^{3}H]paclitaxel concentration versus free/bound values as described above. Figure 26 represents the Hanes plot for the *4-epi* analogue.

Sigmoidal concentration-response curves and Hanes plot suggest that the *epi*-analogue, similar to discodermolide, showed mixed inhibition pattern. This could again be because of overlapping binding sites or presence of more than one isoform of tubulin in the protein aliquot used for inhibition studies. Hanes analysis showed shallow slopes compared to discodermolide owing to the fact that the 4-*epi* analogue had a lower affinity for binding to taxoid site on tubulin polymer. The slopes were not the same for all the inhibitor concentrations. The K_i values calculated from the high and low affinity sites were 0.2 and 2.55 μM, respectively.

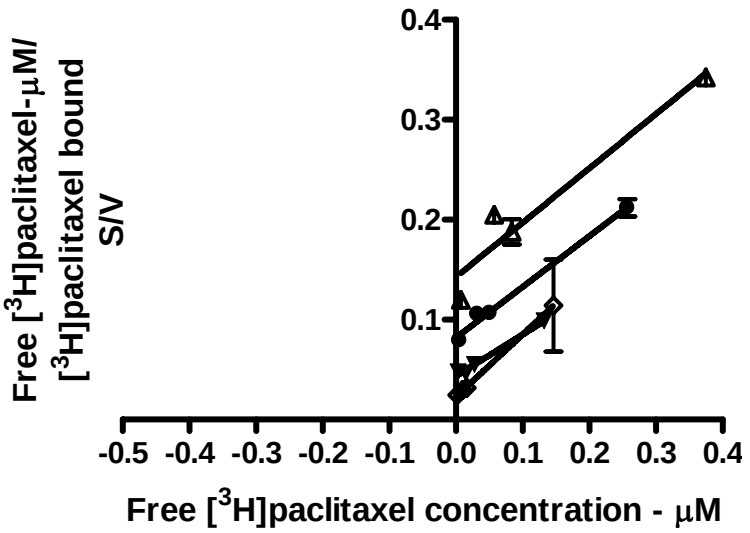

Figure 26. Hanes plot of 4-*epi* analogue (NC86) inhibition kinetics

Inhibition experiments were performed as described in Figure legend 24. Concentrations of the inhibitor, 4-*epi* analogue, ranged from 0.25 to 10 μM. Data is expressed as mean±S.D (N=3). Each data point represents free [^{3}H]paclitaxel (μM) plotted against free [^{3}H]paclitaxel over [^{3}H]paclitaxel bound both in μM. Abcissa (*X*-axis): Free [^{3}H]paclitaxel (μM); Ordinate (*Y*-axis): free [^{3}H]paclitaxel over [^{3}H]paclitaxel bound to tubulin polymer, both in μM. 4-*epi* analogue concentrations were 10 μM (open triangles); 4 μM (circles); 1 μM (closed triangles); 0 μM (open squares). *Note:* slopes not equal, depicts mixed inhibition.

Graphical analysis of log concentration of dictyostatin versus percent inhibition data suggests a competitive inhibition pattern for this molecule (Figure 27). The profile shown here

looked almost similar to that observed for discodermolide (Figure 24). Sigmoidal concentration-response curves from non-linear regression analysis of log concentration and % inhibition data

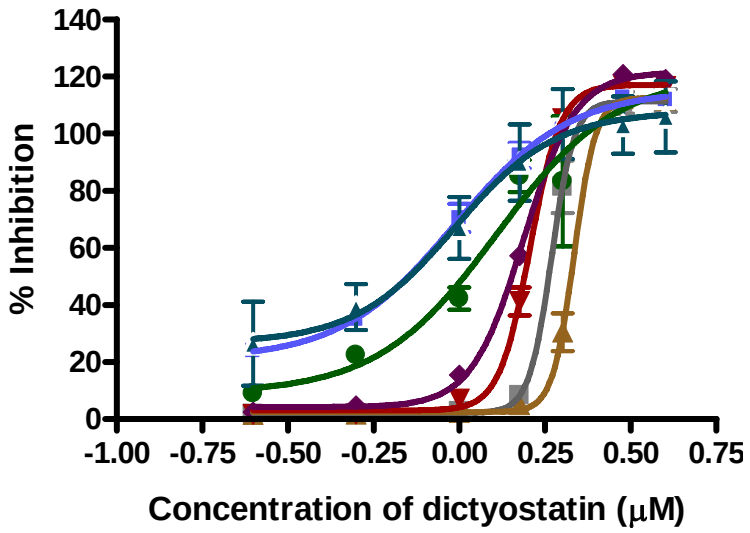

Figure 27. Graphical representation of dictyostatin inhibition kinetics

Inhibition experiments were performed at concentrations of [^{3}H]paclitaxel that ranged from 0.01 μM-5.0 μM and dictyostatin concentrations ranging from 0.25 to 4 μM. Reaction mixtures consisted of 0.74 M MSG (pH 6.6), ddGTP-induced microtubule polymer, [^{3}H]paclitaxel and discodermolide in the concentration range studied. Percent inhibition was determined as described in Chapter 2. Data is expressed as mean±SEM (N=3). Each data point represents percent inhibition values plotted against concentration of dictyostatin in log scale. [^{3}H[paclitaxel concentrations include: 0.05 μM (gray); 0.1 μM (rust); 0.5 μM (brown); 1 μM (purple); 2 μM (olive green); 3 μM (blue); 4 μM (dark green). Abcissa (*X*-axis): μM dictyostatin (log scale); Ordinate (*Y*-axis): % inhibition.

yielded concentartion-response curves with Hill slopes greater than 1.0. The curves were comparable to that observed with discodermolide. Hanes analysis of the dictyostatin inhibition data showed series of lines with slopes not equal to 1.0 suggesting a mixed inhibition pattern (Figure 28). The K_i values determined for high and low affinity sites were, 23.4 and 332 nM, respectively.

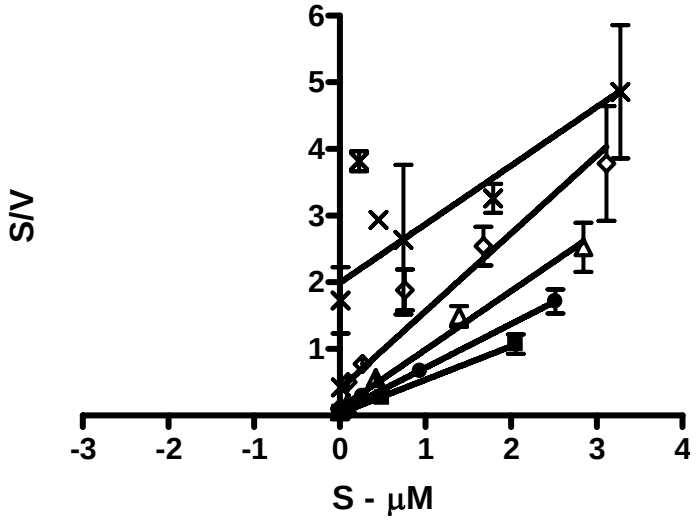

Figure 28. Hanes plot of dictyostatin inhibition kinetics

Inhibition experiments were performed as described in Figure legend 24. Dictyostatin concentrations ranged from 0.25 to 4 μM. Data is expressed as mean±SEM (N=3). Each data point represents free [^{3}H]paclitaxel (μM) plotted against free [^{3}H]paclitaxel over [^{3}H]paclitaxel bound both in μM. Dictyostatin concentrations include: 4 μM (squares); 3 μM (triangles); 2 μM (inverted triangles); 1 μM (diamonds); 0.5 μM (circles); 0.25 μM (small squares); Abcissa (*X*-axis): Free [^{3}H]paclitaxel (μM); Ordinate (*Y*-axis): free [^{3}H]paclitaxel over [^{3}H]paclitaxel bound to tubulin polymer, both in μM. *Note:* slopes not equal, depicts mixed inhibition.

5.6. Fluorescence anisotropy experiments with Flutax-2

Anisotropy experiments were performed using glutaraldehyde-fixed microtubules and fluorescence labeled paclitaxel in the presence and absence of inhibitors. The primary objective of fluorescence anisotropy experiments was to elucidate the binding kinetics of paclitaxel and to relate the kinetics with the thermodynamics involved in ligand-induced assembly reactions. Glutaraldehyde-fixed microtubules were used since cross-linked microtubules withstand dilution- and temperature-induced microtubule disassembly (Andreu and Barasoain 2001). Microtubules were quite stable when checked under EM at 100-fold as well as 1000-fold dilutions (Figure 35 in the Appendix). The concentration of free binding sites on microtubule polymer was determined from anisotropy experimental data. Cross-linked polymer, in the concentration range 0.04-12.5 μM, was studied in the presence of 25 nM Flutax-2. The equilibrium binding constant associated with it was determined using WINNONLIN version 3.0. Figure 29 represents the observed and predicted data from WINNONLIN obtained for this set of anisotropy data. The best model was chosen based on the Akaike Information Criterion (AIC) (Motulsky and Ransnas 1987). The lower the AIC value for a given model, the better fit is the model. The best-fitted values for r_{min} and r_{max} were 0.079 and 0.163, respectively. The equilibrium binding constant calculated based on the best-fit values for r_{min} and r_{max} was 0.00347.

The number of binding sites for Flutax-2 and the equilibrium binding constants for Flutax-2 at room temperature and at 37 ^{o}C were determined. The anisotropy data from experiments done with varying concentrations of Flutax-2 (0-100 nM) was fitted into the equation and iterations were performed using WINNONLIN as mentioned above.

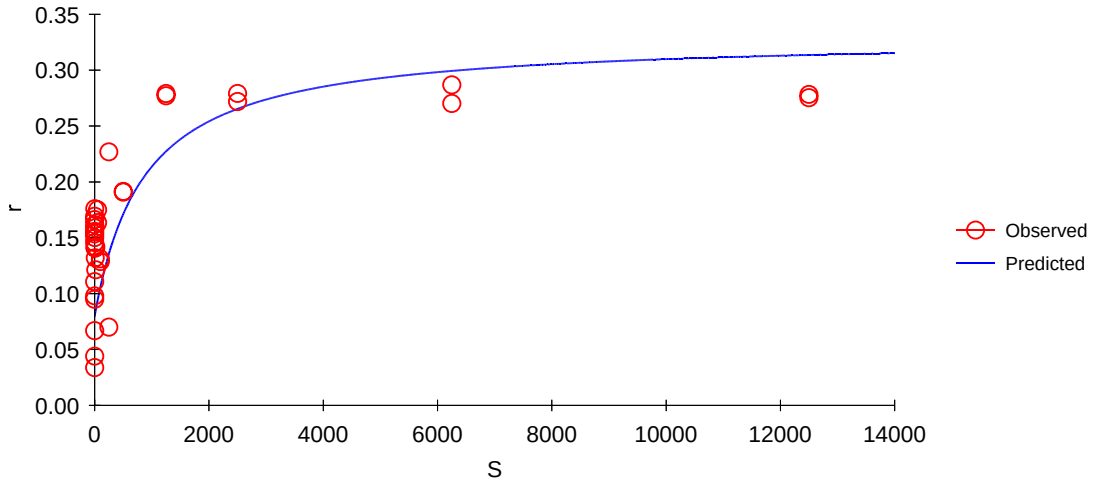

Figure 29. Determination of microtubule binding parameters

Glutaraldehyde-fixed microtubules were studied in the range of 0.4-12.5 μM. The concentration of Flutax-2 used was 25 nM. The concentration of binding sites and equilibrium binding constant. Each data point represents N = 3. Abcissa (*X*-axis): Concentration of cross-linked microtubules (nM); Ordinate (*Y*-axis): anisotropy values.

The data obtained from best-fit modeling strategy for experiments done at 37 ^{o}C and at RT are represented in Figures 30 and 31, respectively. Flutax-2 binding kinetics data at RT indicated the number of binding sites to be around 0.7. The equilibrium binding constant was 0.078 nM. Upon increase in temperature from RT to 37 ^{o}C, the equilibrium binding constant observed was 0.01 nM at 37 ^{o}C and the number of binding sites was around 1.0. This data correlates with the previously reported studies on Flutax-2 kinetics. The number of binding sites close to 1.0 correlated with the data obtained when radiolabeled paclitaxel was used for determining

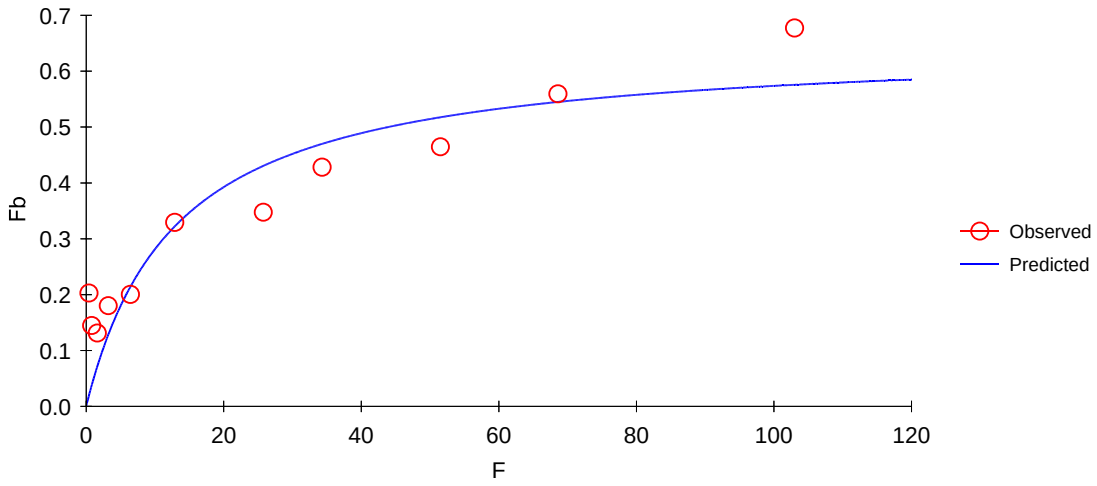

Figure 30. Determination of Flutax-2 binding parameters at 37 ^{o}C

Flutax-2 studied in the concentration range of 1-100 nM. The concentration of cross-linked microtubules was 100 nM. The number of binding sites and equilibrium binding constants for Flutax-2 were determined. Each data point represents N = 3. Abcissa (X-axis): Concentration of Flutax-2 (nM); Ordinate (Y-axis): fraction bound.

stoichiometry of paclitaxel binding to tubulin polymer (*vide supra*). Thermodynamic parameters for Flutax-2 binding to tubulin polymer at two different temperatures were determined from Van't Hoff plot (lnk versus 1/T). The association constant 'k' is the inverse of the equilibrium binding constant. Figure 32 represents the Van't Hoff plot. The data yielded negative enthalpy values suggesting that the thermodynamics of Flutax-2 binding to microtubules is an exothermic process. This is an expected result since Flutax-2 stabilized the formation of microtubules, the reaction is driven to the left (more stable microtubule formation).

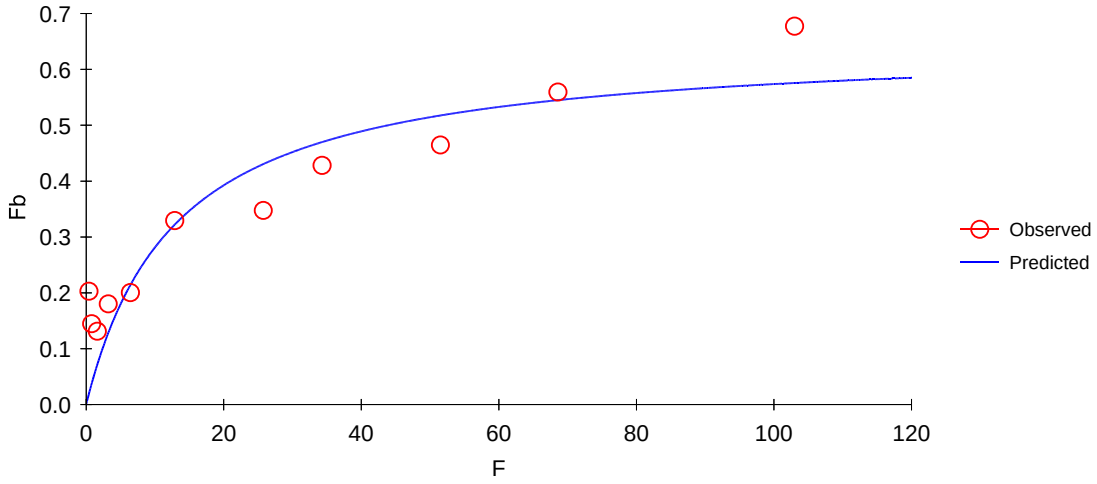

Figure 31. Determination of Flutax-2 binding parameters at RT

Flutax-2 was studied in the concentration range of 1-100 nM. The concentration of cross-linked microtubules was 100 nM. The number of binding sites and equilibrium binding constants for Flutax-2 were determined. Each data point represents N = 3. Abcissa (*X*-axis): Concentration of Flutax-2 (nM); Ordinate (*Y*-axis): fraction bound.

5.7. Discussion

Saturation binding experiments with [^{3}H]paclitaxel suggested a stoichiometry about 0.8 when total [^{3}H]paclitaxel bound values were considered for determination of the molar ratio of [^{3}H]paclitaxel bound to tubulin polymer. However, the molar ratio for specific binding of [^{3}H]paclitaxel bound to tubulin polymer was ~ 0.6 when docetaxel was used to account for non-specific binding values. The reported literature value was about 1:1 stoichiometry for [^{3}H]paclitaxel bound to tubulin heterodimer in similar experiments (Diaz *et al*. 1993; Caplow *et al*. 1994; Hung *et al*. 1996b; Hamel *et al*. 1999), but it is not known whether non-specific binding was considered for the data presented in the literature. Since, > 25% of the added tracer

bound to the protein at concentrations lower than the K_D value, the free concentrations of tracer were not to be assumed the same as total tracer added. This phenomenon is defined as ligand depletion and was understood to occur owing to non-specific binding of the labeled compound to

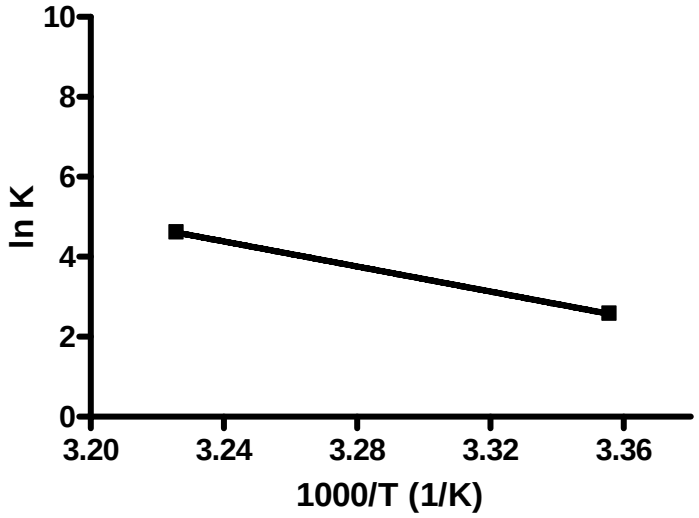

Figure 32. Van't Hoff plot of ln k versus 1/ K

The slope and intercept values were used to determine enthalpy and entropy terms, respectively for Flutax-2 binding to tubulin polymer. Each data point represents N = 4.

the protein (Morton *et al*. 2002). Assumptions made in deriving Langmuir binding isotherms no longer hold true in this case, and correction for non-specific binding should be done to account for ligand depletion. The Hill slope is a good estimate that provides clues for the existence of more than one affinity sites and/or heterogeneity in ligand binding to the protein. Hence, the data obtained in stoichiometry experiments were corrected for non-specific binding and Hill coefficients evaluated. The Hill slopes were different for total and specific binding of

[^{3}H]paclitaxel bound to tubulin polymer (1.6 versus 1.0) indicating paclitaxel bound to non-specific sites on tubulin polymer. This data suggests a one-site model for [^{3}H]paclitaxel binding to tubulin polymer. It is also shown that depending on the nucleotides used for inducing tubulin assembly, reaction conditions like protein and radioligand concentrations, the stoichiometry of paclitaxel binding to microtubules ranged anywhere between 0.7-1.0 (Caplow *et al*. 1994; Hamel 1999; Diaz *et al*. 2003). These same studies have shown that radioligand binding assays with [^{3}H]paclitaxel always yield maxima of about 80% of tracer bound to the polymer. This value when represented on a molar basis with respect to the number of moles of protein used in the assay would yield a value of about 0.8. Hence, 0.8:1 mol stoichiometry observed in the present studies is reasonable. Similar calculations were done for the protein aliquot used for discodermolide and 4-*epi* analogue inhibition study. The stoichiometry was about 0.5:1 or 0.3:1 moles of [^{3}H]paclitaxel bound per mole of tubulin polymer after accounting for non-specific binding. The lower stoichiometry could be due to another isoform of tubulin in the protein aliquot.

Inhibition analyses show that discodermolide, its 4-*epi* analogue (NC2-86) and dictyostatin had competitive effects at one site on the binding kinetics of paclitaxel. The two-site binding model did not converge. However, sigmoidal concentration-response curves afforded Hill slopes > 1.0 for discodermolide and dictyostatin, indicating there could be more than one high affinity site for discodermolide. Steeper slopes were observed regardless of whether non-specific or specific bound values were considered for inhibition plots. Similar plots for the 4-*epi* analogue yielded Hill slopes of > 1.0 at lower concentrations but ~ 1.0 at higher concentrations. The steeper slopes observed in the presence of inhibitors could be because of several reasons, including ligand depletion. Stoichiometry determination after accounting for ligand depletion

yielded Hill slope of 1.0. However, specifically bound values considered for inhibition plots resulted in Hill slopes greater than unity. One possible explanation for this could be that the correction for ligand depletion takes into account only the traceable ligand, *i.e.*, [^{3}H]paclitaxel. Ligand depletion could also occur for nonradioactive ligands or competitors, which were not accounted for in the equations described. This heterogeneity in binding in a heterologous competition experiment, like this one, accounts only for the non-specific binding of the tracer and not the competitor as well. Ligand depletion for inhibitors could be due to inhibitors themselves binding to some other site or have an overlapping binding site with respect to that of the tracer. Another reason could be attributed to the mechanism of action of the competitors. The steep Hill coefficients observed could be due to the high affinity with which the competitors (discodermolide and dictyostatin, in particular) bind to tubulin polymer and/or exert a positive co-operativity for binding of the substrate ([^{3}H]paclitaxel) to microtubule polymer. Literature reports suggest that agonists for a protein or a receptor have this characteristic feature. Since, the molecules have a stabilizing effect on microtubules, the action of one ligand may have an agonistic effect on the microtubule stabilization properties of the other. The presence of more than one isoform of tubulin or MAPs could also explain this effect. Yet another explanation could be due to existence of non-equilibrium conditions in the reaction mixture. This could be a remote possibility since the incubation time was long enough for equilibrium condition to have reached. In these experiments, since the two-site model did not quite fit well for any of the inhibitors, positive co-operativity seems to be the most plausible explanation for Hill slopes to be > 1.0. These results are supported by Hanes analysis which suggested discodermolide, the 4-*epi* analogue of discodermolide and dictyostatin to have a mixed inhibition pattern. Results from Hanes plots also highlight the possibility of minimum overlapping binding sites for

discodermolide, the 4-*epi* analogue of discodermolide, and dictyostatin with respect to paclitaxel on tubulin polymer. The presence of two different isoforms of tubulin contributing to the mixed kinetics cannot be overruled. Discodermolide showed high and low affinity K_i values of 34 and 178 nM, respectively. The K_i value reported in the literature for discodermolide was 0.4 μM, this is because total [^{3}H]paclitaxel concentrations were considered for Hanes analysis versus the free tracer concentrations that were used in the present calculations. Discodermolide seemed to have an allosteric effect on paclitaxel binding to tubulin polymer. A similar effect was observed with the 4-*epi* analogue. However, the possibility for the presence of another isoform of tubulin in the protein aliquot cannot be ruled out, especially considering the variable binding interactions and stoichiometries observed for the tubulin aliquot. We previously reported that [^{3}H]paclitaxel exhibited differential binding and inhibition kinetics on tubulin polymer in the presence of discodermolide and the 4-*epi* analogue (Madiraju *et al*. 2004). Data from these experiments revealed the radioligand to tubulin stoichiometry to be ~ 0.4 and ~ 0.3 moles of total- and specifically-bound radiolabeled paclitaxel per mole of tubulin polymer, respectively, a value half that observed in the previous study. The differences in stoichiometry between the two protein aliquots could be due to solution variables, nucleotide content, or another isoform being present in the tubulin aliquot. Dictyostatin inhibition kinetics with the protein aliquot that showed a 0.8:1 stoichiometry showed a competitive inhibition pattern with higher concentrations of the tracer. Dictyostatin yielded K_i values of 23 and 300 nM at high and low affinity sites, respectively This data suggests that dictyostatin might also have an allosteric effect on paclitaxel binding kinetics.

The reasons behind the positive co-operativity and mixed inhibition pattern observed could be many. Discodermolide and paclitaxel, as suggested in the literature and as discussed

above, might share an overlapping binding site for exerting an allosteric effect and/or positive co-operativity. This latter term is reflected in Hill slopes > 1.0. The presence of any of the inhibitors (known to be microtubule stabilizers) might stabilize the binding conformation of the protofilaments better, making the site amenable for facile binding of paclitaxel on tubulin polymer. However, the presence of more than one isoform or subtype of tubulin might also contribute to the differential binding kinetics. The latter could also be part of the explanation for mixed inhibition observed in these studies. This is because, stoichiometry experiments done with tubulin aliquot used for these studies suggested a mol:mol [^{3}H]paclitaxel to tubulin ratio of <0.5 (Figure 33 in the Appendix). This data suggests there are two moles of protein to which [^{3}H]paclitaxel bound. The mixed inhibition pattern observed for discodermolide could be due to inhibition of [^{3}H]paclitaxel bound to two moles of protein in the reaction mixture. The K_{app} values changed in the presence of discodermolide as compared to the K_D value observed in the presence of no inhibitor, suggesting a competitive pattern of inhibition. However, the slopes of the lines in the presence of inhibitor were not comparable to the one with no inhibitor, indicating that there is a change in B_{max} values as well. Hill slopes also provide similar result. Ideally, one should observe a slope of ~ 1 for a one-site competitive inhibition profile (Edler *et al*. 2005). The Hill slopes of > 1.0 observed in our studies and the proposed mechanism of positive co-operativity between microtubule provide a reasonable explanation for synergism observed in the suppression of microtubule dynamics in the presence of discodermolide and paclitaxel. Studies done to evaluate the cellular effects in the presence of MT-targeting agents suggest a synergism between paclitaxel and discodermolide in their effects on *in vivo* suppression of MT dynamics (Honore *et al*. 2004). This effect was attributed to the accelerated senescence observed for discodermolide- and not paclitaxel-treated cells. The accelerated senescence and synergistic

effect in the presence of these molecules could be due to the presence of mutually exclusive binding sites for paclitaxel, overlapping binding sites, positive co-operativity, to the existence of more than one isoform of tubulin, or higher affinity of the ligands to the polymer all of which bring out sequelae of events starting from hypernucleation, potent stabilization, and suppression of microtubule dynamics to the initiation of mitotic cell death events.

Studies done towards understanding the relationship between stoichiometry of paclitaxel binding to tubulin α,β-dimer and microtubule polymerization dynamics have shown that paclitaxel suppresses dynamic instability of microtubules differently depending on the stoichiometry of paclitaxel bound to tubulin polymer (Derry *et al*. 1995). Results from these studies show that at high stoichiometries > 0.1 mol paclitaxel to mol microtubule polymer, the dynamic instability of microtubules was completely suppressed with a significant change in polymer mass. At lower stoichiometries tubulin polymer dynamics were suppressed with out much change in the polymer mass. Earlier, it was shown that heterogeneous binding sites exist for paclitaxel on microtubule polymer induced by GTP, one a low affinity site and the other a high affinity site (Li *et al*. 2001). Paclitaxel was understood to bind to the high-affinity sites located at the GTP-cap on the polymerizing end or positive-end of the microtubules. Upon GTP hydrolysis, this site becomes the low-affinity site and is either internalized or is located at the depolymerizing end or negative-end of the microtubules (Li *et al*. 2001; Caplow *et al*. 1994). It was recently reported that paclitaxel exhibits two mutually exclusive binding sites one on the outer surface of microtubules (external site) and the other on the luminal side of microtubules (internal site) affording a stoichiometry of 1:1 (Diaz *et al*. 2005). While understanding the mechanism binding kinetics of paclitaxel, it was proposed that paclitaxel or taxoid site binding agents bind to the outer microtubule surface, induce a conformational change, diffuse into the

luminal surface, and bind to the inner side of the microtubules. Structural and biochemical evidence suggests that paclitaxel binds to the luminal surface of the microtubule (Nogales *et al*. 1999). In our studies, the ligands showed an overall mixed inhibition pattern, had Hill slopes greater than unity indicating an allosteric effect and/or positive co-operativity, and showed one-site competitive inhibition. However, at this point it cannot be stated with certainty that the ligands bound to the external or the internal site to show a competitive inhibition effect. Regardless, it would be of interest then to study for *in vivo* and *in vitro* synergism between paclitaxel and dictyostatin on tubulin polymerization dynamics. Studies done to examine the possibility of two binding sites for paclitaxel also suggest that induction of microtubule assembly occurred regardless of whether paclitaxel bound to the external site or the internal site but induction of assembly was shown to be rapid when paclitaxel bound to the external surface (Diaz *et al*. 2005). Hence, from a drug design perspective it would be important to investigate where exactly the ligands bind to the polymer, and ligands that bind to the external surface might have a better efficacy as microtubule stabilizers.

Data obtained from fluorescence anisotropy experiments for Flutax-2 binding kinetics correlated with radioligand binding data. Fluorescence anisotropy is a more sensitive and a robust technique. Hence, lower concentrations of Flutax-2 were studied to understand binding kinetics in a wide concentration range. Like in radioligand binding assay, Flutax-2 showed a unitary binding site on the microtubule polymer. Inhibition studies with Flutax-2 are currently in progress. Thermodynamic evaluation of Flutax-2 binding to tubulin polymer suggests that the binding mechanism is exothermic and an entropy-driven process. Previous studies have suggested that paclitaxel binding to microtubules is an exothermic process. Inhibition studies are

worth doing to understand the binding affinities and energetics of both the tracer and the inhibitor.

The presence of overlapping binding sites for discodermolide-paclitaxel and/or dictyostatin-paclitaxel might be a possibility since in silico modeling studies done in the Day lab suggest that a paclitaxel binding model might not truly fit the ligands that were studied (Hu and Day 2005). Modeling studies showed that discodermolide is away from the B9-B10 helix (Phe270 residue) and *via* hydrophilic interactions is positioned towards the M-loop. This is supported by biological studies done on mutated ovarian carcinoma cell lines that have Phe270 residue mutated (1A9PTX22), where in it was shown that 14-normethyldiscodermolide was as active as the parent molecule (Smith *et al*. 2001). Recently, it was also shown that epothilone A had a pharmacophore model different from that proposed for paclitaxel. These studies suggest that epothilone A to have many hydrophilic interactions with the residues on M-loop of the β-tubulin subunit of the polymer. In contrast to 14-normethyldiscodermolide, the analogous C16-methyl group of dictyostatin was shown to orient towards Phe270, and mutation of this residue led to loss of activity of C16-normethyldictyostatin (Chapter 4). However, the parent molecule, dictyostatin, seemed not be sensitive to these mutations indicating a binding conformation possibly similar to discodermolide, but different from C16-normethyl analogue. Studies directed towards understanding the binding kinetics and conformations are ongoing.

6. CONCLUSIONS

The investigations performed for this dissertation were aimed at pharmacological evaluation and structure-activity relationship studies of discodermolide, dictyostatin and their synthetic analogues for microtubule-targeting and perturbing activities. A structurally diverse set of natural product-derived molecules and synthetic analogues have been identified to have potent microtubule-stabilizing actions (Chapter 1). A few of them are going though clinical trials. The marine sponge-derived discodermolide had shown potent microtubule-targeting activities in in silico and biochemical studies. The SAR data on discodermolide was sparse at the time when this project began. Hence, discodermolide analogues were evaluated for microtubule-targeting activities.

The experiments for performing evaluations were established to understand the pharmacological activity and SAR for microtubule-stabilizing agents (Chapter 2). The first library of discodermolide analogues gave valuable clues on the structural elements important for biological activity (Chapter 3). Modifications done on the diene and carbamate moieties of discodermolide yielded analogues with poor activity. These two positions were sensitive for modifications. The 11*S* and 17*R* stereochemistry is important for activity, since modification of the configuration at these positions led to compounds with very weak microtubule-stabilizing activities. The lactone functionality afforded little more flexibility for SAR studies. Bulkier esters like the ^{t}butanoyl replacing the lactone moiety yielded analogues with reasonably good microtubule-targeting activities. The second library had interesting set of analogues (Chapter 3). One of the analogues, the 4-*epi* analogue NC86, was designed from a rational drug design

approach and the biological activity data is in agreement with the proposal that hydrogen bonding interaction between the C-3-OH and the nitrogen of the carbamate at C-19 stabilizes better the conformation of discodermolide. NC86 has the C3-OH group replaced with an extended spacer, a methoxymethyl ether group, and had shown activity in low micromolar range and inhibited [^{3}H]paclitaxel from binding to tubulin polymer to an extent of about 57% (Chapter 3). Hence, conformational analogues of discodermolide might yield analogues with better microtubule-targeting activity profiles. The third set of analogues set the scope for the future of this project. The hypothesis that because dictyostatin and discodermolide resemble each other structurally and macrocyclic analogues of discodermolide should therefore retain biological activity, proved to be supported by one of the macrocyclic hybrids, YSS133, which had antiproliferative activity in the low micromolar range (Chapter 3).

Synthetic dictyostatin is the present molecule of interest. Studies on MT binding properties, MT-stabilization effects and anti-proliferative activities revealed dictyostatin to be a very potent MT stabilizer (Chapter 4). Preliminary results strongly suggest dictyostatin to be having a potent MT perturbing effect. The inhibition of [^{3}H]paclitaxel and [^{14}C]epothilone B from binding to tubulin polymer by dictyostatin was comparable to discodermolide. However, dictyostatin had a lower ability to inhibit [^{3}H]discodermolide from binding to MTs. This could be because of higher affinity of discodermolide for MTs than dictyostatin. Tubulin polymerization studies showed a comparative profile for dictyostatin, discodermolide and paclitaxel under various reaction conditions. Dictyostatin, like similar to discodermolide, hypernucleated tubulin assembly starting at 0 ^{o}C onwards. Paclitaxel lacked this ability at lower temperatures. MAPs and GTP showed a differential effect on the regulation of polymerization dynamics in the presence of dictyostatin, discodermolide, and paclitaxel. These studies show

that dictyostatin and discodermolide induce tubulin assembly regardless of the presence of MAPs and/or GTP. In addition, the polymer inducing ability of paclitaxel was equal to that of dictyostatin and discodermolide at 30 ^{o}C in complete system consisting of MAPs and GTP. This differential effect could be due to better stabilization of paclitaxel-bound tubulin conformation in the presence of MAPs and GTP. There could be some positive cooperativity of MAPs on the stabilization of binding conformation of paclitaxel to MTs. Since dictyostatin and discodermolide bind to tubulin polymer with higher affinity than paclitaxel, the stabilization of the M-loop conformation at the interprotofilament interface of the polymer might be better in the presence of these agents, thus precluding the requirement for MAPs and/or GTP. Electron microscopic images showed MT polymer in the presence of dictyostatin when polymerization experiments were done in complete system containing MAPs and GTP. Abnormal polymer forms were noticed in the system lacking MAPs and GTP and these were more commonly seen for discodermolide-induced polymer. These subtle differences in polymer morphology could be due to small, but significant, binding site differences. *In vitro* studies show the rank order of potency to be: dictyostatin ~ discodermolide > paclitaxel. Dictyostatin, like discodermolide, is active in paclitaxel-resistant mutated β-tubulin cell lines. Immunfluorescence experiments on HeLa cells showed dictyostatin to be the most potent of all the agents studied. MT bundling, antimitotic effects and condensation of nuclear chromatin were more extensive in the presence of dictyostatin than that observed for either paclitaxel or discodermolide. The minimum detectable effective concentrations of dictyostatin were lower than those of paclitaxel and discodermolide. The rank order of potency of these agents on *in vivo* cellular effects is that: dictyostatin > paclitaxel > discodermolide. This discrepancy between *in vitro* and *in vivo* findings could be that the transport of discodermolide might not be sufficient and discodermolide may be metabolically

more labile. These two features might contribute to the needed dose escalation of and subsequent toxicity observed with discodermolide that led to termination of its clinical trials. Dictyostatin, like epothilone B, is a more rigid, cyclic molecule, and for these features could also be a good candidate for clinical evaluation.

SAR evaluation studies on dictyostatin analogues showed that the macrolactone and the bottom half of dictyostatin are essential for activity (Chapter 4). The top half is crucial for binding of the molecule to the target. The 16-normethyl analogue was less active in [^{3}H]paclitaxel inhibition studies. The 16-normethyl analogue is the interesting molecule with antiproliferative activity profile similar to that of the parent molecule. Interesting is the observation that this molecule showed differential activity profile against two mutated ovarian cancer cell lines that was not seen with dictyostatin. In one cell line (1A9PTX10), it showed activity similar to that observed in the parental cell line, while in the other mutated cell line it showed very weak activity (1A9PTX22). This suggests the orientation of the C16-Me is towards Phe270 and modeling studies support this hypothesis.

Analyses of binding kinetics showed ~ 0.8:1 stoichiometry for [^{3}H]paclitaxel bound to tubulin polymer (Chapter 5). There could be mutually exclusive binding sites for paclitaxel. The inhibitors, discodermolide, dictyostatin and the 4-*epi* analogue NC86 showed mixed inhibition patterns with Hill slopes greater than 2.0. These inhibitors might be exerting an allosteric effect or positive cooperativity on the binding kinetics of paclitaxel. Studies done to understand the binding energetics suggest dictyostatin to be similar to discodermolide in having lower binding energetics. Fluorescence anisotropy experiments with Flutax-2 suggest that the binding thermodynamics is an exothermic and an entropy-driven process (Chapter 5). Inhibition studies are in progress.

The future holds much promise for dictyostatin and its synthetic analogues. It would be of interest to determine any synergism between dictyostatin and paclitaxel. This is suggested because the present results suggest an allosteric effect and/or positive cooperativity of dictyostatin on paclitaxel binding kinetics. It is known that discodermolide and paclitaxel exhibit synergism in suppressing cellular MT dynamics and in causing cytotoxicity. The binding/pharmacophore model for dictyostatin, discodermolide and 16-normethyldiscodermolide needs to be established *via* in silico approaches to help give a better understanding of the binding kinetics. [^{3}H]Discodermolide binding kinetic parameters would be of great help to understand differences in binding interactions between paclitaxel and discodermolide. SAR studies can be pursued further. Finally, synthetic analogues of dictyostatin with modifications on the diene and the bottom half, conversion of the macrolactone (cyclic ester) functionality of dictyostatin to a macrolactam (cyclic amide) would also be of great interest. The challenges now are in the hands of the synthetic chemists.

APPENDIX

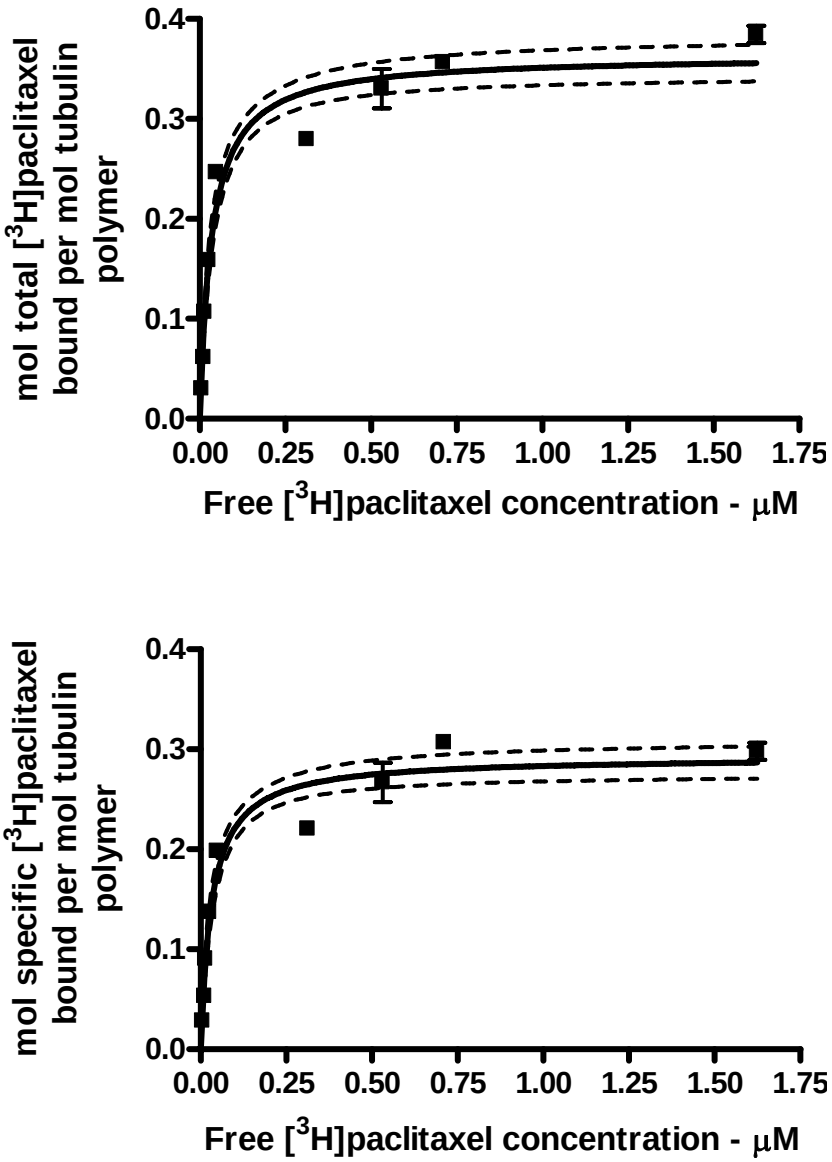

Figure 33. Saturation binding kinetics with previous tubulin aliquot

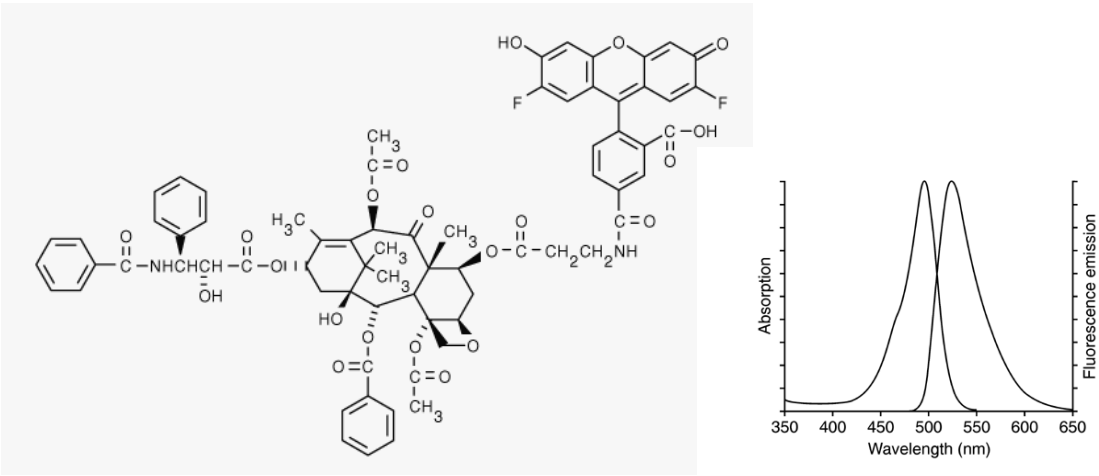

Figure 34. Structure of Flutax-2 and its spectrofluorimetric characteristics

(Adapted from: http://probes.invitrogen.com/servlets/structure?item=22310 and http://probes.invitrogen.com/servlets/spectra?fileid=6380ph8, respectively).

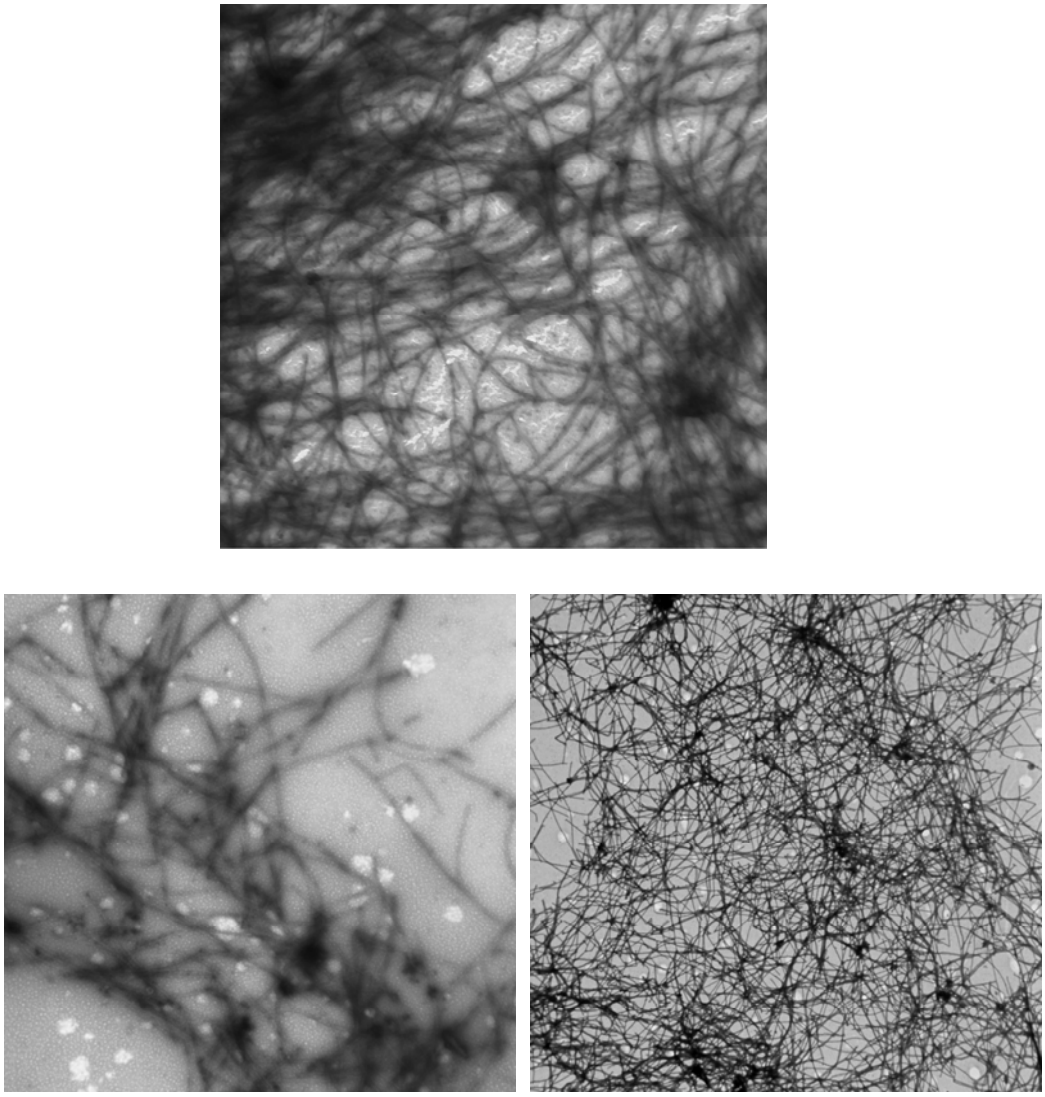

Figure 35. Electron microscopic images of glutaraldehyde-fixed microtubules

Upper image: undiluted fixed microtubules

Image on the left: fixed microtubules after 1000-fold dilution

Image on the right: fixed microtubules after 100-fold dilution

BIBLIOGRAPHY

Abraham, V. C., Taylor, D. L., and Haskins, J. R. (2004) High content screening applied to large-scale cell biology, *Trends Biotechnol*. *22*, 15-22.

Altmann, K. H., Bold, G., Caravatti, G., Florsheimer, A., Guagnano, V., and Wartmann, M. (2000a) Synthesis and biological evaluation of highly potent analogues of epothilones B and D, *Bioorg. Med. Chem. Lett*. *10*, 2765-2768.

Altmann, K-H., Wartmann, M., and O'Reilly, T. (2000b) Epothilones and related structures--a new class of microtubule inhibitors with potent *in vivo* antitumor activity, *Biochem. Biophys. Acta*. *1470*, M79-M91.

Andersen, S. S., Ashford, A. J., Tournebize, R., Gavet, O., Sobel, A., Hyman, A. A., and Karsenti, E. (1997) Mitotic chromatin regulates phosphorylation of Stathmin/Op18, *Nature 389*, 640-643.

Andreu, J. M., and Barasoain, I. (2001) The interaction of baccatin III with the taxol binding site of microtubules determined by a homogeneous assay with fluorescent taxoid, *Biochemistry 40*, 11975-11984.

Balachandran, R., ter Haar, E., Welsh, M. J., Grant, S. G., and Day, B. W. (1998) The potent microtubule-stabilizing agent (+)-discodermolide induces apoptosis in human breast carcinoma cells-preliminary comparisons to paclitaxel, *Anticancer Drugs 9*, 67-76. Erratum in: *Anticancer Drugs* (1998) *9*, 369-370.

Ballone P, and Marchi M. (1999) A density functional study of a new family of anticancer drugs: paclitaxel, taxotere, epothilone, and discodermolide. *J. Phys. Chem. A 103*, 3097–3102.

Belmont, L. D., and Mitchison, T. J. (1996) Identification of a protein that interacts with tubulin dimers and increases the catastrophe rate of microtubules, *Cell 84*, 623-631.

Bollag, D. M., McQueney, P. A., Zhu, J., Hensens, O., Koupal, L., Liesch, J., Goetz, M., Lazarides, E., and Woods, C. M. (1995) Epothilones, a new class of microtubule-stabilizing agents with a taxol-like mechanism of action, *Cancer Res*. *55*, 2325-2333.

Borisy, G. G., and Taylor, E. W. (1967a) The mechanism of action of colchicine. Binding of colchincine-^{3}H to cellular protein, *J. Cell Biol*. *34*, 525-534.

Borisy, G. G., and Taylor, E. W. (1967b) The mechanism of action of colchicine. Colchicine binding to sea urchin eggs and the mitotic apparatus, *J. Cell Biol*. *34*, 535-547.

Buey, R. M., Díaz, J. F., Andreu, J. M., O'Brate, A., Giannakakou, P., Nicolaou., K. C., Sasmal., P. K., Ritzén, A., and Namoto, K. (2004) Interaction of epothilone analogs with the paclitaxel binding site: relationship between binding affinity, microtubule stabilization, and cytotoxicity, *Chem. Biol*. *11*, 225-236.

Burlingame, M. A., Shaw, S. J., Sundermann, K. F., Zhang, D., Petryka, J., Mendoza, E., Liu, F., Myles, D. C., LaMarche, M. J., Hirose, T., Freeze, S. B., and Smith, A. B III. (2004) Design, synthesis and cytotoxicity of 7-deoxy aryl discodermolide analogues, *Bioorg. Med. Chem. Lett*. *14*, 2335-2338.

Caplow, M., Shanks, J., and Ruhlen, R (1994) How taxol modulates microtubule disassembly, *J. Biol. Chem*. *269*, 23399-23402.

Carazo-Salas, R. E., Guarguaglini, G., Gruss, O. J., Segref, A., Karsenti, E., and Mattaj, I. W. (1999) Generation of GTP-bound Ran by RCC1 is required for chromatin-induced mitotic spindle formation, *Nature 400*, 178-181.

Carazo-Salas, R. E., Gruss, O. J., Mattaj, I. W., and Karsenti E. (2001) Ran-GTP coordinates regulation of microtubule nucleation and dynamics during mitotic-spindle assembly, *Nat. Cell Biol*. *3*, 228-234.

Chen, W., Bair, K. W., Lassota, P. T., Ramsey, T. M., Sorensen, E., Wang, R. M., and Kinder, F. R. Jr. (2004) Synthesis of discodermolide analogs with isosteric replacements of the C^{1}-^{5} lactone ring with simplified aromatic groups, *ACS National Meeting Presentation,* 790.

Choy, N., Shin, Y., Nguyen, P. Q., Curran, D. P., Balachandran, R., Madiraju, C., and Day, B. W. (2003) Simplified discodermolide analogues: synthesis and biological evaluation of 4-*epi*-7-dehydroxy-14,16-didemethyl-(+)-discodermolides as microtubule-stabilizing agents, *J. Med. Chem*. *46*, 2846-2864.

Ciomei, M., Albanese, C., Pastori, W., Grandi, M., Pietra, F., D'Ambrosio, M., Guerriero, A., and Battistini, C. (1997) Sarcodictyins: A new class of marine derivatives with mode of action similar to taxol, *Proc. Am. Assoc. Canc. Res*. *38*, 5.

Commercial Insight: Cytotoxics - Generic adversity facing major cytotoxics Datamonitor, July 2005, Pages: 126.
http://www.the-infoshop.com/study/dc31717-cytotoxics.html

Corley, D. G., Herb, R., Moore, R. E., Scheuer, P. J., and Paul, V. J. (1988) Laulimalides: new potent cytotoxic macrolides from a marine sponge and a nudibranch predator, *J. Org. Chem*. *53*, 3644-3646.

Correia, J. J., and Lobert, S. (2001) Physiochemical aspects of tubulin-interacting antimitotic drugs, *Curr. Pharm. Des. 7*, 1213-1228.

Cragg, G. M., and Newman, D. J. (2004) A tale of two tumor targets: topoisomerase I and tubulin, The Wall and Wani contribution to cancer chemotherapy, *J. Nat. Prod*. *67*, 232-244.

Curran, D. P., and Furukawa, T. (2002) Simultaneous preparation of four truncated analogues of discodermolide by fluorous mixture synthesis, *Org. Lett*. *4*, 2233-2335.

D'Ambrosio, M., Guerriero, A., and Pietra, F. (1987) Sarcodictyin A and Sarcodictyin B, novel diterpenoidic alcohols esterified by (*E*)-*N*(1)-methylurocanic acid. Isolation from the mediterranean Stolonifer *Sarcodictyon roseum, Helv. Chim. Acta*. *70*, 2019-2027.

Dabydeen, D. A., Florence, G. J., Paterson, I., and Hamel, E. (2004) A quantitative evaluation of the effects of inhibitors of tubulin assembly on polymerization induced by discodermolide, epothilone B, and paclitaxel, *Cancer Chemother. Pharmacol*. *53*, 397-403.

Davidson, N. G. (1995) Single-agent paclitaxel at first relapse following adjuvant chemotherapy for breast cancer, *Semin. Oncol. 22*, *Suppl*. *14*, 2-6.

Davidson, N. G. (1996) Single-agent paclitaxel as first-line treatment of metastatic breast cancer: the British experience, *Semin. Oncol*. *23*, *Suppl*. *11*, 6-10.

Day, B. W., Kangani, C. O., and Avor, K. S. (2002) Preparation of C1–C7 and C17–C24 fragments of (+)-discodermolide, *Tetrahedron: Asymmetry 13*, 1161-1165.

Derry, W. B., Wilson, L., and Jordan, M. A. (1995) Substoichiometric binding of taxol suppresses microtubule dynamics, *Biochemistry 34*, 2203-2211.

Desai, A., and Mitchison, T. J. (1997) Microtubule polymerization dynamics, *Annu. Rev. Cell Dev. Biol*. *13*, 83-117.

Desai, A., Verma, S., Mitchison, T. J., and Walczak, C. E. (1999) Kin I kinesins are microtubule-destabilizing enzymes, *Cell 96*, 69-78.

Diaz, J. F., and Andreu, J. M. (1993) Assembly of purified GDP-tubulin into microtubules induced by taxol and taxotere: reversibility, ligand stoichiometry, and competition, *Biochemistry 32*, 2747-2755.

Diaz, J. F., Strobe, R., Engelborghs, Y., Souto, A. A, and Andreu, J. M. (2000) Molecular recognition of taxol by microtubules. Kinetics and thermodynamics of binding of fluorescent taxol derivatives to an exposed site, *J. Biol. Chem*. *275*, 26265-26276.

Diaz, J. F., Barasoain, I., and Andreu, J. M. (2003) Fast kinetics of taxol binding to microtubules. Effects of solution variables and microtubule-associated proteins, *J. Biol. Chem*. *278*, 8407-8419.

Diaz, J. F., Barasoain, I., Souto, A. A., Amat-Guerri, F., and Andreu, J. M. (2005) Macromolecular accessibility of fluorescent taxoids bound at a paclitaxel binding site in the microtubule surface. *J. Biol. Chem*. *280*, 3928-3937.

Dixon, M., Webb, E. C., Thorne, C. J. R., and Tipton, K. F. (1979) *Enzymes*, 3rd ed., Academic Press, New York.

Downing, K. H., and Nogales, E. (1998) New insights into microtubule structure and function from the atomic model of tubulin, *Eur. Biophys. J. 27*, 431-436.

Downing, K. H. (2000) Structural basis for the interaction of tubulin with proteins and drugs that affect microtubule dynamics, *Annu. Rev. Cell Dev. Biol. 16*, 89-111.

Dustin, P. (1984) *Microtubules*, Ed. 2, 482 pp. Berlin: Springer-Verlag.

Edler, M. C., Buey, R. M., Gussio, R., Marcus, A. I., Vanderwal, C. D., Sorensen, E. J., Diaz, J. F., Giannakakou, P., and Hamel, E. (2005) Cyclostreptin (FR182877), an antitumor tubulin-polymerizing agent deficient in enhancing tubulin assembly despite its high affinity for the taxoid Site, *Biochemistry 44*, 11525-11538.

Francavilla, C., Chen, W., and Kinder, F. R. (2003) Formal synthesis of (+)-discodermolide, *Org. Lett. 5*, 1233-1236.

Gapud, E. J., Bai, R., Ghosh, A. K., and Hamel, E. (2004) Laulimalide and paclitaxel: a comparison of their effects on tubulin assembly and their synergistic action when present simultaneously, *Mol. Pharmacol. 66*, 113-121.

Gaskin, F., Cantor, C. R., and Shelanski, M. L. (1974) Turbidimetric studies of the in vitro assembly and disassembly of porcine neurotubules, *J. Mol. Biol. 89*, 737-755.

Geng, P., Bair, K. W., Lassota, P. T., Ramsey, T. M., Sorensen, E., Wang, R. M., and Kinder, F. R. Jr. (2004) Synthesis of a discodermolide analogue with an isosteric replacement of the C^{13}-trisubstituted olefin with an N-methyl amide, *ACS National Meeting Presentation,* 789.

Gerth, K., Bedorf, N., Hofle, G., Irschik, H., and Reichenbach, H. (1996) Epothilons A and B: antifungal and cytotoxic compounds from *Sorangium cellulosum* (Myxobacteria). Production, physico-chemical and biological properties*, J. Antibiot. 49*, 560-563.

Giuliano, K. A., Haskins, J. R., and Taylor, D. L. (2003a) Advances in high content screening for drug discovery, *Assay Drug Dev. Technol. 1*, 565-577.

Giuliano, K. A. (2003b) High-content profiling of drug-drug interactions: cellular targets involved in the modulation of microtubule drug action by the antifungal Ketoconazole, *J. Biomol. Screen. 8*, 125-135.

Giuliano, K. A., Chen, Y. T., and Taylor, D. L. (2004) High-content screening with siRNA optimizes a cell biological approach to drug discovery: Defining the role of p53 activation in the cellular response to anticancer drugs, *J. Biomol. Screen. 9*, 557-568.

Guenard, D., Gueritte-Voegelein, F., Dubois, J., and Potier P. (1993) Structure-activity relationships of taxol and taxotere analogues, *J. Natl. Cancer Inst. Monogr. 15*, 79-82.

Gunasekera, S. P., Gunasekera, M., Longley, R. E., and Schulte, G. K. (1990) Discodermolide: a new bioactive polyhydroxylated lactone from the marine sponge *Discodermia dissoluta*, *J. Org. Chem*. *55*, 4912-4915. Correction in: *J. Org. Chem*. (1991) *56*, 1346.

Gunasekera, S. P., Longley, R. E., and Isbrucker, R. A. (2001) Acylated analogues of the microtubule-stabilizing agent discodermolide: preparation and biological activity, *J. Nat. Prod*. *64*, 171-174.

Grover, S., and Hamel, E. (1994) The magnesium-GTP interaction in microtubule assembly, *Eur. J. Biochem*. *222*, 163-172.

Grover, S., Rimoldi, J. M., Molinero, A. A., Chaudhary, A. G., Kingston, D. G., and Hamel, E. (1995) Differential effects of paclitaxel (Taxol) analogs modified at positions C-2, C-7, and C-3' on tubulin polymerization and polymer stabilization: identification of a hyperactive paclitaxel derivative, *Biochemistry 34*, 3927-3934.

http://mitchison.med.harvard.edu/research/Microtubules.htm

http://probes.invitrogen.com/servlets/structure?item=22310

http://probes.invitrogen.com/servlets/spectra?fileid=6380ph8

Hamel, E., and Lin, C. M. (1984) Separation of active tubulin and microtubule-associated proteins by ultracentrifugation and isolation of a component causing the formation of microtubule bundles, *Biochemistry 23*, 4173-4184.

Hamel, E. (1996) Antimitotic natural products and their interactions with tubulin. *Med. Res. Rev*. *16*, 207-231.

Hamel, E., Sackett, D. C., Vourloumis, D., and Nicolaou, K. C. (1999) The coral-derived natural products eleutherobin and sarcodictyins A and B: effects on the assembly of purified tubulin with and without microtubule-associated proteins and binding at the polymer taxoid site, *Biochemistry 38*, 5490-5498.

Harried, S. S., Lee, C. P., Yang, G., Lee, T. I. H., and Myles, D. C. (2003) Total synthesis of the potent microtubule-stabilizing agent (+)-discodermolide, *J. Org. Chem*. *68*, 6646-6660.

Hood, K. A., West, L. M., Rouwe, B., Northcote, P. T., Berridge, M. V., Wakefield, S. J., and Miller, J. H. (2002) Peloruside A, a novel antimitotic agent with paclitaxel-like microtubule-stabilizing activity, *Cancer Res*. *62*, 3356-3360.

Honore, S., Kamath, K., Braguer, D., Horwitz, S. B., Wilson, L., Briand, C., and Jordan, M. A. (2004) Synergistic suppression of microtubule dynamics by discodermolide and paclitaxel in non-small cell lung carcinoma cells, *Cancer Res*. *64*, 4957-4964.

Horwitz, S. B. (2004) Personal recollections on the early development of taxol. *J. Nat. Prod*. *67*, 136-138.

Hung, D. T., Nerenberg, J. B., and Schreiber, S. L. (1996a) Syntheses of discodermolides useful for investigating microtubule binding and stabilization, *J. Am. Chem. Soc*. *118*, 11054-11080.

Hung, D. T, Chen, J., and Schreiber, S. L. (1996b) (+)-Discodermolide binds to microtubules in stoichiometric ratio to tubulin dimers, blocks taxol binding and results in mitotic arrest, *Chem. Biol*. *3*, 287-293.

Hu, R., and Day, B. W. (2005) *http://www.ccbb.pitt.edu/BBSI/2005/proposal/hu.pdf*

Inoue, S., and Sato, H. (1967) Cell motility by labile association of molecules. The nature of mitotic spindle fibers and their role in chromosome movement, *J. Gen. Physiol*. *50*, *Suppl*. 259-292.

Isbrucker, R. A., Gunasekera, S. P., and Longley, R. E. (2001) Structure-activity relationship studies of discodermolide and its semisynthetic acetylated analogs on microtubule function and cytotoxicity, *Cancer Chemother. Pharmacol*. *48*, 29-36.

Isbrucker, R. A., Cummins, J., Pomponi, S. A., Longley, R. E., and Wright, A. E. (2003) Tubulin polymerizing activity of dictyostatin, a polyketide of marine sponge origin, *Biochem. Pharmacol*. *66*, 75-82.

Jimenez-Barbero, J., Amat-Guerri, F., and Snyder, J. P. (2002) The solid state, solution and tubulin-bound conformations of agents that promote microtubule stabilization, *Curr. Med. Chem. Anti-Cancer Agents*. *2*, 91-122.

Karsenti, E., and Vernos, I. (2001) The mitotic spindle: a self-made machine, *Science*. *294*, 543-547.

Kasai, M. (1969) Thermodynamical aspect of G-F transformations of actin, *Biochim. Biophys. Acta*. *180*, 399-409.

Kinder, F. R. Jr., Bair, K. W., Chen, W., Florence, G., Francavilla, C., Geng, P., Gunasekera, S., Lassota, P. T., Longley, R. E., Palermo, M. G., Paterson, I., Pomponi, A., Ramsey, L., Rogers, M., Sabio, M., Sereinig, N., Sorensen, E., and Wan, R. (2004) Synthesis and antitumor activity of analogs of the novel microtubule stabilizing agent discodermolide, *ACS National Meeting Presentation,* 236.

Kirschner, M. W., and Williams, R. C. (1974) The mechanism of microtubule assembly *in vitro*, *J. Supramol. Struct*. *2*, 412-428.

Klein, L. E., Freeze, S., Smith, A. B. III., and Horwitz S. B. (2005) The microtubule stabilizing agent discodermolide is a potent inducer of accelerated cell senescence, *Cell Cycle 4*, 501-507.

Kowalski, R. J., Giannakakou, P., and Hamel, E. (1997) Activities of the microtubule-stabilizing agents epothilones A and B with purified tubulin and in cells resistant to paclitaxel (Taxol®, *J. Biol. Chem*. *272*, 2534-2541.

Kowalski, R. J., Giannakakou, P., Gunasekera, S. P., Longley, R. E., Day, B. W., and Hamel, E. (1997) The microtubule-stabilizing agent discodermolide competitively inhibits the binding of paclitaxel (Taxol) to tubulin polymers, enhances tubulin nucleation reactions more potently than paclitaxel, and inhibits the growth of paclitaxel-resistant cells, *Mol. Pharmacol*. *52*, 613-622.

Lazo, J.S., Tamura, K., Vogt, A., Jung, J.-K., Rodriguez, S., Balachandran, R., Giuliano, K. A., Day, B. W., and Wipf, P. (2001) Antimitotic actions of a novel analog of the fungal metabolite palmarumycin CP1, *J. Pharmacol. Exp. Ther. 296,* 364-371.

Li, Y., Edsall, R. Jr., Jagtap, P. G., Kingston, D. G., and Bane, S. (2001) Equilibrium studies of a fluorescent paclitaxel derivative binding to microtubules, *Biochemistry 39,* 616-623.

Lindel, T., Jensen, P. R., Fenical, W., Long, B. H., Casazza, A. M., Carboni, J., and Fairchild, C. R. (1997) Eleutherobin, a new cytotoxin that mimics paclitaxel (Taxol) by stabilizing microtubules, *J. Am. Chem. Soc*. *119*, 8744-8745.

Long, B. H., Carboni, J. M., Wasserman, A. J., Cornell, L. A., Casazza, A. M., Jensen, P. R., Lindel, T., Fenical, W., and Fairchild, C. R. (1998) Eleutherobin, a novel cytotoxic agent that induces tubulin polymerization, is similar to paclitaxel (Taxol), *Cancer Res. 58*, 1111-1115.

Lowry, O.H., Rosebrough, N. J., Farr, N. J., and Randall, R. J. (1951) Protein measurement with the folin phenol reagent, *J. Biol. Chem. 193*, 265-275.

Madiraju. C., Choy, N., Curran, D. P., and Day, B. W. (2004) Kinetics of differential binding at two types of taxoid binding sites on tubulin polymer, *AACR Annual Meeting Abstracts*, LB-267.

Madiraju, C., Edler, M. C., Hamel, E., Raccor, B. S., Balachandran, R., Zhu, G., Giuliano, K. A., Vogt, A., Shin, Y., Fournier, J.-H., Fukui, Y., Brückner, A. M., Curran, D. P., and Day, B. W. (2005) Tubulin assembly, taxoid site binding, and cellular effects of the microtubule-stabilizing agent dictyostatin, *Biochemistry 44*, 15053-15063.

Mamounas, E. P., Bryant, J., Lembersky, B., Fehrenbacher, L., Sedlacek, S. M., Fisher, B., Wickerham, D. L, Yothers, G., Soran, A., and Wolmark, N. (1995) Paclitaxel after doxorubicin plus cyclophosphamide as adjuvant chemotherapy for node-positive breast cancer: results from NSABP B-28, *J. Clin. Oncol. 23*, 3686-3696.

Mani, S., Macapinlac, M. Jr., Goel, S., Verdier-Pinard, D., Fojo, T, Rothenberg, M., and Colevas, D. (2004) The clinical development of new mitotic inhibitors that stabilize the microtubule, *Anticancer Drugs 15*, 553-558.

Margolis, R. L., and Wilson, L. (1978) Opposite end assembly and disassembly of microtubules at steady state *in vitro*, *Cell 13*, 1-8.

Margolis, R. L., Wilson, L., and Keifer, B. I. (1978) Mitotic mechanism based on intrinsic microtubule behavior, *Nature 272*, 450-452.

Marshall, J. A., and Johns, B. A (1998) Total synthesis of (+)-discodermolide, *J. Org. Chem. 63*, 7885 -7892.

Martello, L. A., McDaid, H. M., Regl, D. L., Yang, C. P., Meng, D., Pettus, T. R., Kaufman, M. D., Arimoto, H., Danishefsky, S. J., Smith, A. B. III, and Horwitz, S. B. (2000) Taxol and discodermolide represent a synergistic drug combination in human carcinoma cell lines, *Clin. Cancer Res. 6*, 1978-1987.

Martlello, L. A., LaMarche, M. J., He, L., Beauchamp, T. J., Smith, A. B III., and Horwitz, S. B. (2001) The relationship between Taxol and (+)-discodermolide: synthetic analogs and modeling studies, *Chem. Biol. 8*, 843-855.

Mastronarde, D. N., McDonald, K. L., Ding, R., and McIntosh, J. R. (1993) Interpolar spindle microtubules in PTK cells, *J. Cell Biol. 123,* 1475-1489.

Mickel, S. J., Sedelmeier, G. H., Niederer, D., Daeffler, R., Osmani, A., Schreiner, K., Seeger-Weibel, M., Bèrod. B., Schaer. K., Gamboni, R., Chen, S., Chen, W., Jagoe, C. T., Kinder, F. R. Jr., Loo, M., Prasad, K., Repic, O., Shieh, W-C., Wang, R-M., Waykole, L., Xu, D. D., and Xue, S. (2004) Large-scale synthesis of the anti-cancer marine natural product (+)-discodermolide. Part 1: Synthetic strategy and preparation of a common precursor, *Org. Process Res. Dev. 8*, 92-100.

Mickel, S. J., Sedelmeier, G. H., Niederer, D., Schuerch, F., Grimler, D., Koch, G., Daeffler, R., Osmani, A., Hirni, A., Schaer, K., Gamboni, R., Bach, A., Chaudhary, A., Chen, S., Chen, W. C., Hu, B., Jagoe, C. T., Kim, H. Y., Kinder, F. R., Jr., Liu, Y., Lu, Y., McKenna, J., Prashad, M., Ramsey, T. M., Repic, O., Rogers, L., Shieh, W-C., Wang, R-M., and Waykole, L. (2004) Large-scale synthesis of the anti-cancer marine natural product (+)-discodermolide. Part 2: Synthesis of fragments C1-6 and C9-14, *Org. Process Res. Dev. 8*, 101-106.

Mickel, S. J., Sedelmeier, G. H., Niederer, D., Schuerch, F., Koch, G., Kuesters, E., Daeffler, R., Osmani, A., Seeger-Weibel, M., Schmid, E., Hirni, A., Schaer, K., Gamboni, R., Bach, A., Chen, S., Chen, W. C., Geng, P., Jagoe, C. T., Kim, H. Y., Kinder, F. R., Jr., Lee, G. T., McKenna, J., Ramsey, T. M., Repic, O., Rogers, L., Shieh, W-C., Wang, R-M., and Waykole, L. (2004) Large-scale synthesis of the anti-cancer marine natural product (+)-discodermolide. Part 3: Synthesis of fragment C15-21, *Org. Process Res. Dev. 8*, 107-112.

Mickel, S. J., Sedelmeier, G. H., Niederer, D., Schuerch, F., Seeger-Weibel, M., Schreiner, K., Daeffler, R., Osmani, A., Bixel, D., Loiseleur, O., Cercus, J., Stettler, H., Schaer, K., Gamboni, R., Bach, A., Chen, G. P., Chen, W. C., Geng, P., Lee, G. T., Loesser, E., McKenna, J., Kinder, F. R., Jr., Konigsberger, K., Prasad, K., Ramsey, T. M., Reel, N., Repic, O., Rogers, L., Shieh, W-C., Wang, R-M., Waykole, L., Xue, S., Florence, G., and Paterson, I. (2004) Large-scale synthesis of the anti-cancer marine natural product (+)-discodermolide. Part 1: Synthetic strategy and preparation of a common precursor, *Org. Process Res. Dev. 8*, 113-121.

Mickel, S. J., Niederer, D., Daeffler, R., Osmani, Kuesters, E., Schmid, E., H., Schaer, K., Gamboni, R., Chen, W. C., Loesser, E., Kinder, F. R., Jr., Konigsberger, K., Prasad, K., Ramsey, T. M., Repic, O., Wang, R-M., Florence, G., Lyothier, I., and Paterson, I. (2004) Large-scale

synthesis of the anti-cancer marine natural product (+)-discodermolide. Part 5: Linkage of fragments C1-6 and C7-24 and finale, *Org. Process Res. Dev. 8*, 122-130.

Miller, M. L., and Ojima, I. (2001) Chemistry and chemical biology of taxane anticancer agents, *Chem. Rec. 1,* 195-211.

Minguez, J. M., Balachandran, R., Madiraju, C., Giuliano, K. A., Curran, D. P., and Day, B. W. (2002) Synthesis and high content cell-based profiling of simplified analogues of the microtubule stabilizer (+)-discodermolide, *Mol. Cancer Ther. 1*, 1305-1313.

Minguez, J. M., Kim, S. Y., Giuliano, K. A., Balachandran, R., Madiraju, C., Day, B. W., and Curran, D. P. (2003) Synthesis and biological assessment of simplified analogues of the potent microtubule stabilizer (+)-discodermolide, *Bioorg. Med. Chem. 11*, 3335-3357.

Mitchison, T. J. (1993) Localization of an exchangeable GTP binding site at the plus end of microtubules, *Science 261,* 1044-1047.

Monteagudo, E., Cicero, D. O., Cornett, B., Myles, D. C., and Snyder, J. P. (2001) The conformations of discodermolide in DMSO, *J. Am. Chem. Soc*. *123*, 6929-6930.

Mooberry, S. L., Tien, G., Hernandez, A. H., Plubrukarn, A., and Davidson, B. S. (1999) Laulimalide and isolaulimalide, new paclitaxel-like microtubule-stabilizing agents, *Cancer Res*. *59*, 653-660.

Morton, M. F., Harper, E. A., Tavares, I. A., and Shankley, N. P. (2002) Pharmacological evidence for putative CCK(1) receptor heterogeneity in human colon smooth muscle, *Br. J. Pharmacol*. *136*, 873-882.

Motulsky, H. J., and Ransnas, L. A. (1987) Fitting curves to data using nonlinear regression: a practical and nonmathematical review, *FASEB J*. *1*, 365-374.

Nabeshima, K., Kurooka, H., Takeuchi, M., Kinoshita, K., Nakaseko, Y., and Yanagida, M. (1999) p93dis1, which is required for sister chromatid separation, is a novel microtubule and spindle pole body-associating protein phosphorylated at the Cdc2 target sites, *Genes Dev*. *9,* 1572-1585.

Nettles, J. H, Li, H., Cornett, B., Krahn, J. M., Snyder, J. P., and Downing, K. H. (2004) The binding mode of epothilone A on alpha,beta-tubulin by electron crystallography, *Science 305*, 866-869.

Nogales, E., Wolf, S. G., Khan, I. A., Luduena, R. F., and Downing, K. H. (1995) Structure of tubulin at 6.5 A^o and location of the taxol-binding site, *Nature 375*, 424-427.

Nogales, E., Wolf, S. G., and Downing, K. H. (1998) Structure of the alpha beta tubulin dimer by electron crystallography, *Nature 391,*199-203. Erratum in: *Nature (*1998) *393,* 191.

Nogales, E., Whittaker, M., Milligan, R. A., and Downing, K. H. (1999) High-resolution model of the microtubule, *Cell 96,* 79-88.

Nogales, E. (2001) Structural insight into microtubule function, *Annu. Rev. Biophys. Biomol. Struct. 30,* 397-420.

Novartis AG, Annual Report Pursuant to Section 13 or 15(d) of the Securities Exchange Act of 1934 for the fiscal year ended December 31, 2004. Securities Exchange Commission file number 1-15024, Form 20-F, filed January 28, 2005, p. 42.

Ojima, I., Chakravarty, S., Inoue, T., Lin, S., He, L., Horwitz, S. B., Kuduk, S.D., and Danishefsky, S. J. (1999) A common pharmacophore for cytotoxic natural products that stabilize microtubules, *Proc. Natl. Acad. Sci. U S A. 96,* 4256-4261.

Oosawa, F., and Kasai, M. (1962) A theory of linear and helical aggregations of macromolecules, *J. Mol. Biol*. *4*, 10-21.

Palermo, M. G., Bair, K. W., Chen, W., Guo, Q., Lassota, P. T., Sorensen, E., Wang, R., Ramsey, T. M., and Kinder, F. R. Jr. (2004) Synthesis of discodermolide analogues with isosteric replacements of the C^{21}-^{24} diene group, *ACS National Meeting Abstracts,* 791.

Paterson, I., Florence, G. J., Gerlach, K., and Scott, J. P. (2000) Total Synthesis of the antimicrotubule agent (+)-discodermolide using boron-mediated aldol reactions of chiral ketones, *Angew. Chem. Int. Ed*. *39*, 377-380.

Paterson, I., Florence, G. J., Gerlach, K., Scott, J. P., and Sereinig, N. (2001) A practical synthesis of (+)-discodermolide and analogues: fragment union by complex aldol reactions, *J. Am. Chem. Soc*. *123*, 9535-9544.

Paterson, I., Britton, R., Delgado, O., and Wright, A. E. (2004a) Stereochemical determination of dictyostatin, a novel microtubule-stabilising macrolide from the marine sponge *Corallistidae* sp., *Chem. Commun*. *6*, 632-633.

Paterson, I., Britton, R., Delgado, O., Meyer, A., and Poullennec, K. G. (2004b) Total synthesis and configurational assignment of (-)-dictyostatin, a microtubule-stabilizing macrolide of marine sponge origin, *Angew. Chem. Int. Ed. Engl*. *43*, 4629-4633.

Perez, E. A. (1998) Paclitaxel in Breast Cancer, *Oncologist 3*, 373-389.

Perez, E. A. (1999) Paclitaxel plus nonanthracycline combinations in metastatic breast cancer, *Semin. Oncol*. *26*, *Suppl. 2*, 21-26.

Pettit, G. R., Cichacz, Z. A., Gao, F., Boyd, M. R., and Schmidt, J. M. (1994) Isolation and structure of the cancer cell growth inhibitor Dictyostatin, *Chem. Commun*. 1111-1112.

Quinoa, E., Kakou, Y., and Crews, P. (1988) Fijianolides, polyketide heterocyclics from a marine sponge, *J. Org. Chem*. *53*, 3642-3644.

Rao, S., Orr, G A., Chaudhary, A. G., Kingston, D.G.I., and Horwitz, S. B. (1995) Characterization of the taxol binding site on the microtubule. 2-(m-Azidobenzoyl)taxol photolabels a peptide (amino acids 217-231) of beta-tubulin, *J. Biol. Chem*. *270*, 20235-20238.

Rieder, C. L., and Salmon, E. D. (1998) The vertebrate cell kinetochore and its roles during mitosis, *Trends Cell Biol. 8,* 310-318.

Rowinsky, E. K., Cazenave, L. A., and Donehower, R. C. (1990) Taxol: a novel investigational antimicrotubule agent, *J. Natl. Cancer Inst. 82,* 1247-1259.

Sackett, D. L., and Fojo, T. (1999) Taxanes and other microtubule stabilizing agents, *Cancer Chemother. Biol. Response Modif. 18*, 59-80.

Salmon, E. D., Leslie, R. J., Saxton, W. M., Karow, M. L., and McIntosh, J. R. (1984) Spindle microtubule dynamics in sea urchin embryos: analysis using a fluorescein-labeled tubulin and measurements of fluorescence redistribution after laser photobleaching, *J. Cell Biol*. *99*, 2165-2174.

Saxton, W. M., Stemple, D. L., Leslie, R. J, Salmon, E. D, Zavortink, M., and McIntosh, J. R. (1984) Tubulin dynamics in cultured mammalian cells, *J. Cell Biol*. *99,* 2175-2186.

Schiff, P. B., Fant, J., Auste, L. A., and Horwitz, S. B. (1978) Effects of taxol on cell growth and *in vitro* microtubule assembly, *J. Supramolec. Struct*. *8*, *Suppl. 2*, 328.

Schiff, P. B., Fant, J., and Horwitz, S. B. (1979) Promotion of microtubule assembly *in vitro* by taxol, *Nature 277*, 665-667.

Shaw, S. J., Sundermann, K. F., Burlingame, M. A., Myles, D. C., Freeze, S. B., Xian, M., Brouard, I., and Smith, A. B. III (2005) Toward understanding how the lactone moiety of discodermolide affects activity, *J. Am. Chem. Soc*. *127*, 6532-6533.

Shelansky, M. L., and Taylor, E. W. (1967) Isolation of a protein subunit from microtubules, *J. Cell Biol*. *34*, 549-554.

Shin, Y., Choy, N., Turner, T. R., Balachandran, R., Madiraju, C., Day, B. W., and Curran, D. P. (2002) Discodermolide/Dictyostatin hybrids: synthesis and biological evaluation, *Org. Lett*. *4*, 4443-4446. Erratum in: *Org. Lett*. (2003) *5*, 603.

Shin, Y., Fournier, J. H., Fukui, Y., Bruckner, A. M., and Curran, D. P. (2004) Total synthesis of (-)-dictyostatin: confirmation of relative and absolute configurations, *Angew. Chem. Int. Ed. Engl*. *43*, 4634-4637.

Shin, Y., Fournier, J. H., Balachandran, R., Madiraju, C., Raccor, B. S., Zhu, G., Edler, M. C., Hamel, E., Day, B. W., and Curran, D. P. (2005) Synthesis and biological evaluation of (-)-16-normethyldictyostatin: a potent analogue of (-)-dictyostatin, *Org. Lett. 7*, 2873-2876.

Shin, Y., *et al*. (2005) - Manuscript in preparation.

Smith, A. B. III., Kaufman, M. D., Beauchamp, T. J., LaMarche, M. J., and Arimoto, H. (1999) Gram-scale synthesis of (+)-discodermolide, *Org. Lett*. *1*, 1823-1826. Erratum in: *Org. Lett.* (2000) *2*, 1983.

Smith, A. B. III., LaMarche, M. J., and Falcone-Hindley, M. (2001) Solution structure of (+)-discodermolide, *Org. Lett*. *3*, 695-698.

Smith, A. B III., Freeze, S. B., LaMarche, M. J., Hirose, T., Brouard, I., Rucker, P. V., Xian, M., Sundermann, K. F., Shaw, S. J., Burlingame, M. A., Horwitz, S. B., and Myles, D. C. (2005) Toward understanding how the lactone moiety of discodermolide affects activity, *Org. Lett*. *7*, 311-314.

Snyder, J. P., Nettles, J. H., Cornett, B., Downing, K. H., and Nogales, E. (2001) The binding conformation of Taxol in beta-tubulin: a model based on electron crystallographic density, *Proc. Natl. Acad. Sci. U. S. A. 98*, 5312-5316.

Soifer, D. (1986) Factors regulating the presence of microtubules in cells, *Ann. N Y Acad. Sci*. *466*, 1-7.

ter Haar, E., Rosenkranz, H. S., Hamel, E., and Day, B. W. (1996) Computational and molecular modeling evaluation of the structural basis for tubulin polymerization inhibition by colchicine site agents, *Bioorg. Med. Chem*. *4*, 1659-1671.

ter Haar, E., Kowalski, R. J., Hamel, E., Lin, C. M., Longley, R. E., Gunasekera, S. P., Rosenkranz, H. S., and Day, B. W. (1996) Discodermolide, a cytotoxic marine agent that stabilizes microtubules more potently than taxol, *Biochemistry 35*, 243-250.

Tournebize, R., Popov, A., Kinoshita, K., Ashford, A. J., Rybina, S., Pozniakovsky, A., Mayer, T. U., Walczak, C. E., Karsenti, E., and Hyman, A. A. (2000) Control of microtubule dynamics by the antagonistic activities of XMAP215 and XKCM1 in *Xenopus* egg extracts, *Nat. Cell Biol*. *2*, 13-19.

Vasquez, R. J., Gard, D. L., and Cassimeris, L. (1999) Phosphorylation by CDK1 regulates XMAP215 function *in vitro, Cell Motil. Cytoskeleton*. *43*, 310-321.

Verde, F., Dogterom, M., Stelzer, E., Karsenti, E., and Leibler, S. (1992) Control of microtubule dynamics and length by cyclin A- and cyclin B-dependent kinases in *Xenopus* egg extracts, *J. Cell Biol. 118*, 1097-1108.

Wani, M. C., Taylor, H. L, Wall, M. E., Coggon, P., and McPhail, A. T. (1971) Plant antitumor agents. VI. The isolation and structure of taxol, a novel antileukemic and antitumor agent from *Taxus brevifolia, J. Am. Chem. Soc. 93*, 2325-2327.

Weingarten, M. D., Lockwood, A. H., Hwo, S. Y., and Kirschner, M. W. (1975) A protein factor essential for microtubule assembly, *Proc. Natl. Acad. Sci. U. S. A. 72*, 1858-1862.

Weisenberg, R. C., and Deery, W. J (1976) Role of nucleotide hydrolysis in microtubule assembly, *Nature 263*, 792-793.

Weisenberg, R. C., Deery, W. J., and Dickinson, P. J. (1976) Tubulin-nucleotide interactions during the polymerization and depolymerization of microtubules, *Biochemistry 15*, 4248-4254.

West, L. M., Northcote, P. T., and Battershill, C. N. (2000) Peloruside A: a potent cytotoxic macrolide isolated from the New Zealand marine sponge *Mycale sp*., *J. Org. Chem*. *65*, 445-449.

Wipf, P., Reeves, J. T., Balachandran, R., Giuliano, K. A., Hamel, E., and Day, B. W. (2000) Synthesis and biological evaluation of a focused mixture library of analogues of the antimitotic marine natural product curacin A, *J. Am. Chem. Soc*. *122*, 9391-9395.

Wittmann, T., Hyman, A., and Desai, A. (2001) The spindle: a dynamic assembly of microtubules and motors, *Nat. Cell Biol*. *3*, E28-34.

Ye, X., and Sloboda, R. D. (1995) A 62-kDa mitotic apparatus protein required for mitotic progression is sequestered to the interphase nucleus by associating with the chromosomes during anaphase, *Cell Motil. Cytoskeleton 30*, 310-323.

Zhai, Y., Kronebusch, P. J, and Borisy, G. G. (1995) Kinetochore microtubule dynamics and the metaphase-anaphase transition, *J. Cell Biol*. *131*, 721-734.